UNIVERSITÀ
DI PAVIA

University of Pavia

FACULTY OF ENGINEERING
Department of Industrial and Information Engineering

Ph.D. Dissertation

Advanced Control of Multiagent Automotive Systems

Supervisor
Prof. Antonella Ferrara, Ph.D.

Candidate
Massimo Zambelli, M.Eng.

A.Y. 2019/2020

Abstract

The latest improvements in automotive technologies are enabling a paradigm shift in transportation systems: shared mobility, electrification, connectivity, and autonomous driving are envisaged as the four major trends in the near future. To support these advancements, advanced control strategies are required for the control of both single vehicles and formations of Connected and Automated Vehicles (CAVs). These, in turn, lead to beneficial features such as greater safety, improved efficiency, and better exploitation of the traffic infrastructure. Autonomously controlled vehicles can exhibit advanced performances which determine an improved safety even in cases where the distances are tight, while the inter-vehicle communication opens a huge number of new possibilities. Among others, unidimensional and bidimensional formations can be employed as dynamic actuators in traffic control.

In this Dissertation a discussion about advanced control techniques for multi-agent automotive systems is provided, proposing novel research results. Starting from a brief introduction to the control of single vehicles (in which electric and hybrid vehicles opened a broad range of new possibilities), the discussion is then extended to the robust control of platoons via the exploitation of Sliding Mode Control techniques. Lastly, an extension to the formation control case is examined, presenting a novel iterative method for the creation and dynamic reshape of formations in highway scenarios.

Sommario

I recenti miglioramenti nelle tecnologie automobilistiche stanno consentendo un cambio di paradigma nei sistemi di trasporto: mobilità condivisa, elettrificazione, connettività e guida autonoma sono le quattro tendenze principali previste nel prossimo futuro. Per supportare tali progressi, sono necessarie strategie di controllo avanzate per il controllo sia dei singoli veicoli che delle formazioni di veicoli connessi e automatizzati (Connected and Automated Vehicles, CAVs). Queste, a loro volta, portano a miglioramenti come una maggiore sicurezza, una migliore efficienza e un migliore sfruttamento delle infrastrutture di trasporto. I veicoli a controllo autonomo offrono prestazioni avanzate che determinano una maggiore sicurezza anche nei casi in cui le distanze inter-veicolo sono ridotte, mentre la comunicazione tra agenti apre un numero enorme di nuove possibilità. Per esempio, formazioni unidimensionali e bidimensionali possono essere impiegate come attuatori dinamici nel controllo del traffico.

In questa Tesi viene fornita una discussione sulle tecniche di controllo avanzate per sistemi automotive multi-agente, proponendo nuovi risultati di ricerca. Partendo da una breve introduzione al controllo dei singoli veicoli (in cui i veicoli elettrici e ibridi hanno aperto una vasta gamma di nuove possibilità), il discorso è poi esteso al controllo robusto dei platoon attraverso l'introduzione delle tecniche di controllo Sliding Mode. Infine, viene esaminata l'estensione al caso del controllo di formazione, presentando un nuovo metodo iterativo per la creazione e il rimodellamento dinamico delle formazioni in scenari autostradali.

Acknowledgement

I need to express my gratitude to all the people who supported me during these years in my Ph.D. journey, making this achievement possible. First of all, a special thank to my family and closest friends, whose love and support have been and are of immense value.

I would like to thank my Advisor, Prof. Antonella Ferrara, for her help and the opportunity she gave me of working as a Ph.D. student at the Identification and Control of Dynamic Systems Laboratory. My gratitude goes also to the reviewers of this Dissertation, Prof. Martin Steinberger (Graz University of Technology) and Prof. Silvia Siri (University of Genova), for their valuable suggestions and very kind comments.

Contents

List of Figures

List of Tables

Chapter 1

Introduction

The control of automotive systems has gained a huge amount of interest in the last years both from the research and the industry point of view. On one hand, the introduction of autonomous driving features (empowered mostly by recent advancements in the field of machine learning[1]) is gradually changing how vehicular systems are designed and employed while, on the other hand, the ever-increasing technological improvements are enabling more and more complex control strategies. These latter make use of suitably developed transportation infrastructures and advanced communication architectures to implement coordination features, whether it is among the vehicles (which become cooperative agents in multi-agent systems) and/or between the vehicles and the infrastructure [214, 1, 42] (one can think, for instance, of vehicles able to negotiate a safe and quick dispatch at an intersection, or of a vehicle communicating with the road infrastructure to adapt its velocity for optimizing the traffic flow according to the state of the traffic lights, [37, 169]).

Looking at the near future, the development of "smart cities" [23] in which the quality of life is expected to be improved through the exploitation of the latest technological advancements (for instance, the so-called Internet of Things [228]) seems the most promising direction. In this context, the evolution of transportation systems appears to be a key element, and thus many solutions are currently being investigated to make them smarter, more comfortable, safer, and more environment-friendly [210, 216]. In turn,

[1] Actually, although the current trend is in the direction of adopting machine learning-based solutions for autonomous driving, a general discussion should also consider recent advancements in computer vision, control engineering, and artificial intelligence in general.

the adoption of advanced communication and control architectures enabled by the latest technological advancements is of paramount importance for empowering effective and robust automatic control strategies.

Figure 1.1: Modern electric cars are currently setting new standards in the vehicles industry. Among many other factors, the new control opportunities provided by EVs open interesting problems to be addressed in advanced automotive control systems.

The ever increasing development and marketing of electric vehicles (EVs) [97] and hybrid electric vehicles (HEVs) [64, 65] is already revolutionizing the automotive field from an energetic point of view [115], but also offering completely new control opportunities [182, 178, 183]. On one side, in fact, new strategies can be investigated to reduce the energy consumption in lithium-ion batteries [151], which in turn require the development of advanced Battery Management Systems (BMSs) [152] and optimal charging

solutions [204]. On the other side, the usual adoption of independent electric motors allows for more flexible and effective control strategies. The latest years have witnessed a gradual evolution of the on-board control systems both from the point of view of the control algorithms and the devices available for control (sensors, communication units, etc.).

To support these advancements, a key feature remains the development of safe and reliable control strategies. In particular, the introduction of robustness has always constituted one of the major aspects in the design of control systems and nowadays its importance is evident more than ever. As a matter of fact, the adoption of increasingly more sophisticated architectures must be strictly supported by reliable systems able to implement the required behaviors in a variety of different situations and under uncertain conditions.

Thus, several results proposed in the present Thesis are dedicated to the development of robust strategies for the control of single EVs/HEVs and multi-agent automotive systems. Throughout the entire discussion, different levels of automotive control problems are considered, introducing gradually more complex architectures. At first the robust control of the dynamics of single vehicles[2] is considered. Then, the problem of effectively control unidimensional formations (i.e., platoons) is addressed. Finally, the extension of formation control to 2-dimensional formations is discussed for the specific case of highway scenarios. Original solutions are proposed for problems regarding these three aspects of the advanced automotive control, with a special focus on robustness. This latter, in particular, is enforced through the adoption of techniques based on Sliding Mode Control (SMC) [207] as will be thoroughly discussed in the remainder of the Dissertation.

A brief overview is provided in the following of this chapter on the main problems faced by modern automotive control systems and considered in the proposed research works. For further reference, the reader is referred to, among many other possibilities, [76, 95].

[2]The focus of the present Thesis being on multi-agent automotive systems, these results are only briefly introduced in the following of this introductory chapter. The reader is referred to the respective published manuscripts for a thorough presentation.

Figure 1.2: An efficient transportation infrastructure constitutes a key element in the development of advanced, smart cities.

1.1 Automotive Control

1.1.1 Vehicle Dynamics Control

The introduction of advanced control strategies for modern automotive systems must cover, first of all, Advanced Driver Assistance Systems (ADAS) [116, 132], which provide safety and reliability to the drivers through more or less invasive automation aimed at improving the driving experience while avoiding accidents and, in general, dangerous circumstances. These strategies comprise slip/skid [140], (lateral) stability [8] and chassis control architectures (considering the anti-rollover systems as part of the latter). Although such features are the most basic ones that a vehicle dynamics controller must address effectively [76, 95], the introduction of more sophisticated control systems that can exploit EVs/HEVs architectures to achieve better performance is a currently active field of research.

Diving deeper in the discussion of the mentioned problems, slip control is concerned with the avoidance of slipping phenomena that may lead to a loss of handling due to abrupt braking especially on low-friction terrains (the Anti-lock Braking System, ABS, is an example of such mechanisms). Anti-skid controllers, on the opposite side, prevent skidding during accelerations thus increasing the vehicle handling and the force exercisable on the ground. To address these two complementary problems, for instance, the authors in [88] propose a gain-scheduled LQR slip controller, while in [80, 4, 46] Sliding Mode Control based solutions are proposed. Fuzzy control is instead employed in [153], while in [46] a slip controller is developed specifically for EVs with independent in-wheels motors (see, e.g., [47, 48, 78]).

Stability control, instead, relates to the lateral dynamics of the vehicles and entails the enforcement of a quasi-kinematic cornering behavior during turnings. This is to say that, despite the complex dynamic interactions determining its lateral behavior, the vehicle must be forced to assume a trajectory prescribed by the driver as it would occur if the vehicle proceeded at very low speed (see, e.g. [163]). Many occasions may arise where a loss of handling is experienced, often with disastrous consequences, especially in low-friction conditions (for instance, sharp turnings on wet or icy grounds). Lateral dynamics control comes commonly in the form of the so-called yaw rate control, where the yaw rate of the vehicle is controlled directly through the exertion of a momentum with respect to the vertical axis of the vehicle

itself. Such momentum can be generated via an (automated) steering wheel input and/or differences in the forces generated by the wheels of the same axle[3]. The problem of yaw rate control is addressed in many works in the literature. For instance, in [233, 202] a lateral dynamics control is proposed based on Sliding Mode Control, while authors in [96] present a solution relying specifically on the in-wheels motors architecture of modern electric vehicles. Active stability control not only allows to improve safety during stressing lateral maneuvers, but also extends the limit of stability of the vehicles during cornering [117], providing more freedom and safety to the driver.

Notice that, in contrast with the past when the different control tasks were carried out somehow independently from different onboard controllers, nowadays effort is being made to develop reliable centralized controllers able to work in many different scenarios (see, e.g. [77, 205, 136, 220])[4]. This shift in the design has been made possible by technological advancements that led to more powerful computation units as well as more complex algorithms. The primary consequence is that the couplings existent between the different exerted control actions are explicitly taken into account, providing better-tailored solutions to the mentioned control problems. Additionally, advanced strategies can be considered, for instance taking into account the particular tire-road interaction or the various dynamics of the powertrain. With the aim of effectively implement centralized, multi-function active control systems, an effort has been devoted to exploiting model-based architectures relying, for instance, on Model Predictive Control (MPC) (refer to, e.g., [75, 121, 118, 32]). In particular, the flexibility offered by EVs and HEVs allowed the development of effective solutions able to address physical and safety constraints in a rather flexible and efficient way. Besides the solution of general combined slip-stability control problems, addressed for instance in works as [108, 167], this enabled researchers to propose solutions able to effectively tackle the problem of stability even in limit conditions, i.e. during aggressive cornering maneuvers at the limit of handling. The works

[3]This latter technique is generally faster in terms of the response of the system with respect to the action on the steering wheel and is particularly easy to implement in EVs with independent in-wheel motors [48, 78].

[4]Another aspect of the vehicle dynamics control, not mentioned explicitly here but equally important and often considered in integrated control solutions, is chassis control (see, for instance, [74, 186, 40, 219]).

[24, 35, 190, 81] are special examples that rely on integrated control systems acting on both the longitudinal and the lateral vehicle dynamics (by means of the wheels torques and the steering angle).

Despite the proven effectiveness of such approaches, the problem of enforcing robustness in sophisticated model-based strategies is still one of the most crucial issues and is addressed in [165] as an original contribution of the research work reported in this Thesis. In particular, a multi-rate architecture comprising an MPC nominal controller and an Integral Sliding Mode (ISM) Control component is exploited for yaw-rate control. The results show great improvement in the performance when vehicles proceed in cornerings on terrains which exhibit abrupt and unexpected changes in the tire-road friction coefficients[5]. The introduced robustness (provided acting on the steering angle with fast corrections) allows to quickly compensate for such effects, allowing the vehicles to maintain stability where non-robustified schemes are shown to fail, leading to potentially destructive losses of handling.

Observers in Vehicle Dynamics Control

Independently of the particular dynamics control problem under investigation or the employed algorithm adopted to solve it, a fundamental element for reliably closing control loops is the ability to reconstruct quantities of interest in real-life scenarios. Output-based control strategies require a prompt and precise reconstruction of the necessary measurements, while the usually more sophisticated model-based algorithms necessitate usually of full states availability. In this respect different solutions have been proposed in the literature, relying for instance on on-line states observers (see, e.g. [94, 211, 39, 120, 13, 57]) or sensors fusion techniques [124]. While observation systems allow the design of control loops in case sensors are not directly available or the measurements are not sufficiently reliable, the exploitation of the reconstructed quantities can also enable fault detection

[5]Notice that, despite the major effects are visible during such unaccounted for changes in the tire-road friction forces (which determine very appreciable differences between the adopted model and the true vehicle behavior), also other effects are mitigated via the adoption of the proposed scheme. For instance, the mismatches introduced by the discretization of the model considered as matched uncertainty is completely compensated for. With regard to the unmatched component of the uncertainty, it is guaranteed that it is not amplified by the introduction of the ISM-injected control through the adoption of the technique developed in [170].

or the introduction of fault-tolerant control schemes (see, e.g., [138]).

Figure 1.3: Advanced vehicle dynamics controllers provide safety and efficiency, greatly improving the performance of both manned and autonomous vehicles.

Authors in [83, 230, 131] propose solutions to reconstruct the vehicle velocity, while the more sophisticated problem of estimating the vehicle sideslip angle is addressed in [58, 60, 191, 192]. Other interesting quantities describing the dynamical state of the vehicle such as, for instance, the roll and bank angle, are estimated in [176, 157].

One of the most challenging problems, though, is the reliable estimation of the tire-road contact forces [218, 11, 12, 59, 156, 160], which constitutes a key feature to empower complex and effective control algorithms. In fact, being able to promptly reconstruct the tire-road contact forces not only enables the design of precise slip/skid and yaw control systems but in principle can enable more advanced features relying on the knowledge of the terrain type. Despite sensors exist able to provide such measurements, their impressive cost make thems unavailable for commercial purposes. Thus, the adoption of observers (or, said differently, virtual sensors) is mandatory and constitutes a key element in the automotive control research.

An original proposal, part of the research related to this Dissertation, has been published in [164] and successively extended in [161], in which a tire-road forces reconstruction algorithm is developed based on the inherent

ability of Sliding Mode Control to estimate uncertain dynamics acting on the considered systems. Specifically, virtual sensors are developed for both the longitudinal and lateral forces exerted instantaneously by the vehicle wheels coupling Second-Order Sliding Mode Control and a Kalman filter. While the former delivers a fast reconstruction of the forces (see, e.g., [194, 73, 234] and references therein for a general understanding of the concept), the latter improves the precision via a model-based Extended Kalman Filter (EKF) which greatly reduces the chattering effects. Notice that the Sliding Mode-based stage, which relies on the Sub-Optimal algorithm[6], adopts an adaptive strategy to inherently reduce the chattering. In fact, as described in [146, 199], the algorithm automatically adapts the gain based on both a switched and a time-based law to exert only the actually required control effort to effectively contrast the uncertainty. The experimental results conducted on a real prototypical car and included in [161] evidence the great effectiveness of the developed strategy, which can precisely reconstruct the forces in real-life scenarios[7].

1.1.2 Platoon Control

While the development of robust and effective vehicle dynamics control systems is of course of paramount importance, in the last few years a shift towards the control of multi-agent vehicular systems happened rapidly due to the availability of new communication and control solutions [109, 5]. In particular, the control of platoons [112, 87] (1D formations of vehicles which follow a leader while maintaining a specified inter-vehicle distance) has attracted a lot of interest due to its simplicity and effectiveness in providing safety, comfort and reduced fuel consumption, while allowing for improvements in traffic regulation [208, 22]. Many studies have been carried out from both the control and the network architecture perspectives (see, e.g., [112, 87] and references therein), to improve the effectiveness and practical realizability of the proposals in real-world scenarios. Platoons can, in fact, provide a vast amount of benefits in the presence of connected and automated vehicles (CAVs), especially on highways, depending on the pen-

[6]Described in Section (2.1.2).

[7]The experiments have been carried out on prototypical vehicles equipped with specific tire-road forces sensors. These, though, as already highlighted are hugely expensive and cannot be equipped on consumer vehicles, hence requiring observation systems for closing the control loops involving such (virtual) measurements.

etration rate. Among them, energy efficiency and road occupation appear to be enhanced if tight inter-vehicle distances are kept, with particular reference to heavy-duty vehicles (e.g. trucks, see [2]). Additionally, platoons can be employed as moving bottlenecks (see, e.g. [144]) to act as dynamic actuators in traffic control architectures [143].

Starting from the concept of Adaptive Cruise Control (ACC), according to which single vehicles can adapt their velocity based on their distance with respect to the preceding one, strings can be built where the agents only exploit local information (see, e.g., [197]). The task, seemingly simple in the presence of sufficiently automated vehicles, is in fact quite challenging since string stability (see, among many others, [66, 215, 148, 149] for an overview of the concept) must be enforced in order to avoid disruptive effects which may lead to crashes. It is clear now that this structural property is mainly determined by the selection of the spacing policy [217, 198, 197, 180] and, at a successive level, via the adoption of proper communication systems augmenting the information available to every vehicle. In this direction, exploiting Vehicle-to-Vehicle (V2V) and Vehicle-to-Infrastructure (V2I) communication systems, Cooperative Adaptive Cruise Control (CACC) solutions have been proposed in the literature (see, among many others, [147, 126, 52]). The adoption of such interconnected frameworks hugely broadens the range of possible strategies which may be implemented, both to enhance particular features of the platoons themselves or to include them into more complex control architectures (again, think about platoons on highways which can be dynamically created and dissolved to promptly implement traffic control strategies and regulate the flow of the entire highway portion).

In the literature, different control methodologies have been effectively proposed over the years. With respect to the former linear controllers (see, among many others, [198]), improvements have been achieved by more recent solutions relying on Sliding Mode Control, which has effectively been introduced in platoon control in works as [187, 70, 3, 172, 175, 173]. Consensus Control (see, e.g., [124, 71] and references therein) has also been adopted as a framework to control platoons (see e.g. [53, 113]), often with promising results. The most popular technique remains, in any case, Model Predictive Control (see, for instance, [61, 223]). With regard to the latter, thanks to the advancements in communication technologies additional

requirements can be addressed based on (distributed) optimal control concepts [33], to further enhance the effectiveness of the platoon formations [62, 61, 98]. In fact, advanced requisites such as the respect of safety and physical constraints can be effectively addressed by MPC, which can also provide various additional features (often in CACC frameworks) [231].

Figure 1.4: The traffic can be effectively regulated introducing platoons of CAVs, especially on highways.

Independently of the complexity of the platoon control systems, robustness occupies a premium position in the requirements list for an effective real-life adoption. In particular, it is known that the longitudinal dynamics models usually adopted to describe the behavior of the vehicles in the platoon are highly uncertain. On one hand, in fact, they are obtained through feedback linearization [215] based, thus, on a nominal description of the powertrain and the vehicle kinematics (for instance, aerodynamic drags and rolling resistances are almost impossible to estimate precisely). On the other hand, many disturbance phenomena and external factors act on the vehicles at any time during real-life applications (e.g. lateral wind, turbulences, road irregularities, and terrain changes). The uncertainty in the modeling of the vehicle dynamics can disrupt the performance, especially when model-based control solutions are adopted (which is very common, since they usually allow one to consider optimality measures and constraints). As a consequence, not only the local and string stability can be disrupted, but also accessory ef-

fects manifest such as for instance the loss of coherence (see, e.g., [114, 112]). This latter is the ability of a platoon to keep the required end-to-end length over time (one can see that as the distance between the first and last vehicle in the string). At a steady speed, this quantity must be constant, but local perturbations can determine visible effects if not damped correctly inside of the platoon, with some possible consequences for example on the traffic-regulation ability of the system. In fact, for instance, shockwaves could be generated in the following traffic flow.

In this dissertation, two proposals are presented to address the problem of robust platoon control exploiting the inherent robustness of Sliding Mode Control, as will be thoroughly described in Chapter 3.

1.1.3 Formation Control

During the last decades, the control of multi-agent systems (MAS) has emerged as one of the most appealing topics in the Control Engineering field. In a MAS, agents are required to act considering the underlying aim of enforcing specific features and global-level goals [188]. The inspiration for the control of such systems comes from nature observation: in nature, in fact, many collective behaviors can be witnessed providing survival benefits for the involved subjects. For instance, extended sensing capabilities and coordinated actions can advantage predators, while cooperative tactics can lead to a better defense of the preys.

Similarly, groups of artificial agents can be controlled to achieve complex goals, enabling the solution of more or less specific problems efficiently through cooperation. For instance, it is possible to exploit groups of agents to provide distributed surveillance thus enlarging the spanned range (see, e.g. [137] and applications in [179, 26]) and provide robustness through redundancy in sensors. Different strategies can be referred to the broad category of MAS control, including flocking [133, 201] consensus control[8] [150, 134] and formation control [38, 55, 50, 36]. This latter is one of the most appealing topics in the control engineering research. Works as [25, 6, 212, 56] propose different strategies for the formation control of Unmanned Aerial Vehicles (UAVs), with applications ranging from cooperative surveillance [209] to transportation [125]. Automated Underwater Vehicles (AUVs) strategies

[8] Briefly discussed in Section 2.1.4.

[45] are instead developed in works as [44, 107] and Automated Ground Vehicles (AGVs) are considered for instance in [16, 90]).

Particularly, the control of formations of autonomous vehicles (or, more generally, CAVs) is currently occupying an interesting position in research, based on the number of new applications it can enable [89, 129]. For instance, the introduction of groups of collectively controlled vehicles can lead to the possibility of dynamically create moving bottlenecks (see, e.g. [144]), functioning as flexible actuators in traffic control strategies. In this respect, coupling the control of single formations with high-level traffic control systems seems a promising strategy to control the traffic flow and provide significantly better exploitation of the transportation infrastructure (especially in highways) [31, 142, 144, 143] .

Many strategies have been developed for the control of formations, which may be roughly grouped for convenience in three main classes:

- Leader-follower strategies [41]: an agent is considered as the leader, and proceeds independently according to a specific objective. The followers are required, in general, to keep a predefined distance and orientation with respect to the leader[9].

- Behavior-based strategies [14, 128]: several simultaneously desired behaviors are considered (for instance, cohesion among the agents, collision avoidance, and trajectory following)[10] and combined to derive the instantaneous action according to the adopted design. Especially in the context of mobile robot control, the renowned method of potential fields is often used as part of the control algorithm.

- Virtual structure approaches [10]: a single virtual rigid structure is considered for the formation, with a fixed geometric structure.

In the present Dissertation, a novel algorithm for the online creation and control of CAVs formations in highway scenarios is proposed (see Chapter 4).

[9] Notice that platoon control, as described in Section 1.1.2, falls into this category.
[10] Flocking algorithms fall straightforwardly in this category.

1.2 Contributions of the Thesis

The major contributions of the present thesis rely on the introduction of Sliding Mode Control (SMC, see Section 2.1) for the development of advanced automotive control systems, involving one or more vehicles, and the proposal of a novel formation control algorithm for highway scenarios. Particular importance is given to robustness, achieved through proposed algorithms directly based on SMC, which are inherently invariant to matched disturbances, or injecting rubustifying terms in advanced MPC-based strategies.

The already introduced works [164, 165, 161] provide solutions for single-vehicle systems, and will not be discussed further in this Dissertation since the focus is mainly devoted to multi-agent automotive systems. In this respect, the results developed and presented in the remaining of the Thesis provide the following contributions:

- In the context of platoon control, two main contributions are proposed. One relies on a multi-rate architecture for the robustification of an original distributed MPC strategy, providing a feasible and lightweight algorithm for robust platoon control (see Section 3.3). The other proves theoretically and in simulation that enforcing second-order sliding modes locally (for each vehicle, with respect to the reference inter-vehicle distance) enables to achieve not only local stability but also Global Disturbance String Stability (GDSS) in a rather general case (i.e. with feedback-linearized vehicle dynamics, described by third-order models). In particular, it proposes a particular formulation for the local spacing policy, able to track at the same time a predefined inter-vehicle distance and a space-dependent reference velocity tracking. This results are presented in Section 3.4.

- In the context of formation control, a novel general two-step asynchronous algorithm for 2D-formations creation and reshaping in highway scenarios is proposed based on discrete Dynamic Programming and continuous trajectory tracking through local MPC (see Section 4.2). With respect to the classification provided above in Section 1.1.3, the proposed control strategy can be considered as mainly based on a virtual structure. Despite that, though, additional flexibility is provided by the two-step asynchronous formulation which relaxes the

inherent rigidity exhibited usually by such kinds of algorithms. Additionally, the modular architecture provides a high degree of flexibility, making the proposal a possible starting point for the development of more advanced solutions.

Besides these main results, minor developed contributions are also briefly discussed in the context of Consensus Control (see 2.1.4) and Constrained Control. Although not straightforwardly employed in the presented automotive control algorithms, such techniques are promising and might be further investigated in automotive applications for improved performance.

1.3 Outline

The remaining of this Dissertation is organized as follows. In Chapter 2, a general overview of the main control techniques adopted in the proposed strategies is provided. In particular, an introduction on Sliding Mode Control and Model Predictive Control is presented in Sections 2.1 and 2.2, respectively. Specifically, in the former First-Order Sliding Mode (FOSM) and Higher-Order Sliding Mode (HOSM) control are presented, with particular emphasis on the Second-Order Sliding Mode (SOSM) control. Additionally, Integral Sliding Modes (ISM) are introduced and proposed in Section 2.1.3 as a straightforward way of introducing robustness with respect to matched uncertainty in MPC formulations. Section 2.1.4, in particular, proposes an overview of the exploitation of Sliding Mode Control in Consensus control problems.

Unidimensional formations (platoons) are considered in Chapter 3. Specifically, in Section 3.1 a brief overview of platoon control is provided to lay the foundations for the subsequent discussion. The longitudinal dynamics modellings employed in platoon control are presented in 3.2. Successively, the two proposals are presented in Section 3.3 and 3.4, respectively.

The extension of automotive formation control strategies to the two-dimensional case is discussed in Chapter 4. In particular, the adopted combined longitudinal and lateral dynamics model upon which the proposed algorithm relies is described in 4.1, and then the novel algorithm is proposed for formation creation and dynamic reshape in highway scenarios, in Section 4.2.

Final conclusions are drawn in Chapter 5, where also an outlook on possible further improvements is proposed.

Chapter 2

Preliminaries

In this chapter, an introduction about the two control strategies on which the results presented in this Thesis rely, namely Sliding Mode Control (SMC) and Model Predictive Control (MPC), is provided. In particular, Section 2.1 introduces at first the concept of First-Order Sliding Mode Control (2.1.1), illustrating the basic mathematical concepts composing the theory and highlighting the main drawbacks, which led subsequently to the adoption of Higher-Order Sliding Mode Control strategies. These latter are introduced in Section 2.1.2, with particular reference to the chattering alleviation features offered by such strategies. Specifically, Second-Order Sliding Mode Control is presented in Section 2.1.2, with specific emphasis on the Sub-Optimal algorithm. This latter, in fact, is adopted in most of the works proposed in this Dissertation and thus deserves a thorough presentation. Additionally, considerations about the possibility of adopting constrained SMC algorithms are drawn. Integral Sliding Mode Control is presented in Section 2.1.3, while the employment of SMC for leader-follower consensus control is discussed in Section 2.1.4, where an original control strategy is also presented.

Lastly, the basics of MPC are introduced in Section 2.2.

2.1 Sliding Mode Control (SMC)

In this section, a brief introduction to Sliding Mode Control [207, 63, 189] is provided, since it constitutes the approach upon which many of the results proposed in this Thesis rely. Nowadays the theory and practice of SMC is very mature and extremely broad, and going through the whole range of different coverable topics is out of the scope of the present work. For this reason, only the concepts useful for the present and subsequent discussion are here introduced, providing to the reader also a number of valuable references covering specific aspects not explicitly considered here.

Specifically, First-Order Sliding Mode (FOSM) Control is first briefly introduced. It forms the historical and mathematical basis for developing all of the subsequent, more advanced, Higher-Order Sliding Mode (HOSM) Control strategies. These latter are then presented for systems with arbitrary relative degree, but special attention is given to Second-Order Sliding Mode (SOSM) Control, it being widely adopted in the literature and in the present work.

As will be made evident, the selection of the *sliding manifold* constitutes a crucial step in SMC, which characterizes the behaviour of the system under control. With this respect, the particular design giving rise to Integral Sliding Mode (ISM) Control is presented and discussed, since it constitutes the fundamental aspect underlying the robustification schemes proposed in this dissertation.

An insight about the possibility of designing constrained sliding mode controllers [225] is also provided: although this technique are not currently resorted to by the proposed strategies, the introduction of constraints can be beneficial in some cases to enlarge the range of applicability of the proposals without changing the theoretical and practical basis on which they rely, and may constitute a valuable objective for further research work. Similarly, a digression about the employment of Sliding Mode Control in Consensus Control is made, presenting also a novel contribution for finite-time leader-follower consensus with prescribed transient, in Section 2.1.4.

2.1.1 First-Order Sliding Mode (FOSM) Control

The basic idea of SMC is that of transforming a system affine in the control, i.e. of the form

$$\dot{x}(t) = f(x(t), t) + g(x(t), t)u(t) \tag{2.1}$$

where $x(t) \in \mathbb{R}^n$, into a Variable Structure System (VSS) by means of a discontinuous control input $u(t) \in \mathbb{R}^m$. The resulting system can generically be expressed as

$$\dot{x}(t) = f_d(x(t), t) \tag{2.2}$$

where the vector function $f_d(x(t), t) \in \mathbb{R}^n$ is discontinuous at some points in $\mathbb{R}^n$. The system in Equation (2.2) can be equivalently seen as composed of a finite number of different subsystems, called *structures*, whose right-hand side is continuous (i.e., the particular shape of $f_d(\cdot)$ is determined in some way, at each time instant, by $x(t)$). The structures switch according to the value of the states and/or time, leading to non-trivial behaviors.

A simple example of VSS can be, for instance,

$$\dot{x} = \begin{cases} 1 & \text{if} \quad x < 0 \\ -1 & \text{if} \quad x > 0 \end{cases} \tag{2.3}$$

In Equation (2.3), the discontinuity set is constituted by $\{x = 0\}$, for which the right-hand side is not defined[1]. In general, the set of values for which the function $f_d(x(t), t)$ is discontinuous are manifolds in $\mathbb{R}^{n+1}$, called *switching manifolds*. A particular behavior of VSSs is the so-called *sliding mode* (or sliding motion), which is the motion of the state trajectory constrained to a particular switching manifold, called thus the *sliding manifold*. This condition arises if the state vector enters a positive *attraction region*, where the positive attraction property holds, i.e. the vector tangential to the state trajectory is always directed towards the sliding manifold. As a direct consequence, a sequence of switches occurring at infinite frequency takes place

[1]This is a characteristic of VSSs, and in particular of the Coulomb friction model reported in Equation (2.3). The discussion of the consequent mathematical details is beyond the scope of the present Dissertation, and the reader is referred e.g. [207] for further details.

across the particular attracting manifold (in general, m sliding manifolds exist and the motion is established on their intersection, see e.g. [49]), thus constraining the trajectory on it.

The description of this behavior is mathematically challenging, and was formerly formalized by Filippov (see [72]). Successively, a simpler methodology called the method of *equivalent control* was proposed by Utkin (refer to [207]). This latter is simple but accurate, and thus it is usually employed in the SMC literature to study the behaviour of the controlled systems during sliding. It will be better described in the following, where it is used to study the equivalent dynamics of systems in sliding motion throughout the whole Dissertation.

Notice that once the sliding mode is attained (in a finite time, as will be made evident in the subsequent discussion) the order of the dynamics of the system is reduced due to the constraint that the trajectories must lie on the manifold. In particular, the so-called *reduced order dynamics* (also referred to as *equivalent dynamics*) is determined by the particular choice of the sliding manifold. Therefore, in general one starts in a situation in which the system states are in the region of attraction of a manifold, and so the system trajectory moves in such a way that eventually convergence to it is attained (during the so called *reaching phase*). After a finite time, convergence is attained and the system trajectory remains constrained indefinitely (*sliding phase*).

Since the values on the basis of which the dynamics switchings occur determine the resulting behaviour of the VSS, being able to arbitrarily design the sliding manifold makes it possible to impose arbitrary reduced-order dynamics, and thus offers a mean to control the system. This feature is achieved in SMC, which entails a two-step procedure for the design of the closed-loop strategy. At first, a *sliding variable* $\sigma(x,t) \in \mathbb{R}^m$ is designed, on the basis of the required behavior of the system once a sliding motion on the manifold

$$\sigma(x,t) = 0 \tag{2.4}$$

is attained and kept. Notice that in this phase the hypothesis that the system eventually reaches such condition in a finite time is made, but needs to be assured in the second stage. The equivalent control method can here be

used to study the reduced-order dynamics in a simple and reliable way. Such procedure consists in finding the equivalent control $u_{eq}(x,t)$ which solves the equation

$$\dot{\sigma}(x,t) = 0 \tag{2.5}$$

and then substituting such expression in the original dynamics. The obtained description is independent of $u(t)$, and composed of $n-m$ ordinary differential equations and m algebraic equations (given by (2.4)). Equation (2.5) makes evident that the reduced-order dynamics is dependent on the choice of $\sigma(x,t)$.

The second step consists in finding a suitable discontinuous control law able to enforce finite-time convergence to the selected manifold (2.4). Specifically, global finite-time stability is required to be enforced. Notice that although in general Multi-Input systems are considered in the SMC theory, from now on only the Single-Input case is considered (i.e. $m = 1$) for the sake of simplicity and because all the subsequent discussion does not require a so general introduction. For a more general discussion, the reader can refer to, e.g., [49, 189]. A commonly adopted input is the relay-like

$$u(t) = -Ksign(\sigma(x,t)) \tag{2.6}$$

where $K > 0$ is the control gain and must be properly chosen. To do so, Lyapunov theory can be exploited: let us select the energy function

$$V(x,t) = \frac{1}{2}\sigma^2(x,t) \tag{2.7}$$

Based on (2.7), it can be shown that ensuring the so-called *η-reachability condition*

$$\dot{V}(x,t) = \sigma(x,t)\dot{\sigma}(x,t) < -\eta|\sigma(x,t)| \tag{2.8}$$

for some $\eta > 0$ proves global finite-time convergence to the manifold (2.4) and the enforcement of a sliding motion on it. An upper bound for the *reaching time* t_R, in this case, is given by

$$t_R \leq \frac{|\sigma(x_0,t_0)|}{\eta} \tag{2.9}$$

from which one can see that higher η values ensure usually a faster convergence.

Condition (2.8) imposes a lower bound on the control gain K, which can be found under the hypothesis that the sliding variable and its first time derivative are bounded by a known constant. In the presence of uncertainty, this usually translates in the requirement of a known constant upper bound for the absolute value of the uncertain terms. Notice that the latter requirement is quite mild, and entails the fact that SMC is robust with respect to matched uncertainty[2]: intuitively, it is sufficient to exert a strong enough control action to contrast the uncertainty in the input channel, provided that such uncertainty does not exceed a known constant value.

In order to clarify the stated concepts, let us consider now a simple linear unstable system (with open-loop eigenvalues $1 \pm 6i$) controlled through the input $u(t)$:

$$\begin{bmatrix} \dot{x}_1 \\ \dot{x}_2 \end{bmatrix} = \begin{bmatrix} 0 & 1 \\ -10 & 2 \end{bmatrix} \begin{bmatrix} x_1 \\ x_2 \end{bmatrix} + \begin{bmatrix} 0 \\ 1 \end{bmatrix} u(t), \quad x(0) = \begin{bmatrix} 10 \\ 4 \end{bmatrix}. \tag{2.10}$$

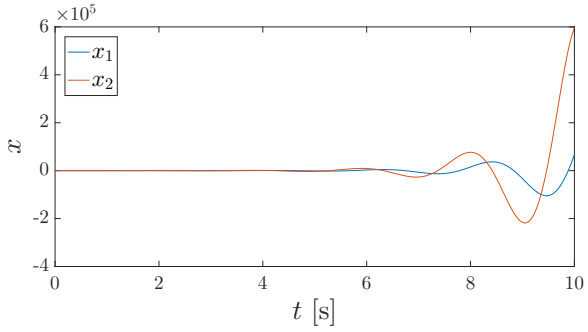

Figure 2.1: Uncontrolled system: evolution in time.

The uncontrolled system is unstable and exhibits a second-order (oscillating) behavior, captured in Figure 2.1. In particular, the origin is an unstable focus, as can be seen in Figure 2.2. One would like to stabilize the origin by means of the control variable $u(t)$ exploiting SMC. To do so, a

[2]The component of the uncertainty affecting a system referred to as "matched" can be informally defined as that which can be written as an additive term with respect to the input. In other words, it is the "projection" of the uncertainty on the input. For further reference and a formal description, please refer to e.g. [170].

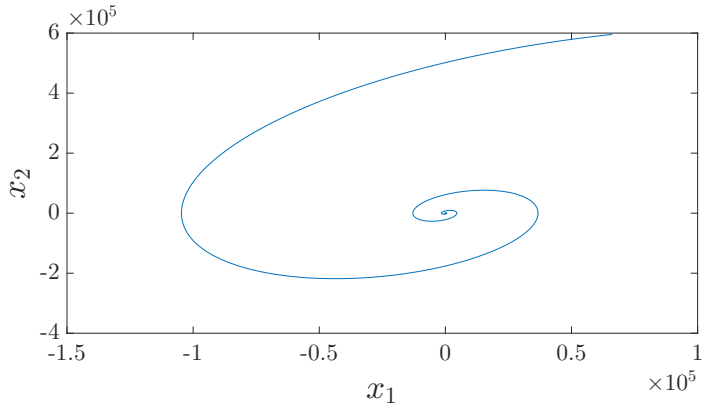

Figure 2.2: Uncontrolled system: phase plane trajectory.

sliding surface must be defined, such as for instance

$$\sigma(x,t) = cx_1 + x_2 = 0 \quad , \quad c > 0 \tag{2.11}$$

which describes a subspace of dimension 1 ($n - m = 2 - 1 = 1$). A standard relay law (2.6) is selected and a suitable gain K is chosen considering the condition (2.8). Specifically, the total time derivative of the Lyapunov function $V(x)$ is considered, i.e.

$$\begin{aligned}\dot{V}(x) &= \sigma(x,t)(c\dot{x}_1 + \dot{x}_2) = \sigma(x,t)[(c+2)x_2 - 10x_1 + u(t)] \\ &= \sigma(x,t)[(c+2)x_2 - 10x_1] - K|\sigma(x,t)| < L|\sigma(x,t)| - K|\sigma(x,t)|\end{aligned} \tag{2.12}$$

for a certain positive constant L such that

$$L > (c+2)x_2 - 10x_1 \tag{2.13}$$

which may be found introducing the assumption that the state vector values are bounded element-wise by known constants. Then, it follows that

$$\dot{V}(x) < -(K-L)|\sigma(x,t)| < -\eta|\sigma(x,t)| \tag{2.14}$$

and so, consequently,

$$K > \eta + L \tag{2.15}$$

In this case the reaching time can be bounded inserting η in Equation (2.9) as

$$t_R \leq \frac{|\sigma(x,t)|}{K-L} \tag{2.16}$$

which evidently depends on the initial value of $\sigma(x,t)$ as well as the bounds on the state vector elements and the chosen gain.

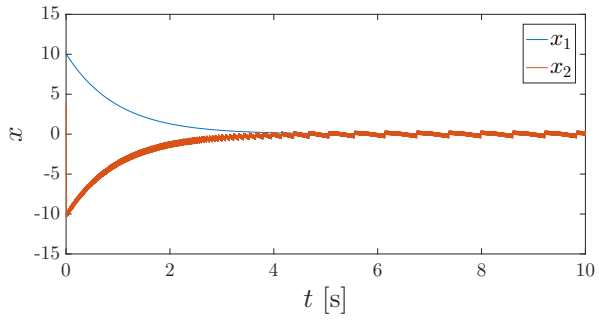

Figure 2.3: FOSM: Time evolution of the controlled system.

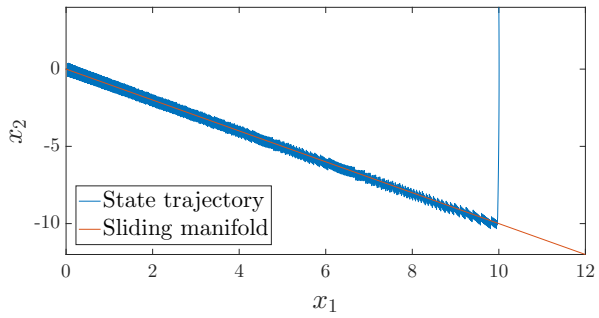

Figure 2.4: FOSM: Phase plane trajectory of the controlled system.

Let us select $c = 1$, so that the sliding surface is $x_2 = -x_1$. In Figure 2.4 the state trajectory is plotted: as it is clear, the selected manifold is reached in finite time (reaching phase) and then the system begins to slide on it (sliding phase). Once in sliding mode, the system behaves as a first-order system and it is asymptotically stable, as can be seen in Figure 2.3.

Suppose that, once on the sliding manifold, the state trajectory continues to lay on it. Then, in this situation both the sliding variable $\sigma(x,t)$ and its first derivative must be vanishing. This means that, referring to the example

under investigation,

$$\dot{\sigma}(x,t) = (c+2)x_2(t) - 10x_1(t) + u(t) = 0 \tag{2.17}$$

The control function that allows to maintain the condition expressed in Equation (2.17) (which means that the sliding manifold is not going to be left), is

$$u_{\text{eq}}(t) = 10x_1(t) - (c+2)x_2(t) \tag{2.18}$$

The equivalent control can be used to determine the dynamics of the controlled system once in sliding mode. In the aforementioned example, inserting Equation (2.18) into (2.10) and considering that on the sliding manifold $x_2(t) = -cx_1(t)$,

$$\begin{cases} \dot{x}_1(t) = x_2(t) = -cx_1(t) \\ \dot{x}_2(t) = -cx_2(t) \end{cases} \tag{2.19}$$

The two states evolve, independently, as first-order systems. In particular,

$$\begin{cases} x_1(t) = x_1(t_r)e^{-ct} \\ x_2(t) = x_2(t_r)e^{-ct} \end{cases} \tag{2.20}$$

for $t \geq t_R$ where $t_R < \infty$ is the time at which sliding manifold is reached. It is clear then how the choice of c (and, thus, of parametrization of the sliding variable) can affect the dynamics of the equivalent system.

In order to show clearly the insensitivity to bounded matched uncertainty, we can introduce now a generic exogenous matched disturbance $d(t)$. The system in Equation (2.10) becomes then

$$\begin{bmatrix} \dot{x}_1 \\ \dot{x}_2 \end{bmatrix} = \begin{bmatrix} 0 & 1 \\ -10 & 2 \end{bmatrix} \begin{bmatrix} x_1 \\ x_2 \end{bmatrix} + \begin{bmatrix} 0 \\ 1 \end{bmatrix} d(t) + \begin{bmatrix} 0 \\ 1 \end{bmatrix} u(t), \quad x(0) = \begin{bmatrix} 10 \\ 4 \end{bmatrix}. \tag{2.21}$$

The control law can be chosen, for instance, as in Equation (2.6), but this time introducing also a continuous term dependent on the (supposed known) states. This latter choice is not related to the enforcement of robustness, and is done here just to highlight the possibility of using SMC together with any other form of control strategy to effectively reject the uncertainty. The

resulting control law is, then,

$$u(t) = (c+2)x_2(t) - 10x_1(t) - Ksign(\sigma(x,t)) \tag{2.22}$$

To guarantee the finite-time convergence, therefore,

$$\begin{aligned}\dot{V}(x) &= \sigma(x,t)(c\dot{x}_1 + \dot{x}_2 + u(t)) = \sigma(x,t)[(c+2)x_2(t) - 10x_1(t) + d(t) + u(t)] = \\ &= \sigma(x,t)d(t) - K|\sigma(x,t)| \leq L|\sigma(x,t)| - K|\sigma(x,t)|\end{aligned} \tag{2.23}$$

where L is a positive constant such that $L > |d(t)|$. This requires obviously that $d(t)$ is bounded. In this case, for a proper choice of K, the controlled system behaves as expected.

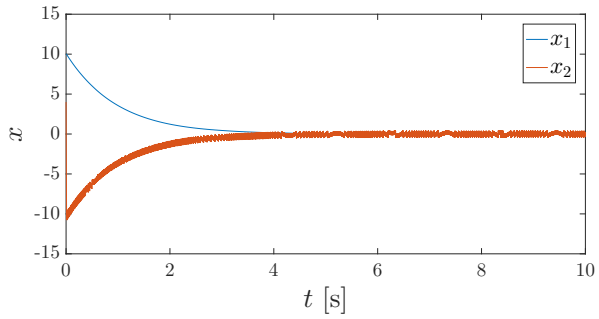

Figure 2.5: FOSM: Time evolution of the controlled (uncertain) system

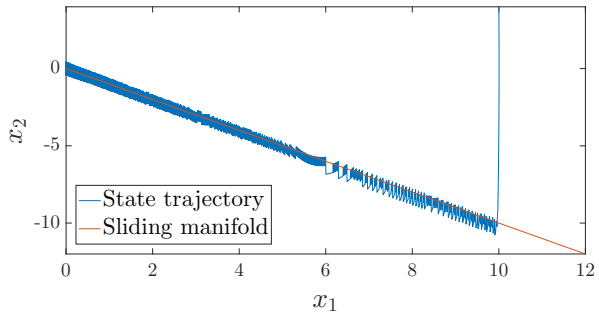

Figure 2.6: FOSM: Phase plane trajectory of the controlled (uncertain) system

For simulation purposes, let us assume that the unknown matched disturbance is $d(t) = 10sin(3t)$. It is not possible to appreciate differences in

the behavior of the uncontrolled system, which still has an unstable focus (as in Figure 2.2) and explodes as in Figure 2.1. In Figures 2.5 and 2.6 the evolution and the trajectory of the controlled system states are plotted. It is evident that the goal is reached despite the disturbance, thus highlighting the invariance property of SMC.

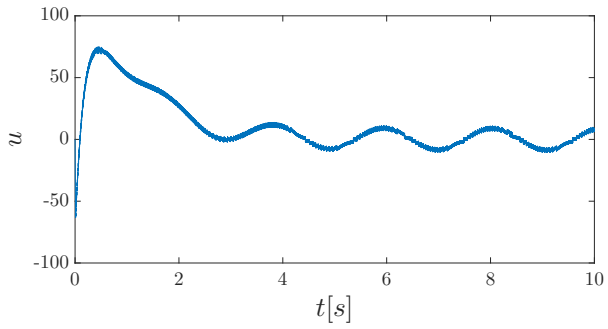

Figure 2.7: FOSM: Equivalent control, corresponding to the opposite of the injected disturbance.

The equivalent control in this case is $u_{eq}(t) = -d(t)$. This is evident from the plot of the (filtered) control law in Figure 2.7. Here a notable property of the Sliding Mode Control appears: the equivalent control can be used to estimate unknown terms that determine the system dynamics. The only assumption needed for this basic implementation is that they are bounded and matched[3].

Main issues of FOSM Control

In spite of the effectiveness of the FOSM strategies, two main problems can be identified, namely:

- Only situations in which the pair $\{\sigma(x,t), u(t)\}$ exhibits *relative degree*[4][99, 91] $r = 1$ can be considered. In other words, only choices of

[3]Such idea is at the basis of the observation system briefly introduced in Section 1.1.1.

[4]The relative degree of an output-input pair can be identified intuitively as the order of the first derivative of the output in which the input appears explicitly.

the sliding variable $\sigma(x,t)$ such that for a system as in Equation (2.1)

$$\begin{aligned}\dot{\sigma}(x,t) &= \frac{\partial\sigma(x,t)}{\partial x(t)}\dot{x}(t) + \frac{\partial\sigma(x,t)}{\partial t} \\ &= \frac{\partial\sigma(x,t)}{\partial x(t)}\left(f(x,t) + g(x,t)u(t)\right) + \frac{\partial\sigma(x,t)}{\partial t} \\ &= \underbrace{\frac{\partial\sigma(x,t)}{\partial x(t)}f(x,t) + \frac{\partial\sigma(x,t)}{\partial t}}_{h(x,t)} + \underbrace{\frac{\partial\sigma(x,t)}{\partial x(t)}g(x,t)}_{p(x,t)}\,u(t) \\ &= h(x,t) + p(x,t)u(t)\end{aligned} \tag{2.24}$$

holds with $p(x,t) \neq 0$ can be effectively considered to produce a sliding motion;

- The so-called *chattering effect* [105], as explained in the following, appears due to non-idealities in the switching and can potentially lead to disruptive effects.

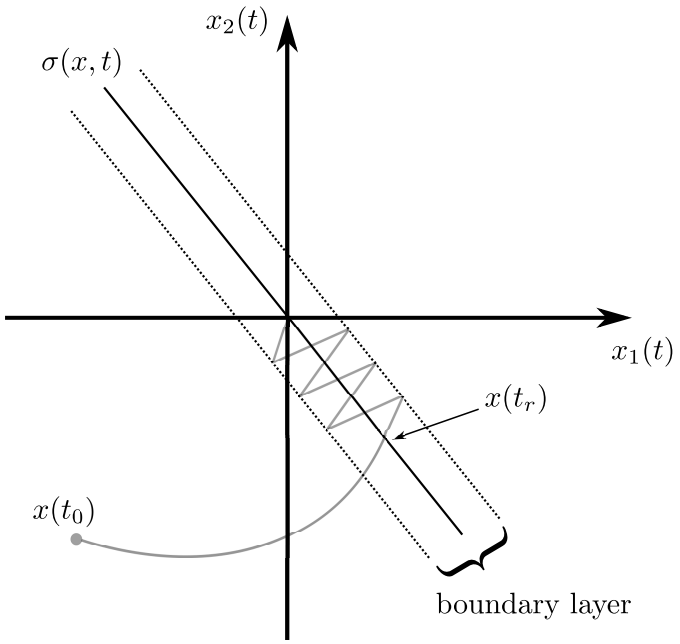

Figure 2.8: Schematic representation of the chattering phenomenon for a two-states system, considering a linear sliding variable of the type $\sigma(x,t) = cx_1(t) + x_2(t)$ for some $c < 0$.

As already described, when

$$\sigma(x,t) = 0 \quad \forall t \geq t_R \tag{2.25}$$

the so-called *ideal sliding mode* occurs, during which the control variable switches at infinite frequency. In practical situations, though, the commutations occur at high (but finite) frequency: a *practical sliding mode* (or *real sliding mode*) is always enforced [146]. It is characterized by the fact that the state trajectory is confined not exactly on the sliding manifold but in a vicinity of it (the so-called *boundary layer*), whose size is inversely proportional to the switching frequency. This is clearly visible in Figure 2.4 and 2.6, and schematically reported in Figure 2.8. In such situation, the control variable exhibits large high-frequency oscillations (*chattering*). Especially if mechanical actuators are employed, the high-frequency ripple appearing in the resulting control law can represent an issue. In fact, the actuators are stressed and can be seriously damaged if, for instance, resonating modes are excited. For this reason, some techniques have been developed in order to reduce such effect.

The most trivial one is the introduction of a low-pass filter for the control signal: the fast dynamics, attributable to the chattering effects, are filtered out according to the time constant of the filter. This approach can be effective in practice, but exhibits a number of issues. First of all, the filter must be slow enough to eliminate chattering but also sufficiently fast to preserve the control action, since strong filtering can lead to delays and degradations of the performance. The choice of fixed time constants can be tricky since, at least in presence of disturbances, the resulting control law is unpredictable. Issues like this have led to the development of more advanced techniques.

For instance, an effective approach can be the induction of a *quasi-sliding mode*: the main idea is to enforce a smoother behavior of the control variable, approximating the *sign* function with a similar but continuous shape. The *sigmoid* function can be used for instance, i.e.

$$sign(\sigma(x,t)) \approx \frac{\sigma(x,t)}{|\sigma(x,t)| + \epsilon}, \quad \epsilon > 0. \tag{2.26}$$

Point-wise, if ϵ is small enough, the sigmoid tends indeed to the *sign* func-

tion while retaining smoothness properties. In practice, a tradeoff choice must be performed for the value of ϵ: the bigger it is, the smoother is the resulting function (less chattering) at the cost of more non-ideal performances. Although usually the resulting behavior resembles the ideal one in an acceptable way, the major drawback is the loss of accuracy and robustness. Additionally, the control law cannot provide exact finite-time convergence since the sliding variable does not approach the origin, but rather a vicinity of it.

Another possible solution relies on the idea that, if the discontinuity is moved to the first derivative of the control variable by means of the adoption of an auxiliary sliding manifold

$$\Sigma(x,t) = \sigma(x,t) + c\dot{\sigma}(x,t) \tag{2.27}$$

for some $c > 0$, the resulting control law is a smooth continuous function. This idea leads to induce an *asymptotic sliding mode*, since the sliding variable $\sigma(x,t)$ vanishes only asymptotically (exponentially, and not in finite time). Notice in fact that when

$$\Sigma(x,t) = 0 \tag{2.28}$$

is attained in a finite time, a subsequent motion of the original sliding variable to zero starts. In fact,

$$\dot{\sigma}(x,t) = -\frac{1}{c}\sigma(x,t) \tag{2.29}$$

holds. In view of the choice reported in Equation (2.28), the control input appears already in the expression of $\Sigma(x,t)$. Thus, the pair $\{\Sigma(x,t), \dot{u}(t)\}$ exhibits relative degree $r = 1$, and one can adopt $v(t) = \dot{u}(t)$ as a dummy discontinuous input. Notice that this technique, besides the asymptotic convergence which does not guarantee the theoretical properties established by the classical choices of the sliding variable, the need to know the time derivative $\dot{\sigma}(x,t)$ of the sliding variable arises. In practical situations this can be an issue, and the introduction of additional observers to estimate it may become mandatory.

2.1.2 Higher-Order Sliding Mode (HOSM) Control

Both the problems introduced in 2.1.1 can be effectively solved via the adoption of Higher Order Sliding Mode (HOSM) Control [101, 189]. In fact, a k-th order sliding motion[5] [99] is attained when the *sliding set* attains in a finite time the origin, i.e.

$$\sigma(x,t) = \dot{\sigma}(x,t) = \cdots = \sigma^{(k-1)}(x,t) = 0 \tag{2.30}$$

and thus systems with relative degree $r = k$ can be effectively considered[6].

Additionally, the generation of HOSM is one of the most effective techniques for chattering alleviation. In fact, it allows to reduce the chattering without losing all the properties of sliding mode, like finite time convergence and disturbance rejection[7]. Supposing the relative degree of the $\{\sigma(x,t), u(t)\}$ pair is $r > k$, it is possible to integrate the control input $u(t)$ generated by a k-th order HOSM algorithm $l = r - k$ times to produce an input suitable for the original system (see the discussion in Section 2.1.2 and the proposal described in Section 3.3 for further clarification).

Different HOSM algorithms are available in literature, as for instance the ones in [101, 102, 103, 54]. Among them, those belonging to the Second Order Sliding Mode (SOSM) Control class ($k = 2$) are widely used.

Second-Order Sliding Mode Control

SOSM Control [18, 21] entails generating a sliding mode of order $k = 2$, thus producing a reduced-order dynamics constrained to the subspace

$$\sigma(x,t) = \dot{\sigma}(x,t) = 0 \tag{2.31}$$

If, for the considered system as in (2.1), the relative degree of the $\{\sigma(x,t), u(t)\}$ pair is $r = 2$, it is straightforward to derive that the input $u(t)$ appears for the first time in $\dot{\sigma}(x,t)$ thus requiring (at least) a SOSM to reach a sliding

[5] The order of a sliding mode (*sliding order*) is defined as the number of continuous total derivatives minus one (including the 0-th, in case of FOSM) of the sliding variable $\sigma(x,t)$ which define the sliding motion when attain and keep a null value. It represents, in some sense, the degree of smoothness of the motion constrained to the manifold [99].

[6] Clearly, FOSM corresponds to $k = 1$ and therefore in Equation (2.30) no derivatives are included.

[7] In fact, it can be proved that the size of the boundary layer is inversely proportional to the k-th power of the sampling frequency (being k the order of the sliding motion) [99].

motion. Considered in fact Equation (2.24), one has that if $p(x,t) = 0$[8],

$$\begin{aligned}\ddot{\sigma}(x,t) &= \frac{\partial h(x,t)}{\partial x(t)}\dot{x}(t) + \frac{\partial h(x,t)}{\partial t} \\ &= \frac{\partial h(x,t)}{\partial x(t)}\left(f(x,t) + g(x,t)u(t)\right) + \frac{\partial h(x,t)}{\partial t} \\ &= \frac{\partial h(x,t)}{\partial x(t)}f(x,t) + \frac{\partial h(x,t)}{\partial t} + \frac{\partial h(x,t)}{\partial x(t)}g(x,t)u(t)\end{aligned} \tag{2.32}$$

holds. The discussion becomes then trivial and overlaps that already made for the FOSM case except that the original dynamics is reduced of two orders instead of one.

If, instead, $r = 1$ for the system under consideration, chattering alleviation can be enforced by means of any SOSM algorithm. In fact, considered again Equation (2.24), it can be derived that

$$\begin{aligned}\ddot{\sigma}(x,t) &= \underbrace{\frac{\partial h(x,t)}{\partial x(t)}\dot{x}(t) + \frac{\partial h(x,t)}{\partial t} + \left(\frac{\partial p(x,t)}{\partial x(t)}\dot{x}(t) + \frac{\partial p(x,t)}{\partial t}\right)u(t)}_{\phi(x,t)} \\ &\quad + p(x,t)w(t) \\ &= \phi(x,t) + p(x,t)w(t)\end{aligned} \tag{2.33}$$

where $w(t) = \dot{u}(t)$ is the considered (virtual) input such that the pair $\{\sigma(x,t), w(t)\}$ has relative degree 2. It follows, then, that taking the integral of $w(t)$ produces a suitable input for the considered (original) system, which is continuous thus producing a smooth input. In addition, the chattering is reduced due to the fact that, as already highlighted, the "width" of the boundary layer is greatly reduced during a real sliding motion.

Among the most popular algorithms effectively solving this problem, the Sub-Optimal [19, 20] (S-SOSM) algorithm is presented below, since it is the strategy adopted in the following of the discussion.

Sub-Optimal Sliding Mode Control

The S-SOSM algorithm relies on the adoption of a control law derived from the idea of a bang-bang algorithm for two-states systems. To formally state the control problem, making use of the results derived in the previous dis-

[8] This is required, since otherwise the relative degree would be $k = 1$.

cussion (Equations (2.24) and (2.33) or (2.32)), an auxiliary dynamics can be introduced posing $\zeta_1(t) = \sigma(t)$ for any system with $r = 2$[9]. By means of the respective diffeomorphism[10], one obtains

$$\begin{cases} \dot{\zeta}_1(t) = \zeta_2(t) \\ \dot{\zeta}_2(t) = \phi(\zeta_1(t), \zeta_2(t), t) + p(\zeta_1(t), \zeta_2(t), t)v(t) \end{cases} \tag{2.34}$$

where, $v(t) = w(t)$ in case of chattering alleviation ($k = 1$) or $v(t) = u(t)$ if for the original system $r = 2$ holds. The Sub-Optimal strategy, then, aims at enforcing in a finite time a sliding motion on the subset $\zeta_1(t) = \zeta_2(t) = 0$ under the following assumption.

Assumption 1. *There exist known positive constants Φ, P_1 and P_2 such that*

$$|\phi(\cdot)| \leq \Phi, \quad P_1 \leq p(\cdot) \leq P_2 \tag{2.35}$$

holds.[11]

By means of the following control input

$$v(t) = -\alpha(t) K sign\left(\zeta_1(t) - \frac{\zeta_1^*}{2}\right), \tag{2.36}$$

where α is a modulation parameter, K is the gain and $\zeta_1^* = \zeta_1(t^*)$ with t^* the last time instant at which $\zeta_2(t) = 0$, a SOSM is enforced. In particular, the selection of K and α must fulfil the following conditions

$$\alpha = \begin{cases} \alpha^* & \text{if } \left(\zeta_1(t) - \frac{1}{2}\zeta^*\right)(\zeta^* - \zeta_1(t)) > 0 \\ 1 & \text{otherwise} \end{cases} \tag{2.37}$$

$$K > \max\left(\frac{\Phi}{\alpha^* P_1}; \frac{4\Phi}{3P_1 - \alpha^* P_2}\right) \tag{2.38}$$

[9] As already described, this can be the actual relative degree of the $\{\sigma(x,t), u(t)\}$ pair, or that obtained introducing a virtual input $w(t)$ to the end of achieving chattering alleviation. Equation (2.34) reports the case described in Equation (2.33) (chettering alleviation) to maintain coherence with respect to the paper [20]. Anyway, in the other case very similar considerations can be made employing the same notation to describe the quantities in Equation (2.32).

[10] This diffeomorphism always exists, see for instance [91, Chapter 13].

[11] If $p(\cdot) < 0$, similar bounds hold considering $-v(t)$ as the input.

with

$$\alpha^* \in (0,1] \cap \left(0, \frac{3P_1}{P_2}\right) \tag{2.39}$$

a parameter to be arbitrarily chosen. The reader can refer to [20] for the complete proof of convergence.

Notice that, to implement an n-th order sliding mode control law, the knowledge of the first $n-1$ time derivatives of the sliding variable is usually mandatory. This increases the complexity of the resulting schemes, in which additional sensors or differentiators must be introduced (see, e.g. [100, 104, 43]). On the contrary, one of the peculiarities of S-SOSM is that no derivatives of $\sigma(t)$ are needed (in particular, the value of $\zeta_2(t)$ is not required), as can be seen in (2.36). In fact, in real implementations, ζ_1^* can be determined using commercial peak detectors or looking at successive measurements of $\zeta_1(t) = \sigma(x,t)$. If the difference $\Delta\zeta_i = \zeta_1(t_i) - \zeta_1(t_{i-1})$ between the last two acquired values has opposite sign with respect to $\Delta\zeta_{i-1}$, it means that $\zeta_2(t_i) = 0$ happened. This is an approximation, which implies that some non-idealities are introduced in practice with respect to a perfect knowledge of $\dot{\sigma}(x,t) = \zeta_2(t)$, but they are typically negligible for sufficiently high sampling frequencies.

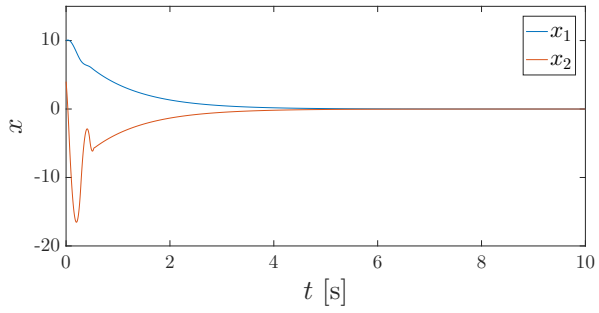

Figure 2.9: S-SOSM: Time evolution of the controlled (uncertain) system.

An example is obtained applying the S-SOSM to system (2.21) in chattering alleviation form. The results are reported in Figures 2.9 and 2.10, where the time evolution and the phase plane of the controlled system are plotted, respectively. With respect to the choice $\sigma(t) = x_1(t) + x_2(t)$, made also in the example of Section (2.1.1) where the $c = 1$ was considered, the plot of the phase plane for the pair $(\sigma(t), \dot{\sigma}(t))$ is reported in Figure 2.11.

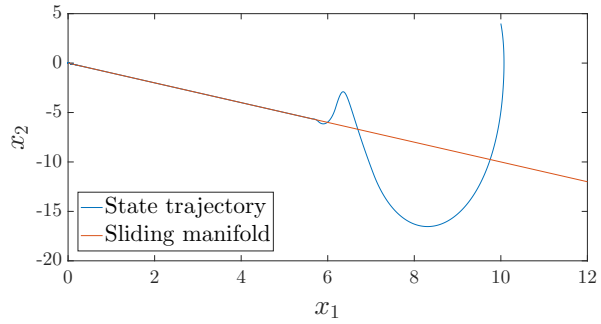

Figure 2.10: S-SOSM: Phase plane trajectory of the controlled (uncertain) system

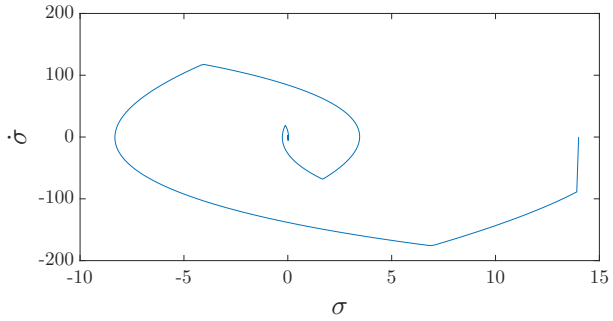

Figure 2.11: S-SOSM: Phase plane trajectory of the sliding variable and its first time derivative.

Notice the shape of the resulting trajectory, which is composed of parabolic branches: this is one of the two typical behaviors enforced by the S-SOSM algorithm, and highlights the affinity of it with the bang-bang control approach in second-order systems.

Additionally, comparing Figures 2.6 and 2.10, it is possible to clearly appreciate the chattering alleviation feature of the adopted strategy. In fact, the two simulations are carried out with the same sampling time, but the boundary layer obtained from the application of the S-SOSM is visibly tighter.

Constrained SMC

When dealing with HOSM, an important aspect concerns actuators and states saturations. Although constraints on the system state vector or the input are not explicitly accounted for in standard HOSM control algorithms,

advanced solutions exist to take into account physical or safety limitations in real systems. A broad overview of the available techniques is provided in [225], which constitutes a side result of the work on which this Dissertation is based[12]. Specifically, as an example one can consider actuators saturations which may arise when chattering alleviation is performed. In fact, in case a discontinuous control action is exerted (thus, based on Equation (2.32)), the input signal $u(t)$ is bounded in absolute value by the selected gain. On the contrary, the chattering alleviation form entails the exertion of a control signal which corresponds to the integral of the discontinuous input. Thus, $u(t)$ could in principle grow unbounded: as can be seen in Equation (2.33), this could lead to unbounded $\phi(x,t)$ terms which may prevent the respect of Assumption 1. Particular selections of the control law can prevent this, leading to a more robust and safe implementation which is guaranteed to converge.

Many additional types of constraints, for techniques enforcing different sliding mode orders, are available in the literature but are out of the scope of the present Thesis. Nevertheless, it can be envisaged that introducing constrained sliding mode techniques in the solutions proposed in the following could lead to improved strategies in most circumstances.

2.1.3 Integral Sliding Mode (ISM) Control

ISM control was formerly introduced in [206] in the context of FOSM with the aim of enforcing robustness (and, in general, the features offered by SMC) from the first time instant, avoiding the reaching phase typical of classic SMC algorithms. Such condition is achieved introducing an auxiliary sliding manifold $\Sigma(x,t)$ obtained in general combining the "original" sliding manifold $\sigma(x,t)$ with an integral term $z(x,t)$, such that

$$\Sigma(x,t) = \sigma(x,t) + z(x,t) \tag{2.40}$$

is defined. As will be more clear in the following, the term *integral sliding mode* refers to the fact that no order reduction is achieved during such motion (i.e., the equivalent dynamics is of the same order as the original system). Obviously, in the controller design Equation (2.40) is to be considered,

[12] Additionally, a novel constrained sliding mode control algorithm is proposed by the author in [222], exploiting a linearization-based approach to constrain the trajectories of the controlled systems.

which may change the bounds to consider (see Assumption 1).

The choice of $z(x,t)$ must be made such that

$$\Sigma(x,t_0) = 0 \tag{2.41}$$

and thus a sliding motion on it is kept from the initial time instant. In particular, the function $z(x,t)$ can be chosen based on two different main aims:

- To prescribe the transient dynamics, in case $z(x,t)$ is made to vanish eventually so that a sliding motion is established (asymptotically or in a finite-time) on the originally designed manifold $\sigma(x,t)$;
- To introduce robustness, using the ISM to compensate for matched uncertain dynamics.

Both the cases will be discussed in the following, considering for generality the HOSM case (the FOSM case is naturally included).

ISM for Prescribing the Transient Dynamics

A general, well presented overview on the subject is given in [106], which provides both the motivations and the theoretical basis on which Higher-Order Integral Sliding Modes (HOISM) generation relies[13]. In general, when designing $z(x,t)$ to prescribe the transient phase for HOSM different requirements can be addressed through the degrees of freedom offered by the selection of such function[14]. For instance, one could considered smoothness requirements for the entrance on the motion on $\sigma(x,t)$, or the possibility of enforcing a prescribed-time convergence. In any case, the following condition has to be ideally attained to effectively pursue this aim

$$\begin{cases} z(x(t_0),t_0) & = -\sigma(x(t_0),t_0) \\ \dot{z}(x(t_0),t_0) & = -\dot{\sigma}(x(t_0),t_0) \\ & \dots \\ z^{(k-1)}(x(t_0),t_0) & = -\sigma^{(k-1)}(x(t_0),t_0) \end{cases} \tag{2.42}$$

[13]The reader is referred to the mentioned reference for further details, which rely on a deeper analysis of HOSMs not provided in this Dissertation.

[14]Notice that the $z(x,t)$ function must anyway be taken $(k-1)$-smooth, where k is the order of the enforced sliding motion.

and

$$z(x,t) = 0, \quad t \geq t_f \tag{2.43}$$

with t_f a finite time instant (called the entrance moment). The authors in [106] propose a $(k-1)$-regular polynomial shape for $z(x,t)$, i.e.

$$z(x,t) = (t - t_f)^k \rho(t) \tag{2.44}$$

with

$$\rho(t) = c_0 + c_1(t - t_0) + \cdots + c_{k-1}(t - t_0)^{k-1} \tag{2.45}$$

where t_f is to be designed[15]. The coefficients $c_0, \cdots, c_{k-1}$ are to be chosen at the beginning of the control so as to respect the conditions in (2.42) and (2.43). An example of algorithm exploiting HOISM for transient prescription is provided in Section 2.1.4[16].

ISM for Matched Uncertainty Rejection

Considering a system with dynamics as in Equation (2.1), the uncertainty affecting the dynamics can be modelled generically with a $d(t)$ term. Therefore, the dynamics of the system can be equivalently described as

$$\dot{x}(t) = \bar{f}(x,t) + \bar{g}(x,t)u(t) + d(t) \tag{2.46}$$

where $\bar{f}(\cdot)$ and $\bar{g}(\cdot)$ are vector functions representing the *nominal* description of the system (i.e. without uncertainty). In this context, one may consider an input signal $u(t)$ as

$$u(t) = \bar{u}(t) + u_{ism}(t) \tag{2.47}$$

where $\bar{u}(t)$ is a nominal control input and $u_{ism}(t)$ is an ISM discontinuous control signal [206] of any type.

As described for instance in [170], the $d(t)$ term in (2.46) can always be

[15] Constant values for $t_f - t_0$ lead to unbounded required control gains, since this latter depends on the initial values of $\sigma(x,t)$. Therefore, an homogeneous law is proposed in [106] to make t_f dependent on the initial conditions thus enabling (at least formally) a guaranteed convergence.

[16] Another case is [67], while an adaptive HOISM strategy is proposed in [86].

decomposed in two parts, i.e. a matched and an unmatched component. Considering, for simplicity, a system comprising only the matched component[17] $d_m(x,t)$, one has that the dynamics correspond to

$$\dot{x}(t) = \bar{f}(x,t) + \bar{g}(x,t)u(t) + d_m(t) \tag{2.48}$$

with a slight abuse of notation (in the general case, Equation (2.48) should only refer to the part of the dynamics which is affected by the matched component of $d(t)$).

Considered the nominal dynamics in Equation (2.48), the selection of the integral function $z(x,t)$ can be made as[18]

$$\dot{z}(x,t) = -\frac{\partial \sigma(x,t)}{\partial x}\left(\bar{f}(x,t) + \bar{g}(x,t)\bar{u}(t)\right), \quad z(x(t_0),t_0) = -\sigma(x(t_0),t_0) \tag{2.49}$$

Analysing the equivalent dynamics of (2.48), one must consider the usual equation $\dot{\Sigma}(x,t) = 0$. Considered that

$$\dot{\Sigma}(x,t) = \dot{\sigma}(x,t) + \dot{z}(x,t) = \frac{\partial \sigma(x,t)}{\partial x}\left(\bar{g}(x,t)u_{ism}(t) + d_m(t)\right) \tag{2.50}$$

one has, thus, that

$$\bar{g}(x,t)u_{ism}(t) = -d_m(t) \tag{2.51}$$

Therefore, the dynamics followed by the controlled system corresponds to

$$\begin{aligned} \dot{x}(t) &= \bar{f}(x,t) + \bar{g}(x,t)\bar{u}(t) + \bar{g}(x,t)u_{ism}(t) + d_m(t) \\ &= \bar{f}(x,t) + \bar{g}(x,t)\bar{u}(t) - d_m(t) + d_m(t) \\ &= \bar{f}(x,t) + \bar{g}(x,t)\bar{u}(t) \end{aligned} \tag{2.52}$$

which is the nominal dynamics driven by the nominal input $\bar{u}(t)$. This latter can therefore be designed basing only on the nominal (completely

[17] For additional considerations, the reader can refer to the discussion in [170]. In particular, the of the mentioned work propose a strategy to design the ISM controller in such a way that the unmatched component of the uncertainty does not amplify (which may generally happen in case the selection of the integral function is not cleverly made).

[18] Notice that in the specific considered case, where the uncertainty is completely matched, no considerations regarding the amplification of the unmatched component need to be made. In general, though, an additional term should be included according to [170].

known) description of the system, thus pursuing additional control objectives robustly with respect to the bounded (see, again, Assumption (1)) matched disturbances. As a special case, the adoption of MPC algorithms for the nominal control law $\bar{u}(t)$ has been vastly investigated in the literature (see, e.g., [84, 85]).

Notice that an extension to HOSM control is possible, although the property of robustness from the initial time instant is in general lost. In particular, using (2.40) as the sliding variable, one has that during the HOSM $\Sigma(x,t) = 0$, thus providing for all the discussion developed above. Anyway, although condition (2.41) can easily be respected, the same does not hold in general for the time derivatives of $\Sigma(x,t)$, which cannot be imposed as null. Thus, the sliding set

$$\Sigma(x,t) = \dot{\Sigma}(x,t) = \cdots = \Sigma^{(k-1)} = 0 \tag{2.53}$$

is attained in a finite time $t_r > 0$. This fact in practice should not constitute a major problem, but nevertheless at least it must be considered at least theoretically that a reaching phase (of unpredictable duration) still exists. An example of adoption of such strategy is provided by the proposal presented in Section 3.3, where a Second-Order ISM is induced to robustify an MPC nominal control scheme via a multi-rate approach.

2.1.4 SMC in Leader-Follower Consensus Control

In the following discussion an application of SOSM is proposed, both for its relevance in the context of multi-agent systems and to provide a practical example of the features offered by sliding mode control based solutions. In particular, the adoption of an Integral SOSM control strategy is presented to achieve robust prescribed-time leader-follower consensus as one of the results of the research work related to this Thesis (published originally in [71]).

Consensus control in multi-agent systems (MAS) has become a relevant topic in control systems research (see [226], whch constitutes one of the side contributions of the research work reported in this Dissertation), due to the increase of engineering applications relying, by nature or by design, on such concept [134, 168]. It entails, in particular, the attainment (consensus reaching) of a common value for a function of the state vector of the agents

involved in the MAS, which can be described by means of a graph[19]. Such function can be chosen differently dependent on the particular considered task, giving rise to different forms of consensus control.

Specifically, leader-follower consensus [82, 141, 130] holds a primary role, since it is the reference structure for a large variety of practical problems including formation control [159] and platooning [181], which are the main subjects of the present Dissertation. Due to the relevance of the topic, great effort is being made in solving consensus problems under different conditions: for instance, directed and/or dynamically changing topologies, presence of delays and faults, and finite-time convergence (see, e.g., [135, 213, 111, 154]).

The introduction of SMC-based techniques has gained significant attention in the last few years, since it provides complete robustness against bounded matched uncertainty and the ability to enforce finite-time convergence [226]. Among many possible examples, FOSM control strategies are succesfully employed in works as [93, 51, 155][20]. Discontinuous control laws, however, might induce the so-called chattering effect, already discussed in Section 2.1.2. This issue has been considered in consensus problems only in few works (see, for instance, [145, 127]).

As pointed out in Section 2.1.3 the robustness of SMC in sliding mode is not exhibited during the so-called reaching phase (i.e. when the sliding motion is not yet established): the invariance principle does not apply, and thus robustness cannot be guaranteed. This implies that the controlled system dynamics is completely dependent on uncertainty, which can disrupt performance and lead to disastrous consequences. In order to overcome these limitations, the adoption of integral sliding manifolds is proposed in works as [145, 92], where it is employed in the classical FOSM formulation to add robustness to nominal consensus controllers through the rejection of matched disturbances.

In the following of the discussion, a second-order sliding mode (SOSM) control strategy, inspired to the so-called Sub-Optimal algorithm (see Section 2.1.2), is proposed for robust finite-time leader-follower consensus con-

[19]To formally study consensus control algorithms, reference is commonly made to the graph algebraic theory, which allows to model the agents as nodes. A brief introduction is provided in the following of the Section, while the interested reader may refer to [124] for a detailed discussion.

[20]It is worth noticing that a consistent portion of the results rely on Terminal Sliding Modes (TSM) generation, able to enforce finite-time convergence once the designed sliding manifold is attained.

trol in MASs with directed topologies (thus, in a general case). The considered agents can exhibit first or second-order (perturbed) chain of integrators dynamics, and the network graph is only assumed to contain a directed spanning tree [168] with the leader as the root. With respect to the majority of the works about consensus already present in the literature, a first contribution is that only partial information is required, namely the relative distance between the first state of each agent and those of its neighbours. This constitutes a valuable feature for instance in the case of vehicular or mobile robot agents, since it implies that information exchange (with all the subsequent network-related issues) can be avoided if simple range sensors are present on board. Additionally, it is sufficient that the control signal driving the leader is bounded for the second-order agents case or with bounded first derivative in the first-order case, with no specific assumptions about the particular shape, enabling for a wider range of applications.

A further contribution lies in the introduction of second-order integral sliding manifolds (see [106] and Section 2.1.3), never used previously in MAS consensus problems, as an effective design element able to eliminate the reaching phase (thus guaranteeing robustness from the beginning of the control process) and enforcing prescribed-time consensus attainment. Thus guarantees the respect of possible time constraints dictated by the particular application[21].

Due to the establishment of a SOSM, chattering alleviation arises naturally in the proposed approach for first-order agents, while for second-order agents specific chattering alleviation strategies can be adopted together with our approach, as will be pointed out in the following.

Graph Theory in MAS Control

Before diving into the details of the proposed strategy, a brief introduction about graph theory in the context of leader-follower MAS control is provided. In fact, the most commonly adopted description for the agents in a MAS and their connections (in terms of "information availability", it being through sensors or direct/indirect communication) makes use of graph

[21] This feature is also of particular importance since, in asymptotic consensus-seeking protocols, the speed of convergence is tightly related to the graph algebraic connectivity [134]. However, higher connectivity, which usually implies faster convergence, can also decrease the tolerance to disturbances and faults, so that a trade-off is required. This drawback is avoided if the proposed approach is adopted.

algebraic methods (see [124]).

Consider a generic networked MAS of $N+1$ agents (an uncontrolled leader and N followers), indexed by the subscript $i = 0, \cdots, N$, with the leader corresponding to $i = 0$ without loss of generality. One can then describe the network topology by means of a non-empty directed graph $G = (V, E)$, with $V = 0, \cdots, N$ the set of nodes modelling the agents and $E \subset V \times V$ the edges describing the information exchange. In particular $(i, j) \in E$ if and only if $j \in N_i$, with $N_i = \{j \in V : (i, j) \in E\}$ the set of *neighbours* of agent i, i.e. the agents from which agent i can gather information about the states. This, in general, can happen through a communication channel or by any other mean (e.g. sensors, or virtual links).

Definition 1. *A directed tree is a directed graph where every node, apart from the root, has one and only one parent. The root has a directed path to every node. A directed spanning tree of G is a directed tree that contains all the nodes of G.*

From the literature, it is known that a directed graph G has a (directed) *spanning tree* if and only if it has at least one node (in this case, the leader) with a directed path to all other nodes [168]. The leader-follower network topology can be described also by means of an adjacency matrix

$$A = \begin{bmatrix} 0 & 0 & \cdots & 0 \\ a_{10} & & & \\ \vdots & & \bar{A} & \\ a_{N0} & & & \end{bmatrix}, \; \bar{A} = \begin{bmatrix} a_{11} & \cdots & a_{1N} \\ \vdots & \ddots & \vdots \\ a_{N1} & \cdots & a_{NN} \end{bmatrix} \tag{2.54}$$

$$a_{jj} = 0, \; a_{ij} = 1 \iff j \in N_i, \; 1 \leq i \leq N, \; 0 \leq j \leq N$$

Defining the followers graph degree matrix $\bar{D} = diag\{d_1, \cdots, d_N\}$ with $d_i = \sum_j a_{ij}$, one can finally write the Laplacian of a digraph $\bar{G}$ comprising only the N followers as

$$\bar{L} = \bar{D} - \bar{A} \; \in \mathbb{R}^N \tag{2.55}$$

The Laplacian of the entire graph G, which is not explicitly reported here since it will not be useful in the following discussion, can be obtained similarly to (2.55) considering $d_0 = 0$ and the complete adjacency matrix A.

Defining $b_i = a_{i0}$ for convenience, the pinning matrix

$$\bar{B} = diag([b_1, \cdots, b_N]) \tag{2.56}$$

can now be introduced.

The following result, fundamental for the remaining of the discussion, holds:

Theorem 1 ([93])**.** *If the digraph G has a directed spanning tree, then $\bar{L}+\bar{B}$ is invertible.*

With the adopted convention and terminology, the problem of enforcing a leader-follower consensus can be stated as follows.

Problem 1. *[Leader-Follower Consensus] Enforce and keep the following relationship for every agent $i = 1, \cdots, N$ in the MAS*

$$\begin{cases} x_{1_i}(t) & = x_{1_0}(t) - \Delta_i \\ x_{h_i}(t) & = x_{h_0}(t), \quad \forall h = 2, \cdots, n \end{cases} \tag{2.57}$$

with n the order of the considered agents and $\Delta_i > 0$ the desired distance between the first state of the i-th agent and that of the leader.

The Proposed Strategy

In this section, the Integral Sub-Optimal SOSM (IS-SOSM) strategy is presented to robustly solve Problem 1 in a prescribed (arbitrary) time. Firstly, second-order agents dynamics (thus, with $r = 2$[22]) are considered, where a bounded discontinuous control signal is produced. In this case, particular techniques can be adopted to reduce the chattering effect. Then, the strategy is adapted for chattering alleviation producing a continuous control signal in case of first-order agents (for which, thus, $r = 1$ holds).

[22]This follows straightforwardly from the fact that the considered dynamics are in form of (perturbed) chains of integrators, see Equation (2.58), and the choice of the sliding variable as in Equation (2.59).

Second-Order Agents The dynamics of the i-th agent can be modelled as

$$\begin{cases} \dot{x}_{1_i}(t) &= x_{2_i}(t) \\ \dot{x}_{2_i}(t) &= \gamma_i(t) + u_i(t) \end{cases} \tag{2.58}$$

with $\gamma_i(t)$ being an unknown sufficiently smooth function, respecting the following assumption.

Assumption 2. *$|\gamma_i(t)| \leq \Gamma_i$ with Γ_i known constants possibly different for the different agents i*[23]*.*

The following further hypothesis are also introduced:

Assumption 3. *G contains a spanning tree, as per Definition 1.*

Assumption 4. *Every follower i, $i = 1, \cdots, N$ can get in real time the first state relative information $(x_{1_i}(t) - x_{1_j}(t))$ with respect to all neighbouring agents $j \in N_i$.*

Assumption 5. *The input of the leader is bounded and with bounded first time derivative. This is to say, $|(u_0(t) + \gamma_0(t))| \leq U_0$ and $|(\dot{u}_0(t) + \dot{\gamma}_0(t))| \leq \bar{U}_0$, with U_0 and $\bar{U}_0$ known positive constants.*

The task is to design a distributed control strategy solving the leader-follower consensus problem (Problem 1) in a prescribed finite time $T > 0$ in spite of any possible realizations of $\gamma_i(t)$, thus providing robustness with respect to matched uncertainty. To do so, the following local sliding variable is selected for agent i.

$$\sigma_i(t) = \sum_{j \in N_i} (x_{1_i} - x_{1_j} + \Delta_i - \Delta_j) + b_i(x_{1_i} - x_{1_0} + \Delta_i) \tag{2.59}$$

As already anticipated, it is evident that the pair $\{\sigma_i(t), u_i(t)\}$ exhibits relative degree $r = 2$. Additionally, it is worth noticing that only the relative measurements $(x_{1_i}(t) - x_{1_j}(t))$ and possibly $(x_{1_i}(t) - x_{1_0}(t))$ (if the agent has the leader as neighbour), available in view of Assumption 4, are required in (2.59).

[23] See Assumption 1.

Then, basing on the discussion provided in Section 2.1.3, the following choice for the auxiliary sliding variable (2.40) is made

$$\Sigma_i(t) = \begin{cases} \sigma_i(t) - (t - t_{f_i})^2(c_0 + c_1(t - t_{0_i})), & t \leq t_{f_i} \\ \sigma_i(t) & t \geq t_{f_i} \end{cases} \tag{2.60}$$

with $t_{f_i} > 0$ being an arbitrarily chosen reaching time. In particular, at time $t = t_{0_i}$ the coefficients c_{0_i} and c_{1_i} in (2.60) are computed solving the algebraic system of equations

$$\begin{cases} c_{0_i} & = \sigma(t_{0_i})(t_{f_i} - t_{0_i})^{-2} \\ c_{1_i} & = \dot{\sigma}_i(t_{0_i})(t_{f_i} - t_{0_i})^{-2} + 2\sigma_i(t_{0_i})(t_{f_i} - t_{0_i})^{-3} \end{cases} \tag{2.61}$$

where $\dot{\sigma}_i(t)$ is estimated as θ_{1_i} via a Levant exact differentiator [101] converging in a finite time $t_{l_i} \leq t_{0_i}$

$$\begin{cases} \dot{\theta}_{0_i} & = -\lambda_{0_i}|\theta_{0_i} - \sigma_i(t)|^{1/2} sign(\theta_{0_i} - \sigma_i(t)) + \theta_{1_i}) \\ \dot{\theta}_{1_i} & = -\lambda_{1_i} sign(\theta_{0_i} - \sigma_i(t)) \end{cases} \tag{2.62}$$

with $\lambda_{0_i}, \lambda_{1_i} > 0$ constant gains to be designed according to the desired performance [101].

Remark 1. *Notice that due to* (2.62) *the reaching phase elimination actually starts at time $t = t_0$, but in practice this does not constitute an issue since the differentiator convergence time can be made arbitrarily small increasing the gains.*

The following distributed control law, based on (2.36),

$$u_i(t) = -K_i sign\left(\Sigma_i(t) - \frac{\Sigma_i^*}{2}\right) \tag{2.63}$$

is proposed, where $\alpha^* = 1$ is taken for the sake of simplicity with reference to Assumption 1 and (2.37), since $P_1 = P_2 = 1$ holds for (2.58).

Theorem 2. *For a MAS of $N+1$ agents with dynamics as in* (2.58) *and under the stated assumptions, there exist control gains $K_i,\ i = 1, \cdots, N$ such that the control law* (2.63) *robustly solves the leader-follower consensus problem (i.e., Problem 1) with $n = 2$ in a finite prescribed time $T = max(t_{f_i})$.*

Proof. Let us initially define, stacking the respective quantities of the agent dynamics (2.58), the error vectors

$$\begin{aligned} &\mathbf{e}(t) = \mathbf{x}_1(t) - \mathbf{1}x_{1_0}(t) + \boldsymbol{\Delta}(t),\ \dot{\mathbf{e}}(t) = \mathbf{x}_2(t) - \mathbf{1}x_{2_0}(t), \\ &\ddot{\mathbf{e}}(t) = \mathbf{u}(t) + \boldsymbol{\gamma}(t) - \mathbf{1}(u_0(t) + \gamma_0(t)) \coloneqq \mathbf{u}(t) + \mathbf{d}(t) \end{aligned} \tag{2.64}$$

and then define for convenience $\boldsymbol{\kappa}_1(t) = \dot{\mathbf{e}}(t)$. Exploiting the fact that $\bar{L}\mathbf{1} = 0$, and relationships (2.40) and (2.59), one can rewrite (2.60) in vector form as

$$\boldsymbol{\sigma}(t) = (\bar{L} + \bar{B})\mathbf{e}(t) - \boldsymbol{\psi}(t) \tag{2.65}$$

Now, let us consider the system

$$\begin{cases} \dot{\boldsymbol{\kappa}}_1(t) &= \mathbf{u}(t) + \mathbf{d}(t) \\ \dot{\boldsymbol{\sigma}}(t) &= (\bar{L} + \bar{B})\boldsymbol{\kappa}_\mathbf{1}(t) - \dot{\boldsymbol{\psi}}(t) \end{cases} \tag{2.66}$$

which is in the appropriate form for the application of the so-called *method of control hierarchy* [49, Section VI]. This method can be employed to find K_i in (2.63) basing on $\ddot{\boldsymbol{\sigma}}(t)$ for the respect of conditions (2.37) and (2.38), and thus proves the existence of a suitable set of gains guaranteeing robust convergence in spite of the matched disturbance $\mathbf{d}(t)$. Since the considered control law enforces a SOSM, the sliding mode is eventually established both on $\dot{\boldsymbol{\sigma}}(t) = 0$ and $\boldsymbol{\sigma}(t) = 0$ at a certain reaching time $t_r > 0$. Then, as soon as $t = T = max(t_{f_i}) > t_r$, $\boldsymbol{\psi}(t) = \dot{\boldsymbol{\psi}}(t) = 0$ and so, due to the invertibility of $(\bar{L} + \bar{B})$ (Theorem 1), the previous relationships translates directly into (2.57) in view of (2.65) and (2.66), thus solving the stated consensus problem. □

The method of control hierarchy introduced in the proof of Theorem 2 guarantees the possibility of finding suitable gains for the distributed controllers once the topology of the network is known. According to the procedure, the succession of equivalent dynamics $\boldsymbol{\kappa}_\mathbf{1}^{[j]}$, $j = 1, \cdots, N-1$ has to be computed, considering at each iteration j the Utkin-Drazenovic equivalent controls $u_i^{eq}(t)$ for agents $i = 1, \cdots, j$ and $\boldsymbol{\kappa}_\mathbf{1}^{[0]} = \boldsymbol{\kappa}_\mathbf{1}$. These latter are computed as the solution of $\ddot{\sigma}_i^{[i-1]}(t) = (\bar{L} + \bar{B})_i \dot{\boldsymbol{\kappa}}_\mathbf{1}^{[i-1]}(t) - \ddot{\phi}_i(t) = 0$. Then, proceeding backwards, the gains $K_N, \cdots, K_1$ are found considering

successively the obtained systems $\boldsymbol{\kappa}_{\mathbf{1}}^{[j]}$, $j = N-1, \cdots, 0$ for the selection of K_i according to (2.38) (the reader is referred to [49] for a thorough presentation and illustrative examples clarifying the concept).

Remark 2. *It is worth noticing that, at least from simulation results, one can conjecture that also in the case of gains $K_i = K, \forall i$ chosen all equal, there exist a finite value K^* such that $K \geq K^*$ guarantees finite-time convergence, independently of the particular structure of the system. Therefore, the procedure previously described is needed only to prove existence of feasible gains but appears not mandatory in practice. In practical situations and especially if a large number of agents has to be considered, in order to avoid possibly cumbersome computations, a proper set of gains can be found by trial and error in simulation. The formal proof of such a statement is anyway currently subject of further investigation.*

Remark 3. *Theorem 2 deals with the general case in which a reaching phase exists. When a manifold of integral type is employed, the system is in sliding mode from the initial time instant (i.e. $t_r = 0$) or $t_r = max(t_{0_i})$ in case distributed Levant differentiators are employed.*

Remark 4. *Particular chattering alleviation techniques, for instance that proposed in [206] or those relying on the selection of a non-discontinuous law can be adopted also for the second-order case. Alternatively, to maintain unaltered the robustness and increase precision, third-order SMC [54] can be effectively employed.*

First-Order Agents In the case of first-order dynamics, for agent i relationship (2.58) is replaced by

$$\dot{x}_{1_i} = \gamma_i(t) + \bar{u}_i(t) \tag{2.67}$$

with $\gamma_i(\mathbf{x_i}(t), t)$ an unknown sufficiently smooth function with assumed bounded first time derivative, i.e.

Assumption 6. $|\dot{\gamma}_i(t)| \leq \hat{\Gamma}_i$, $\hat{\Gamma}_i$ *being known constants.*

In order to achieve prescribed-time consensus, the same choices (2.59), (2.60) are made as before, and hence also (2.61) keeps holding for the initial time instant t_0. The Sub-Optimal law can be employed here in chattering

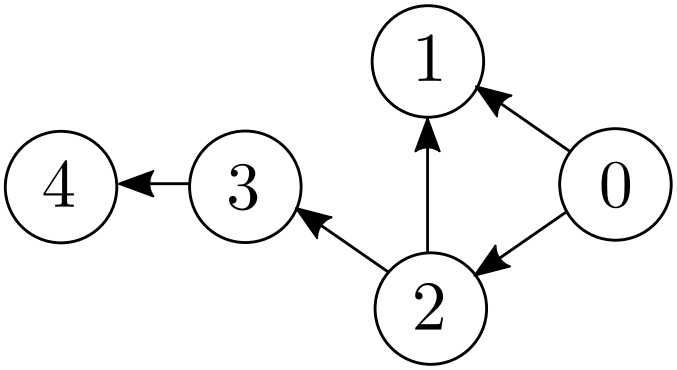

Figure 2.12: Graph representation of the MAS network considered in the simulations. The arrows follow the information flow direction, opposite with respect to the edges of graph G. *From [71].*

alleviation form using as control $\bar{u}_i(t) = \int_0^t u_i(t)\,dt$, with $u_i(t)$ as per (2.63). The same considerations made in the previous case for convergence can easily be adapted for this case under the additional Assumption 6.

Simulation Results

The proposed approach is now tested in simulation, considering a network of 4 agents and an independently controlled leader for both the cases of first and second order chain of integrators dynamics.

The dynamics of the agents are supposed affected by sinusoidal disturbances $\gamma_i(t)$ of different amplitude and frequency generated from a uniform random distribution, as reported in Figure 2.13. The leader is considered as governed by a sinusoidal input signal, generated independently of the presented architecture. The considered task is that of robustly reaching leader-follower consensus, i.e. (2.57), while keeping $\Delta_i = 5i$. A prescribed convergence time of $T = 1s$ is considered as a requirement for the design of the integral manifold, while the initialization time is set as $t_0 = 0.1$ for all the agents.

The gains of the local Levant differentiators are taken as $\lambda_{0_i} = 250$, $\lambda_{1_i} = 70000$, in both the first and second-order cases, while the control gains are chosen according to the introduced procedure for the second-order case and all equal ($K_i = 1000$) for the first-order case. The two different design methodologies are presented simultaneously in order to validate both

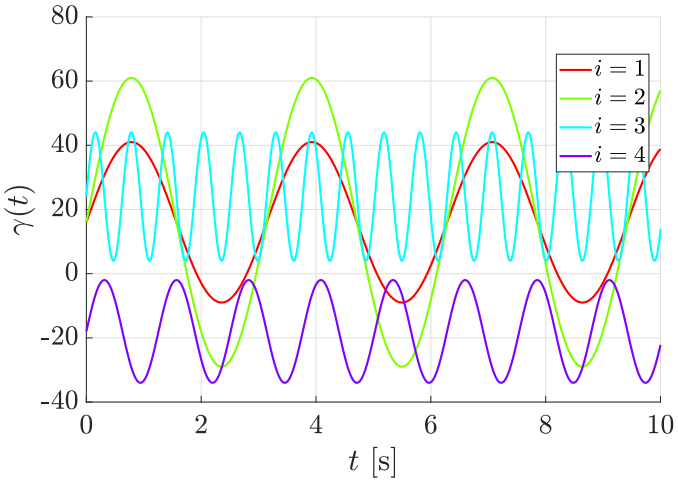

Figure 2.13: Sinusoidal disturbances acting on the agents dynamics. *From [71].*

the formal methodology and the practical Remark 2.

The application of the method of control hierarchy to the considered network with agents ordered as in Figure 2.12 gives the following sufficient conditions for convergence, according to (2.38):

$$\begin{aligned}
K_1 &> 2\Gamma_1 + 2U_0 + K_2 + \Gamma_2 + \sup_{t\in[0,T]}(\ddot{\psi}_1(t)) \\
K_2 &> 2\left(\Gamma_2 + U_0 + \sup_{t\in[0,T]}(\ddot{\psi}_2(t))\right) \\
K_3 &> 2\left(\Gamma_3 + U_0 + \sup_{t\in[0,T]}\left(\sum_{i=2,3}\ddot{\psi}_i(t)\right)\right) \\
K_4 &> 2\left(\Gamma_4 + U_0 + \sup_{t\in[0,T]}\left(\sum_{i=2,3,4}\ddot{\psi}_i(t)\right)\right)
\end{aligned} \tag{2.68}$$

In practice, one could either choose magnitudes so high to consider all the possible realizations of the functions $\psi_i(t)$ or compute suitable values for the gains once the transient functions coefficients become explicitly available by means of (2.61). In the second case, if $t_{0_i} > 0$ for the i-th agent, for $t \in [0, t_{0_i})$ one can simply neglect the existence of the terms $\ddot{\psi}(t)$ in the expression of the lower bound for K_i. For the sake of simplicity, here $K_2 = K_3 = K_4 =$

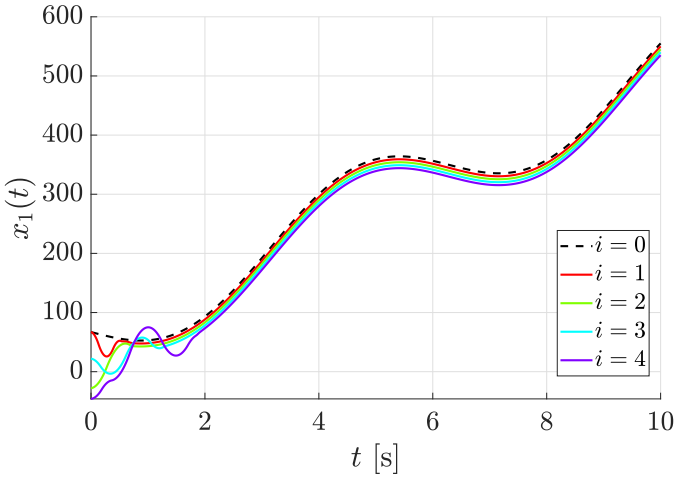

(a) Sub-Optimal law.

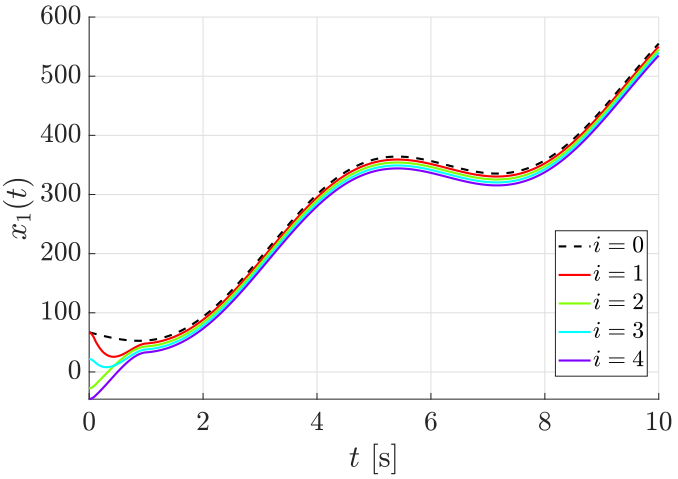

(b) Integral Sub-Optimal law.

Figure 2.14: States $x_1(t)$ for the second-order agents. *From [71].*

$K_5 = 800$, $K_1 = 1500$ were conservatively selected.

The time evolution of the states of the second-order agents are reported in Figure 2.14 and 2.15, respectively. It is evident that the adoption of the proposed Integral Second-Order Sub-Optimal Sliding Mode (IS-SOSM) law is capable of enforcing finite-time consensus reaching if suitable gains are selected. Additionally, the benefits of introducing a second-order integral manifold are appreciable, since it allows greater robustness as well as prescribed convergence time. In particular, it is possible to see how during the reaching phase (present if a plain S-SOSM is employed as the local controller

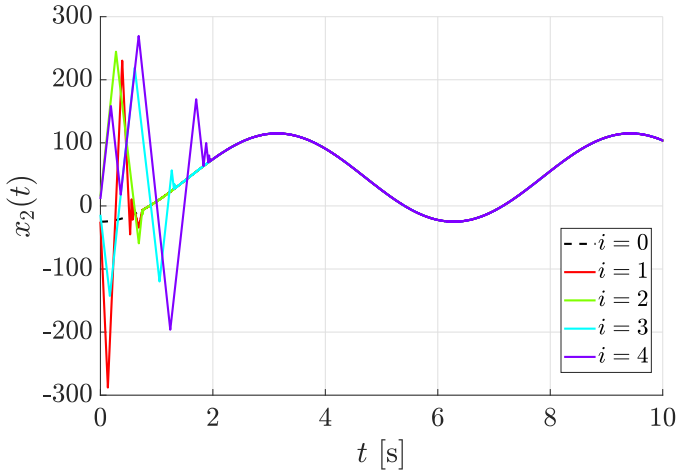

(a) Sub-Optimal law.

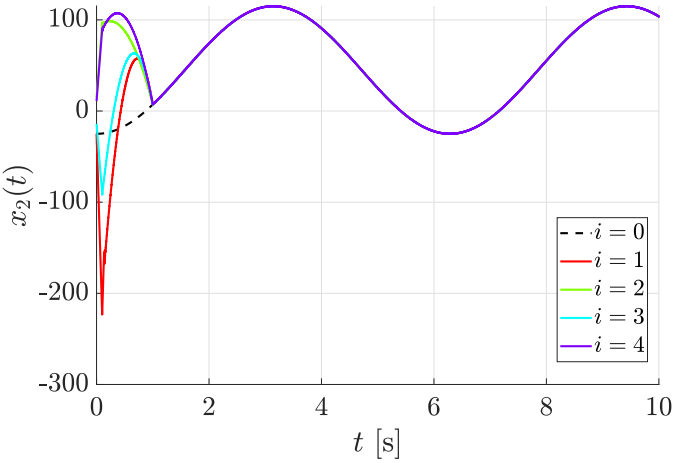

(b) Integral Sub-Optimal law.

Figure 2.15: States $x_2(t)$ for the second-order agents. *From [71].*

for the agents) the dynamics are affected by the sinusoidal uncertainty, while in the proposed IS-SOSM case a robust behaviour is observed. In fact, during the transient phase $\sigma_i(t) = \psi_i(t)$, $\dot{\sigma}_i(t) = \dot{\psi}(t)$ are smooth polynomials independent of the external disturbances.

Similar considerations can be drawn for the first-order agents case, for which the states evolution is depicted in Figure 2.16, with the standard Sub-Optimal controller able to enforce finite-time consensus. Anyway, the superiority of an integral manifold selection appears evident also in this circumstance, for which the continuous input signals are reported in Figure 2.17. Moreover, one can evidence that avoiding the reaching phase trans-

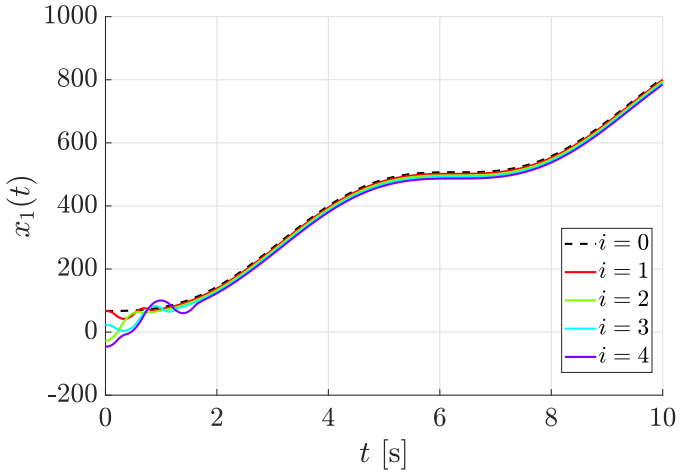

(a) Sub-Optimal (continuous) law.

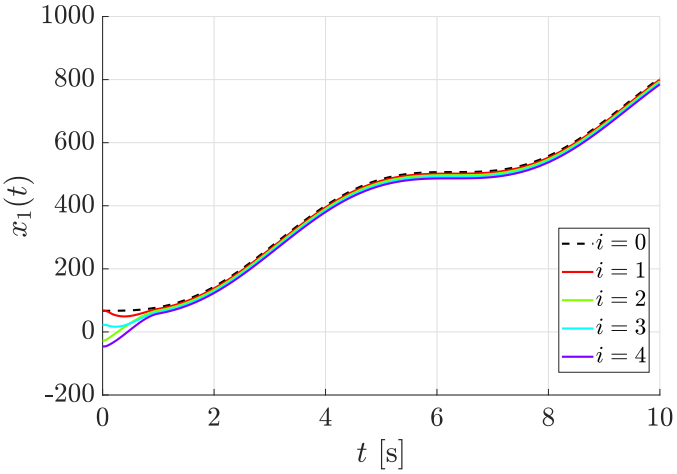

(b) Integral Sub-Optimal (continuous) law.

Figure 2.16: States $x_1(t)$ for the first-order agents. *From [71].*

lates directly into the generation of a smoother control signal: this can be beneficial for instance in vehicular applications (consider the agents as cars with passengers, for which abrupt velocity changes constitute a source of discomfort). In fact, the characteristic "sawtooth" behaviour, which arises from the integration of a constant signal with switching sign, is avoided.

Notice that the degrees of freedom provided by the possibility of designing the transient function could also be exploited to considered advanced features in place of a prescribed transient time. In fact, for instance, collision avoidance capabilities could possibly be embedded in the design of

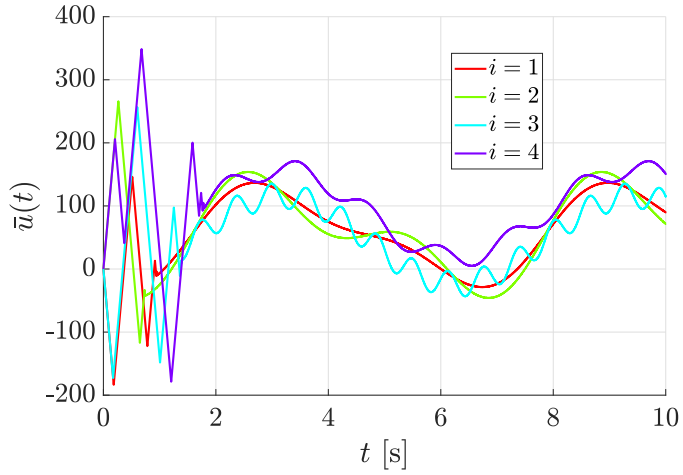

(a) Sub-Optimal (continuous) law.

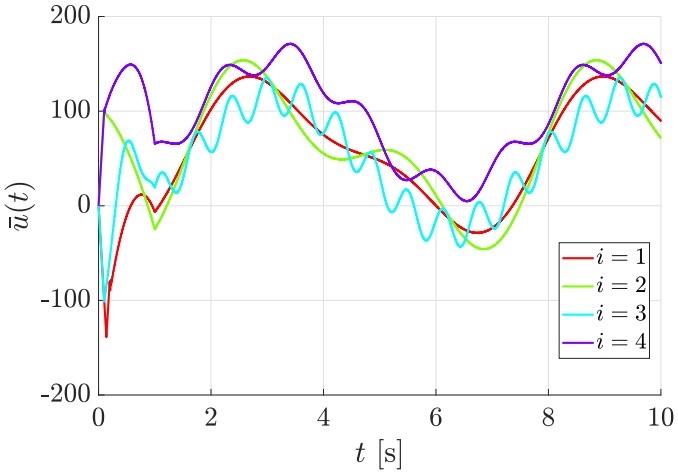

(b) Integral Sub-Optimal (continuous) law.

Figure 2.17: Continuous inputs of the first-order agents. *From [71].*

the functions $\psi_i(t)$, although this is not an issue addressed in the present contribution. As a general rule, stated here on the sole basis of intuition but derivable also from formal computations, notice that the requirement for a fast transient (i.e. small T) or a particularly sharp transient function entail the need for greater control gains. Thus, the trade-off between the contrasting requirements should be considered during the design procedure.

2.2 Model Predictive Control (MPC)

In this section a very brief introduction on Model Predictive Control (MPC) is provided. Although the topic is one of the most extensively treated in the control systems literature (for reference, see for instance [121, 118, 32]), here only the bare minimum concepts are reported in order to understand the solutions adopted in the following of this Dissertation[24].

MPC is a family of optimal control strategies which rely on the model of the system under control to predict the successive state trajectory and select an appropriate sequence of inputs to drive it according to a given cost function, possibly in the presence of constraints. Different algorithms exist, addressing a variety of problems characterized by the cost function, the dynamics of the system, the shape of the constraints and the values upon which the control scheme relies to close the feedback loop. An exhaustive discussion on these different aspects is out of the scope of the present Thesis, which reports the general concept as follows.

Let us introduce a sampling time T_s along with a *prediction horizon* $P \in \mathbb{N}$ which induces a sequence of inputs

$$\bar{u}_k = (u_k, u_{k+1}, \cdots, u_{k+P-1}) \tag{2.69}$$

for every sampling step k (corresponding to the sampling instant kT_s). The formulation adopted here relies on a continuous time framework, so that the input signal is to be considered as a piece-wise constant function[25], namely

$$u(t) = u_k, \quad kT_s \leq t < (k+1)T_s \tag{2.70}$$

Considered also a general dynamics description of a system

$$\dot{x}(t) = f(x(t), t, u(t)) \tag{2.71}$$

with $x(t) \in \mathbb{R}^n$ and $u(t) \in \mathbb{R}^m$, the (nonlinear) MPC algorithms rely on a

[24] A huge amount of different aspects have been addressed in research: just to mention a few among many others, the study of stability (see, e.g. [184, 121, 9]), the proposal of robust solutions such as [27, 119, 122] and the development of stochastic algorithms [123].

[25] This is a commonly adopted framework, although other possibilities (e.g. discrete MPC formulations) can be adopted.

provided cost function

$$J_k = \sum_{i=k}^{k+P-1} j(x((i+1)T_s), iT_s, u(iTs)) + \bar{j}_k \tag{2.72}$$

at every time instant k to compute the respective optimal input sequence $\bar{u}_k$ as in (2.69). In Equation (2.72), the function $j_i(\cdot)$ describes the cost associated to the i-th time step, while $\bar{j}_k$ provides a general term which includes any possible quantity in the prediction horizon $k, \cdots, k+P-1$. In particular, it can be vanishing or correspond to the terminal cost, depending on the adopted formulation. Possibly, constraints can be provided both in terms of the input values, the states, or in general an arbitrary function of states, inputs and time.

The problem of MPC can then be generically stated as follows.

Problem 2 (Nonlinear MPC)**.** *At each time step k, find the optimal sequence $\bar{u}_k$ (as in* (2.69)*) which minimizes the cost function* (2.72) *under the dynamics* (2.71)*, subject to the constraints*

$$g_1(x(t), t, u(t)) < 0 \tag{2.73}$$

$$g_2(x(t), t, u(t)) \leq 0 \tag{2.74}$$

with $g_1(\cdot)$ and $g_2(\cdot)$ an arbitrary vector function of any dimension (possibly null) of states, inputs and time, samples at discrete time instants $k, \cdots, k+P$.

Once computed the optimal sequence $\bar{u}_k$, according to the principle of *receding horizon*, only the first input is applied to the system for the subsequent T_s seconds, before a new optimization is performed at time $k+1$[26] to provide greater robustness.

Among the many possible frameworks in which MPC can be successfully adopted, the linear case is of paramount importance. In fact, if both the dynamics of the controlled system and the constraints are linear, and the cost function is quadratic, the optimization problem becomes a Quadratic Pro-

[26]In this discussion, as always in the theoretical developments about MPC, the assumption that the solution of the optimization problem is instantaneous is made. Of course, this is not the case in real-life applications, where in general performance is of great importance and well-crafted implementations are required to cope with the control requirements. A discussion about these aspects is out of the scope of the present work.

gramming one. Thus, special techniques can be adopted which provide superior performance and guaranteed convergence. Additionally, linear MPC is well studied in the literature and many theoretical results are available.

In that specific case, one has in particular that the MPC cost function can be defined by means of the matrices $Q \succeq 0$ and $R \succ 0$. The general expression becomes then

$$J_k = \sum_{i=k}^{k+P-1} \left(\hat{x}_{i+1}^T Q \hat{x}_{i+1} + u_i^T R u_i \right) \tag{2.75}$$

where $\hat{x}_i$ is the vector of predicted states at step i according to model (4.8) starting from $x(kT_s)$ and sampled over the considered prediction horizon, i.e. at time instants $(k+1)T_s, \cdots, (k+P)T_s$. Thus, $\hat{x}_i$ represents the predicted state at the time step i, obtained sampling the trajectories computed inside the MPC algorithm, dependent on the chosen input sequence $\bar{u}_k$. Also in Equation (2.75) the terminal penalty cost could be included (and it is, indeed, in many formulations). However, in the following of the discussion this additional term is not considered and thus the simplified expression (2.75) is provided here.

Chapter 3

Robust Platoon Control

In this chapter, the problem of robustly control a platoon of arbitrary size is presented and addressed proposing two different approaches relying on Sliding Mode Control. In fact, as will be made more clear in Section 3.2, uncertainty always exists in practical platoon control applications and could in principle disrupt the performance or even determine unstable behaviors, possibly leading to crashes. Therefore, independently of the specific adopted control strategy, robustness remains one of the major issues to address in order to deploy effective platoon control systems in real-life scenarios [193], especially in the presence of tightly spaced vehicles. The inherent robustness of SMC, together with its low computational complexity, constitute then a promising feature which can be effectively exploited in this context.

Specifically, in the present Dissertation,

- A first solution, presented in Section 3.3 (and published originally in [223]) deals with the specific problem of robustifying a nonlinear distributed MPC platoon control system by means of a multi-rate local control scheme including a fast, lightweight Integral Sliding Mode (see Section 2.1.3) correction loop. While the local MPC is in charge of tracking the inter-vehicle distance and consider energy efficiency[1], the corrective term is injected at a high frequency to reject the matched disturbance acting on the vehicle dynamics. This latter, in particular, is considered as a second or third-order system, depending on the

[1] In the present implementation energy efficiency is considered as an additional objective in the optimal control problem. However, this is just to highlight the possibility of effectively including advanced features while controlling the platoon.

dynamics of the powertrain and the working assumptions made (as it will be clarified in the following).

Besides the introduced general robustness, which guarantees better tracking properties and more precise consideration of the constraints, an additional effect is that of enforcing *coherence* in the string. This concept can be informally defined as the ability of the formation to behave like a rigid body, which implies that (at constant velocity) the distance between the leader and the last follower remains constant and equal to a prespecified one [15], obtained as the sum of the steady-state distances between the single adjacent vehicles. When vehicles proceed at a constant relative distance, e.g. during cruising on highways, coherence becomes a valuable feature especially when a large number of agents is considered (see, e.g. [69]). Despite the enforcement of local and string stability, in fact, as highlighted for instance in [114], coherence cannot be guaranteed in principle in the presence of unknown perturbations of the acceleration, determined e.g. by the presence of uncertainty in the description of the dynamics or due to external phenomena. Some proposals exist making use of linear local controllers considering linear dynamics for the vehicles, but the results do not apply in principle to the nonlinear case. The simulation results provided show, instead, how the proposed strategy helps in maintaining coherence while countering the uncertainty acting on the dynamics of each controlled vehicle.

- The results presented in Section 3.4 and published in [224] rely instead entirely on Sliding Mode Control. Specifically, it is shown both theoretically and in simulation that the generation of Second-Order Sliding Modes by means of local controllers guarantees the robust achievement of Disturbance String Stability (DSS, a relatively new concept of string stability considering a wide range of cases, introduced in [30]) in a rather general case, i.e. for vehicles dynamics describable by means of uncertain third-order models. In order to enforce global convergence and string stability, a particular formulation of the spacing policy is introduced, which aims at the attainment of a specified constant inter-vehicle distance and a predefined space-dependent velocity profile. In this respect, it is worth noticing how the particular strategy chosen to

enforce the sliding motion is not important, and therefore any SOSM control algorithm can in principle be adopted considering proper lower bounds for the control amplitude. However, an explicit proof is given for the adoption of the Sub-Optimal SOSM strategy, which is used also in the reported simulations.

Before going through a detailed description of the research results, a brief general introduction on platoon control is provided below in Section 3.1 with the aim of establishing a common knowledge base and a uniform notation.

3.1 Platoon Control Basics

In order to introduce the basic concepts of platoon control, a string composed of $N+1$ vehicles indexed by i in ascending order of position (with $i=0$ corresponding to the leader) is considered. A platoon is enforced with the vehicles following the leader (which may or may not be explicitly controlled) while keeping a determined inter-vehicle distance (of course, while avoiding collisions). The reader may refer to Figure 3.1 for a schematic representation of the concept.

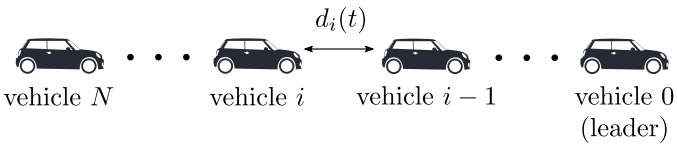

Figure 3.1: Basic idea of a platoon.

Two fundamental requirements, namely *local* and *string stability*, are crucial in platoon control. The former relates to the most classical concept of stability and describes the ability of the single vehicles in the platoon to effectively track the specified inter-vehicle distance with respect to the preceding vehicle. The selection of this distance by means of a suitable *spacing policy*, in turn, is key in determining not only the local (transient) behavior of the vehicles but also the string stability properties of the entire platoon. This latter, roughly speaking, can be identified as the ability of the string to positively respond to perturbations, specifically avoiding their amplification as they propagate backward toward the platoon tail [195, 66, 185, 149, 171].

To dive a little deeper, one can define the distance $d_i(t) > 0$ between vehicle i and $i-1$ as

$$d_i(t) = s_{i-1}(t) - s_i(t), \quad i = 1, \cdots, N \tag{3.1}$$

with $s_i(t)$ the position of vehicle i in a unidimensional space (i.e. along the unique spatial coordinate, which will be referred to as s). Notice that, obviously, the inter-vehicle distance is not defined for the leader, which in general does not have to follow any preceding vehicle. Additionally, near-zero or negative distances mean that a crash has occurred, and thus represent a

situation to avoid. With respect to this particular issue, notice that special considerations must be made in the design of the local controllers in order to avoid undershoots, especially during the transient phase, in the tracking of the inter-vehicle distance. To this end, a minimum safety distance can be imposed as a constraint in MPC-based local controllers (as done, for instance, in [223]) with long enough prediction horizons. As a possible alternative, the authors in [172] propose instead a special formulation of the local tracking control problem with sliding mode onboard controllers.

In general, having in mind the just introduced concepts, the process of designing a distributed platoon control system can be divided into two distinct parts:

- At first, a proper spacing policy is selected to enforce the desired behavior for the controlled vehicles in terms of transient dynamics and string stability. In other words, a reference distance $d_i^*(t)$ is defined to be tracked by each vehicle i;

- Then, a proper local control strategy is developed for the single vehicles to track the desired distance, i.e. to enforce[2]

$$d_i(t) \to d_i^*(t). \tag{3.2}$$

  Notice that local controllers must rely only on the locally available information (whether it comes from sensors or inter-vehicle communication), i.e. distributed control architectures are usually considered.

Among the possible choices for the spacing policy, the most commonly adopted are, by far, the Constant Distance (CD) (see, for instance, [79, 232]) and Constant Time Headway (CTH) [198, 110] ones[3]. For the first,

$$d_i^*(t) = d_s \tag{3.3}$$

[2]The achievement of such inter-vehicle distances is to intend slightly differently, dependent on the adopted controllers. For instance, linear and MPC controllers only guarantee asymptotic convergence, while pure SMC strategies enforce finite-time convergence.

[3]A wide variety of spacing policies can actually be designed, and have been proved to work under certain circumstances, often providing better performance than the CD and CTH ones at the expense of more complex control architectures and/or stability analysis. For instance, among others, the authors in [217, 229] propose nonlinear spacing policies, while the policy proposed in Section 3.4 makes use of information coming from the platoon leader.

holds, with $d_s > 0$ a constant distance to be chosen. The second, instead, relies on the idea of a velocity-dependent spacing. In fact, a time headway $t_h > 0$ is introduced so that the reference spacing becomes

$$d_i^*(t) = d_s + t_h v_i(t) \tag{3.4}$$

where $d_s > 0$ is considered in this case a minimum safety distance (to be kept when the velocity is null). It is well understood in the literature that, due to the inherent filtering features of (3.4), perturbations are attenuated throughout the string of vehicles, thus providing some forms of string stability in many cases. In particular, this can be easily proved for a string of linear systems (refer to, e.g., [3]) under the assumption that the initial perturbations are null. Notice that the same cannot be said, in general, for the CD policy as defined in Equation (3.3), for nonlinear vehicle dynamics or for non-null initial perturbations. In these cases, ad-hoc formulations of the controllers must be developed and specifically studied.

3.2 Longitudinal Dynamics Modelling

For platoon control applications, it is almost always sufficient to rely on the longitudinal dynamics description of the vehicles. In particular, for the modelling of the i-th vehicle, with $i = 0, \cdots, N$, one can consider the following general third-order model

$$\begin{cases} \dot{s}_i(t) = v_i(t) \\ \dot{v}_i(t) = a_i(t) + \phi_i(t) \\ \dot{a}_i(t) = -a_i(t) + u_i(t) + \gamma_i(t) \end{cases} \tag{3.5}$$

where the state vector $x_i(t) = [s_i(t)\ v_i(t)\ a_i(t)]^T$ includes, respectively, the absolute position, velocity and reference acceleration for vehicle i, and $u_i(t)$ is the control input (it can be conceptually seen as a reference commanded acceleration).

In order to provide a formal description of the uncertainty affecting the vehicle models, the unknown terms $\phi_i(t)$ and $\gamma_i(t)$ are here introduced. These account mainly for the following issues:

- The models usually adopted for platoon control applications are often derived by means of I/O linearization (see, e.g., [91]), as described for instance in [215]. Such a technique enables to transform a complex dynamic system (dependent, among other elements, on the engine and powertrain characteristics, the aerodynamic drag, and the rolling resistances) into a chain of integrators (notice that, here, one would be considering the system in (3.5) with $\phi_i(t) = \gamma_i(t) = 0$). Anyway, to do so the exact knowledge of the dynamics to be linearized is mandatory: since it is never the case, due to the fact that a precise description of all the involved complex dynamics is impossible to obtain in practice, it produces approximate descriptions where uncertainty is not explicitly accounted for;

- Some external disturbances and unmodelled effects may act on the system in various forms, introducing further uncertainty;

- Despite (3.5) describes a platoon of homogeneous vehicles, the possible inhomogeneities existing in practice can be included in the model uncertainty.

Notice that in most of the literary works, not explicitly considering the robustness of the proposed strategies, the actually employed model does not comprise the explicit inclusion of the uncertainty. This, thus, can be seen as an initial partial contribution of the following works.

The next assumptions are made[4], which will be useful in the remainder of the chapter.

Assumption 7. *There exist known positive constants* Φ, $\hat{\Phi}$ *and* Γ *such that*

$$|\phi_i(t)| \leq \Phi, \quad |\dot{\phi}_i(t)| \leq \hat{\Phi}, \quad |\gamma_i(t)| \leq \Gamma \tag{3.6}$$

hold for every controlled vehicle i*.*

Assumption 8. *The conditions*

$$v_i(t) > 0, \quad |a_i(t)| < A \tag{3.7}$$

hold for some known positive constant A *and for every controlled vehicle* i*.*

Another possible representation for the longitudinal dynamics of the vehicles in a platoon, often adopted in the literature, considers explicitly the forces exerted at the wheels level (see Assumption 9) and the vehicles parameters. The most simple description is the following two-states model, which anyway still accounts for uncertainty as already discussed, namely

$$\begin{cases} \dot{s}_i(t) = v_i(t) \\ m_i \dot{v}_i(t) = F_{in,i}(t) - F_{loss,i}(t) + \phi_i(t) \end{cases} \tag{3.8}$$

where m is the vehicle mass, while $F_{loss,i}(t)$ encompasses the aerodynamic drag and rolling resistance forces such that

$$F_{loss}(t) = \frac{1}{2}\rho C_a S v^2(t) + C_r m g \tag{3.9}$$

with ρ the air density, C_a the aerodynamic coefficient, S the equivalent vehicle surface, C_r the rolling resistance coefficient and g the gravitational acceleration.

[4]Such assumptions are (almost) always made in the context of (robust) platoon control when the local controllers are of SMC-type. Thus, they do not constitute a limitation with respect to the currently available literature works.

As for the input force $F_{in}(t)$, let us introduce the following assumption (indices i will be omitted for the sake of simplicity, although all the quantities are to refer to all the vehicles under control).

Assumption 9. *The vehicles are equipped with low-level fast enough slip controllers, able to maintain the desired slip ratio while keeping the tire-road friction characteristic in the linear region (see, e.g., [163]). As a consequence, defining $\omega_l(t)$ as the l-th wheel rotational speed, one has*

$$\dot{\omega}_l(t) \simeq 0 \quad \forall t \tag{3.10}$$

That is to say, a steady state condition is considered so that at each time instant the forces exerted at the wheels level can be considered as coincident with that in output from the powertrain. Therefore,

$$\sum_{l \in DW} \frac{T_{in_l}(t)}{R_{e_l}} = F_{in}(t) \tag{3.11}$$

where DW is the set of driving wheels, $T_{in_l}(t)$ is the net torque applied to the l-th wheel (supposed equal for the two wheels on the same axle) and R_{e_l} is its effective radius.

From Assumption 9, two consequences can be directly drawn:

- The scope of validity of model (3.8) coincides with a limited range of input forces $F_{in}(t)$. In particular, it corresponds to the linear region of the tire-road friction characteristic curve (see for instance [76]). This, in turn, implies that for an effective control the forces must be constrained in the range

$$F_{in}(t) \in [F_{min}(t);\, F_{max}(t)] \tag{3.12}$$

  with bounds which depend on the specific properties of the tire-road characteristic curve and, thus, may in principle vary with time.

- Since the major effects of a transient in the generation of the tire-road forces are neglected, it appears reasonable to assume that the force $F_{in}(t)$ actually exerted follows a first-order dynamics with respect to the one requested, namely

$$\tau \dot{F}_{in}(t) = F_u(t) - F_{in}(t) + \gamma(t) \tag{3.13}$$

where τ is the (possibly unknown) time constant and $F_u(t)$ is the requested force, which can be positive or negative.

Notice that the introduction of a third equation leads to a third-order representation analogous to the already introduced kinematic model in (3.5), based on similar considerations but with explicit representation of the forces and the vehicle parameters[5], namely one has

$$\begin{cases} \dot{s}_i(t) = v_i(t) \\ m_i \dot{v}_i(t) = F_{in,i}(t) - F_{loss,i}(t) + \phi_i(t) \\ \tau_i \dot{F}_{in,i}(t) = F_{u,i}(t) - F_{in,i}(t) + \gamma_i(t) \end{cases} \tag{3.14}$$

Remark 5. *Possible residual mismatches due to imperfect knowledge of the effective radius and the real slip control actuation, which are neglected by virtue of Assumption 9, can be lumped into the uncertainty terms $\phi_i(t)$ and $\gamma_i(t)$ as well.*

[5]Also this representation is usually derived by means of feedback linearization, neglecting the real underlying dynamics of the powertrain. Moreover, it is always possible to represent the same vehicle dynamics by means of one model or the other, rescaling suitably the involved variables. For instance, note that the acceleration in (3.5) is represented as the ratio between the exerted force at the wheels level and the vehicle mass in (3.8) and (3.14).

3.3 ISM-Robustified Multirate Distributed MPC for Platoon Control

In the following, a non-iterative non-cooperative Distributed Model Predictive Control (DMPC) scheme is proposed for the robust control of arbitrarily-sized platoons. In particular, a multi-rate scheme is proposed for the local distributed controllers. Its design couples a (relatively slow) nominal DMPC regulator with a fast second-order integral sliding mode controller. This latter compensates for bounded uncertainty, and thus the resulting system is led to follow the trajectory predicted using the nominal model during each control step. As a consequence, any formulation for the distributed model predictive controllers can be exploited to account for distance tracking and, in general, other goals such as energy efficiency. In the present work, in particular, a fleet of EVs is considered and the power flowing out of the batteries is required to be minimized in a multi-objective optimization. Due to the obvious environmental and economic benefits that follow, in fact, energy efficiency appears to be a natural advanced objective in an evolved formation control system [158]. With reference to EVs and HEVs, specifically, the employment of the so-called regenerative braking allows to recover energy while decelerating the vehicle. This feature, of course, makes the control problem non-trivial and rather interesting.

In contrast to already existent robust strategies, that rely on complex MPC formulations, the proposed architecture only introduces a simple and lightweight additional term which can be easily implemented on the on-board vehicles controllers. Additionally, the second-order formulation for the ISM algorithms helps to reduce the chattering phenomena and enables the consideration of either second-order (3.8) or third-order (3.14) dynamics without affecting the design of the basic multi-rate algorithm[6].

As a direct consequence of the robustification, it is evidenced in the following that the closed-loop control scheme becomes far less sensitive to the MPC sampling time, which in principle can be chosen relatively high. This feature may enable less required computational power and lower packet transmission rates, with obvious benefits from both a local and a network standpoint. An internal schematization of the distributed controllers is

[6]Beside introducing an integration step in case of chattering alleviation, as already discussed in Section 2.1.2.

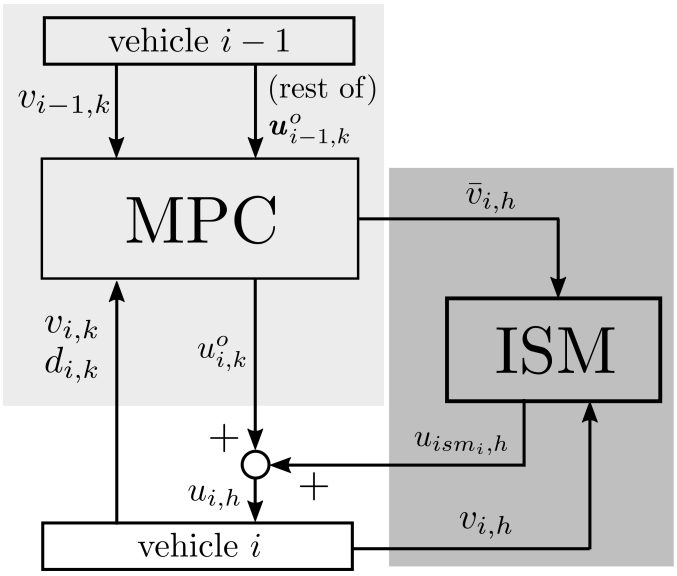

Figure 3.2: Schematic of the multirate control system. The brighter gray box indicates a slower rate (sampling time T_s), while the darker box refers to the higher one (sampling time t_s). *From [223].*

sketched in Figure 3.2, which provides a reference for the entire subsequent discussion.

In order to allow the description of a more general situation, the leader is kept uncontrolled. For instance, a higher-level controller (e.g. a traffic regulation system, which controls the steady-state platoon speed [142]) could be employed to provide reference speeds for the leader. To provide a modern approach to the problem, as already introduced in the previous discussion, electric vehicles are considered, and thus a side objective of the local optimizations is identified in the battery energetic out-flow minimization. In particular, the regenerative braking feature (see, e.g., [28]) is considered, encouraging it over the usage of the mechanical braking system. With reference to models in Equations (3.8) and (3.14), the input force is then taken here as

$$F_{in}(t) = F_e(t) + F_b(t) \tag{3.15}$$

where $F_e(t)$ is the total electric force (which can be either positive or negative, during acceleration or regenerative braking, respectively) and $F_b(t) \leq 0$

is the mechanical braking force, which can only be negative.

A simple model for the electric power flow is then introduced, and will be used in the MPC optimizations to account for the efficiency-related objective. Specifically, the total power utilized by the motors can be written as

$$P_m(t) = \sum_{\mu \in M} T_{in_\mu}(t)\omega_\mu(t)\eta_\mu(T_{in_\mu}(t), \omega_\mu(t))^{-sign(T_{in_\mu}(t))} \tag{3.16}$$

where M is the set of electrical motors driving the vehicle wheels. The efficiency function $\eta_\mu(T_{in_\mu}(t), \omega_\mu(t))$, specific of the particular motor μ, is usually obtained via experiments. In this work, anyway, for the sake of simplicity it is assumed constant over the whole considered working region. The wheels rotational speeds $\omega_l(t)$ in (3.16) can then be approximated through the expression

$$\omega_l(t) = \frac{g_{r_l}}{R_{e_l}} v(t) \tag{3.17}$$

where the gear ratio g_{r_l} is supposed constant, as usually done with EVs[7]. Notice that the $sign(.)$ function at the exponent in Equation (3.16) allows to consider also regenerative braking, during which the power flows "backward" from the wheels to the engine, in a unique expression. Thus, the total power entering (or exiting) the battery pack can be described as

$$P_b(t) = P_m(t)\eta_b^{-sign(F_{in}(t))} \tag{3.18}$$

with $\eta_b \in [0, 1]$ the efficiency of the conversion from mechanical to chemical energy, supposed here constant again for the sake of simplicity.

3.3.1 Distributed MPC

In the proposed approach, every vehicle in the platoon equips an independent controller and a short-distance Vehicle-to-Vehicle (V2V) communication device. The required measured quantities for closing the local feedbacks comprise the instantaneous velocity as well as the distance from the preceding vehicle (obtainable, for instance, via a range sensor on the front bumper). Since the communication frequency is assumed comparable with that of the

[7]Nevertheless, a variable ratio can be considered for canonical vehicle configurations, with a possible additional degree of freedom in the control (anyway, notice that this would in principle require a mixed-integer optimization procedure, which might be quite heavy from the computational point of view).

local DMPC controllers, the resulting architecture is designed based on a non-iterative MPC scheme. At each step, specifically, every vehicle sends the computed optimal control sequence (from the second time step on) to the following one, which at the successive iteration computes an updated prediction of the future distances[8]. The ISM correction term, as will be thoroughly explained in the following, is instead computed locally for each of the vehicles. As a consequence, no fast interaction is required among the neighbors for the transmission of information, thus avoiding the need for a large transmission bandwidth. The main result of the remaining of this section can be summarized as the fact that if all of the vehicles equip the proposed local multi-rate controller, robust control of the entire formation is enforced. This holds for both the considered cases (namely, with models as in Equation (3.8) and (3.14)) under Assumption 7, and allows to achieve coherence of the whole platoon.

For the MPC on-board controller of the i-th vehicle, the following nominal model[9] (i.e. not accounting for uncertainty) is considered based on (3.8)

$$\begin{cases} \dot{\bar{d}}_i(t) = \bar{v}_{i-1}(t) - \bar{v}_i(t) \\ \dot{\bar{v}}_{i-1}(t) = \frac{1}{m_{i-1}}\left(\bar{F}_{in_{i-1}}(t) - \bar{F}_{loss_{i-1}}(t)\right) \\ \dot{\bar{v}}_i(t) = \frac{1}{m_i}\left(\bar{F}_{in_i}(t) - \bar{F}_{loss_i}(t)\right) = \bar{f}_v(\bar{v}_i(t), u_i(t)) \end{cases} \tag{3.19}$$

where the term $\bar{d}_i(t)$ is the nominal relative distance, which is defined as

$$\bar{d}_i(t) = \bar{s}_{i-1}(t) - \bar{s}_i(t) \tag{3.20}$$

as per Equation (3.1). Notice that $\bar{d}_i(t)$ is available for every vehicle through measurement (supposedly with ideal precision) by assumption. The velocity $v_i(t)$ is also assumed to be available, and hence $v_{i-1}(t)$ can be sent to vehicle $i-1$ through short-range communication. Alternatively, it can be estimated through precise enough differentiators (e.g. exact Levant differentiators, see [101]). The second equation in (3.19) is based on the nominal parameters received by i from $i-1$ at connection time, i.e. as soon as vehicle i approaches vehicle $i-1$ and recognizes it as its predecessor in the platoon.

[8]Notice that, in order to match the length of the future predicted trajectory with the received input sequence, the last term of this latter is repeated in the adopted strategy.

[9]The $\bar{\cdot}$ notation indicates nominal quantities, predicted or estimated using the nominal models.

For a generic vehicle $r = \{i-1, i\}$, the control input signal coming from the on-board MPC $u_r(t)$, is decomposed as

$$u_r(t) = u_{1_r}(t) + u_{2_r}(t) = F_{e_r}(t) + F_{b_r}(t) \tag{3.21}$$

according to Equation (3.15). Two cases can be identified in practice with reference to Equation (3.13), which require to slightly different control schemes.

Case 1. *The actuators dynamics can be neglected, i.e.*

$$\tau_r \simeq 0 \;\Rightarrow\; \bar{F}_{in_r}(t) = u_r(t) \tag{3.22}$$

so that the final model is of order two as per Equations (3.8) *and, consequently,* (3.19)*.*

Case 2. *The actuators dynamics cannot be neglected, i.e.*

$$\tau_r > 0 \;\Rightarrow\; \dot{\bar{F}}_{in_r}(t) = \frac{1}{\tau_r}\left(u_r(t) - \bar{F}_{in_r}(t)\right) \tag{3.23}$$

so that the an additional equation must be added to (3.19) *basing on the third-order description in Equation* (3.14)[10]*.*

As described already in Section 2.2, at each discrete time instant k (sampled with period T_s corresponding to the selected MPC time step), vehicle i computes an optimal control sequence $\boldsymbol{u}^o_{i,k} = \{u^o_{i,k}, \cdots, u^o_{i,(k+P-1)}\}$, $\quad u^o_{i,k} = [u^o_{1_i,k}, u^o_{2_i,k}]^T$ solving a constrained optimization problem minimizing a cost function $J_{i,k}$ over the P future steps (i.e. the prediction horizon). Then, following the receding horizon approach, only the first computed input $u^o_{i,k}$ is applied for the entire subsequent interval T_s. The rest of the control sequence is sent to vehicle $i+1$, which in the successive optimization, at time instant $k+1$, predicts $\bar{\boldsymbol{v}}_{i,(k+1)} = \{\bar{v}_{i,(k+1)}, \cdots, \bar{v}_{i,(k+1+P)}\}$ and $\bar{\boldsymbol{d}}_{i,(k+1)} = \{\bar{d}_{i,(k+1)}, \cdots, \bar{d}_{i,(k+1+P)}\}$ applying the received sequence to the stored nominal model of vehicle i (as already anticipated, the last term is duplicated in order to match the required length).

Remark 6. *Even if the leader is considered independently controlled as a generalization, it is nevertheless required that it sends to the following*

[10] In this scenario, in the case of a state-feedback MPC formulation (as the one adopted in this work) also F_{in_r} (the real value, sampled before performing the MPC optimizations) must be available to close the loop.

vehicle the future $P-1$ control inputs, sampled at an according rate so that its nominal evolution can be computed by vehicle 1.

A CTH policy (see Equation (3.4)) is considered in the present proposal, which provides a reference for the first objective of the MPC optimization. Thus, the i-th vehicle should minimize the following cost

$$J_{i,k} = \alpha_d c_{d,k} + \alpha_e c_{e,k} + \alpha_b c_{b,k} \tag{3.24}$$

where

$$c_{d,k} = \sum_{j=k+1}^{k+P} (\bar{d}_{i,j} - \bar{d}^*_{i,j})^2 \tag{3.25}$$

is the cost associated with the distances sequence predicted by means of (3.19),

$$c_{e,k} = \sum_{j=k+1}^{k+P} P_{m_i,j} \tag{3.26}$$

is the net energy outcome from usage and regeneration during the prediction horizon and

$$c_{b,k} = \sum_{j=k+1}^{k+P} F^2_{b_i,j} = \sum_{j=k+1}^{k+P} u^2_{2_i,j} \tag{3.27}$$

is the cost associated with the mechanical braking force. In order to avoid the usage of the mechanical brake, which does not provide energy regeneration, α_b should always be kept large. In this way, the mechanical braking input $F_b(t)$ is avoided unless inevitable thus encouraging regenerative braking to decelerate the vehicle.

The following minimal constraints are introduced, which are fundamental for the practical effectiveness of the proposed algorithm

$$F_{min_i,k} + \kappa \leq u_{1_i,k} + u_{2_i,k} \leq F_{max_i,k} - \kappa \tag{3.28a}$$

$$0 \leq \bar{v}_{i,k} \leq v_{max,k} \tag{3.28b}$$

$$d_{min} \leq \bar{d}_{i,k} \leq d_{max,k} \tag{3.28c}$$

where κ is to be introduced in the following section. Specifically, (3.28a) accounts for relationship (3.12), determined by the physical tire-road friction available, the maximum torque exercisable by the electric motors and the limit braking force. For safety and road speed limit purposes, (3.28b) and

(3.28c) are also enforced with v_{max} and d_{max} possibly varying parameters.

Remark 7. *Notice that, despite in the presented proposal the considered model is nonlinear, a linearization based solution could also be investigated. In particular, the mismatch between the linearized version of the model (which may be performed at every working point, to increase the accuracy of the representation) and the real behavior of the vehicles can be included in the disturbances.*

Remark 8. *A more advanced solution could be based on a lexicographic formulation, where the main objective is that of attaining and keeping the inter-vehicle distances, while the secondary objective could include additional features such as energy efficiency. No changes are required with respect to the proposed multi-rate architecture as per the disturbances compensation*[11].

3.3.2 ISM robustification

The optimal control input $\boldsymbol{u}^o_{i,k}$, computed by the i-th vehicle at the time instant k, is obtained relying on nominal models. Thus, the controllers performance can be heavily degraded due to the fact that, in general, the real dynamics is affected by uncertainty. To face this issue, the fundamental idea of this proposal is that of having a trivially implementable controller able to run at a much higher rate which compensates for the bounded uncertainty so that the real system behaves as the nominal one.

To do so, in particular, a second-order Sub-Optimal Sliding Mode (refer to Section 2.1.2) is resorted to. The resulting law is in chattering alleviation form when it directly affects the acceleration (*Case 1*) but also directly suitable for *Case 2*, when the relative degree is $r = 2$. It is now worth noticing that in a practical implementation the action of the ISM correction must be exerted at discrete time instants. In this regard, one defines t_s as the ISM sampling time, and therefore the computation of the corrective control term is performed at discrete steps h, of length t_s. At these time instants, the velocity measurements are to be acquired and the total control $u_{i,h}$ is to be applied and held for the successive time step (refer again to Figure 3.2 for a schematic representation).

[11] This implementation is currently under investigation.

Under Assumption 7, the local sliding variables are proposed as

$$\sigma_{i,h} = v_{i,h} - \bar{v}_{i,h} \tag{3.29}$$

where $\bar{v}_{i,h}$ is the nominal velocity of vehicle i, computed relying on model (3.19) starting from the most recent previous MPC sampling time instant, i.e.

$$\bar{v}_{i,h} = v_i(kT_s) + \int_{kT_s}^{kTs+ht_s} \bar{f}_v(\bar{v}_i(t), u^o_{i,k})\ dt \tag{3.30}$$

Then, for the two considered cases, the total control input to be used during the h-th time step is

$$u_{i,h} = (u^o_{1_i,k} + u_{ism_i,h}) + u^o_{2_i,k} = \bar{u}_{i,h} + u_{ism_i,h} \tag{3.31}$$

while (3.19) is left evolving under the nominal

$$\bar{u}_{i,h} = u^o_{1_i,k} + u^o_{2_i,k}, \quad \forall h\ :\ kT_s \leq ht_s < (k+1)T_s \tag{3.32}$$

The next propositions hold, respectively, for the two considered cases. Notice that they are stated for simplicity in continuous time.

Proposition 1. *In Case 1, for the generic vehicle i and for a choice of K_i as in Equation* (3.37)*, if the corrective term in Equation* (3.31) *is selected as*

$$u_{ism_i,h} = u_{ism_i}(kT_s) - \int_{kT_s}^{kTs+ht_s} K_i sign\left(\sigma_i(t) - \frac{\sigma_i^*}{2}\right)\ dt \tag{3.33}$$

where σ_i^* is the value of $\sigma_i(t)$ at the last time instant when $\dot{\sigma}_i(t) = 0$, the real velocity evolution tracks in a finite time the nominal one, predicted relying on model (3.19)*.*

Proof. The formal proof of the finite-time convergence for the Sub-Optimal Sliding Mode Control algorithm is given in [20]. Therefore, it suffices to verify that in the present case the needed hypothesis hold. Let us derive the expression of the derivatives of $\sigma_i(t)$, namely

$$\begin{aligned} \dot{\sigma}_i(t) &= \dot{v}_i(t) - \dot{\bar{v}}_i(t) \\ &= \frac{1}{m_i}\left(u_{ism_i}(t) - F_i^*(t) + \delta(t)\right) \end{aligned} \tag{3.34}$$

with $F_i^*(t) = F_{loss_i}(t) - \bar{F}_{loss_i}(t)$ a time-dependent component, locally bounded by $\bar{F}_i^* \geq 0$ and with first time-derivative locally bounded by $\hat{F}_i^* \geq 0$, since in practice velocities and accelerations can only assume values in a closed set. Therefore,

$$\ddot{\sigma}_i(t) = \frac{1}{m_i}\dot{u}_{ism_i}(t) + \frac{1}{m_i}(\dot{\delta}_i(t) - \dot{F}_i^*) \tag{3.35}$$

Introducing also Assumption 7, one has that

$$\frac{1}{m_i}\left|\dot{\delta}_i(t) - \dot{F}_i^*\right| \leq \frac{1}{m_i}\left(\hat{\Delta}_i + \hat{F}_i^*\right) \tag{3.36}$$

so that (3.33) enforces a sliding motion provided that

$$K_i > 2(\hat{\Delta}_i + \hat{F}_i^*) \tag{3.37}$$

Once attained $\sigma_i(t) = 0$, at time instant t_f, $\bar{v}_i(t) = v_i(t)\ \forall t \geq t_f$, which concludes the proof. □

During the sliding mode, since $\bar{v}_i(t) = v_i(t)$, also $F_i^*(t) = 0\ \forall t \geq t_f$ holds. Relying on the concept of equivalent control [207], one can then infer that

$$u_{ism_i}(t) \simeq F_i^*(t) - \delta_i(t) = -\delta_i(t) \leq \Delta_i \tag{3.38}$$

holds in Filippov's sense and therefore in (3.28a) κ must be chosen larger than Δ_i.

In order to guarantee that $|u_{ism_i}(t)| \leq \kappa$ also during the reaching phase (where, in general, this relationship could not hold in view of the fact that (3.38) is not in place), a constrained formulation can be resorted to. Specifically, one can adopt the constrained Sub-Optimal SOSM algoritm proposed in [68], which modifies the usual S-SOSM law in Equation (2.36) leading to

$$\dot{u}_{ism_i}(t) = \begin{cases} -K_i sign(\sigma_i(t) - \frac{\sigma_i^*}{2}) & \text{if} \quad |u_{ism_i}(t)| < \kappa \\ -K_i sign(u_{ism_i}(t)) & \text{if} \quad |u_{ism_i}(t)| \geq \kappa \end{cases} \tag{3.39}$$

in place of (3.33). The proof of Proposition (1) still holds, in view of the convergence proof provided in [68] and the choice of κ.

Proposition 2. *In Case 2, for the generic vehicle i and for a choice of K_i as in Equation* (3.42)*, if the corrective term in Equation* (3.31) *is selected*

Table 3.1: Nominal vehicles parameters

m [Kg]	$C_a \times S$ [m^2]	C_r	g_r	ρ [kg/m^3]
1200	0.8	0.008	10	1.22
η_m	η_t	η_b	τ	$\eta_\mu \ \forall \mu$
0.75	0.85	0.95	0.05	$\eta_m \eta_t$

Table 3.2: Simulation Parameters

N	T_s [s]	t_s	t_{CTH} [s]	K [N]
10	2	0.01	3	350
F_{min} [N]	F_{max} [N]	d_{min} [m]	d_{max} [m]	v_{max} [m/s]
-6500	6500	4	100	50

as

$$u_{ism_i,h} = -K_i sign\left(\sigma_{i,h} - \frac{\sigma_i^*}{2}\right) \tag{3.40}$$

the real velocity evolution tracks in finite time the nominal one, predicted relying on model (3.19)*.*

Proof. Similar argumentations as the ones given above can be used also in this case, where

$$\begin{aligned}\ddot{\sigma}_i(t) = &\frac{1}{m_i\tau_i}\left(\bar{F}_{in_i}(t) - F_{in_i}(t) + \gamma_i(t) + \tau_i\left(\dot{\delta}_i(t) - \dot{F}_i^*\right)\right) \\ &+ \frac{1}{m_i\tau_i}u_{ism_i}(t)\end{aligned} \tag{3.41}$$

with $|\bar{F}_{in_i}(t) - F_{in_i}(t)|$ locally bounded by a certain known positive constant ΔF_{in_i}, since $\bar{F}_{in_i}(t)$ can never grow unbounded in practice. In order to enforce finite-time convergence, the following choice

$$K_i > 2[(\Delta F_{in_i} + \Gamma_i + \tau_i(\hat{\Delta}_i + \hat{F}_i^*)] \tag{3.42}$$

must be made. □

In this case, the κ term in Equation (3.28a) can be simply chosen such that $\kappa_i > K_i$. Moreover, notice how in (3.42) the required control effort decreases with τ_i. In other words, one needs lower control efforts with more "responsive" actuators, according with intuition.

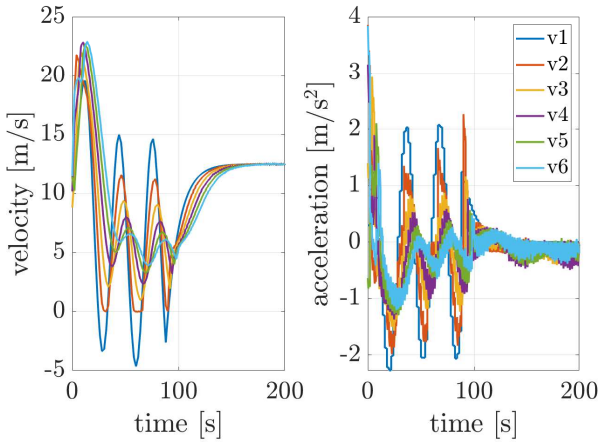

Figure 3.3: *Case 1:* Velocity and acceleration profiles for the vehicles in the platoon, optimal control only.

3.3.3 Simulation Results

A scenario is proposed where the platoon is composed of 6 vehicles, considered here as having all the same nominal dynamics parameters (summarized in Table 3.1) and the settings of the local control schemes reported in Table 3.2. Sinusoidal uncertainty is injected into the vehicle dynamics with the aim of simulating the previously mentioned mismatches between the models and the real systems, as well as possible external forces arising from actuation lags, unaccounted nonlinearities, etc. Specifically, the following shifted low-frequency sinusoid is employed, on which random uniform noise is superimposed

$$\beta_{i_1} + \beta_{i_2} * \left[sin\left(\frac{1}{\beta_{i_3}} t + \beta_{i_4} \right) + r_i(t) \right] \tag{3.43}$$

both for $\delta(t)$ and $\gamma(t)$, where all the parameters β_i are constants randomly picked for each of the vehicles, while $r_i(t)$ is a uniform random variable. In particular, the values are taken such that $\beta_{i_1} \in [-150; 450]$, $\beta_{i_2} \in [0; 450]$, $\beta_{i_3} \in [1; 11]$, $\beta_{i_4} \in [0; 5]$, $r_i(t) \in [0; 0.25]$, and the resulting injected uncertainty is as the one reported in Figure 3.4.

As one can see in Figure 3.3, the maneuver considered here is designed so that the leader initially follows a sinusoidal velocity. Then, it starts to cruise at an almost constant velocity for the rest of the time. All the vehicles start

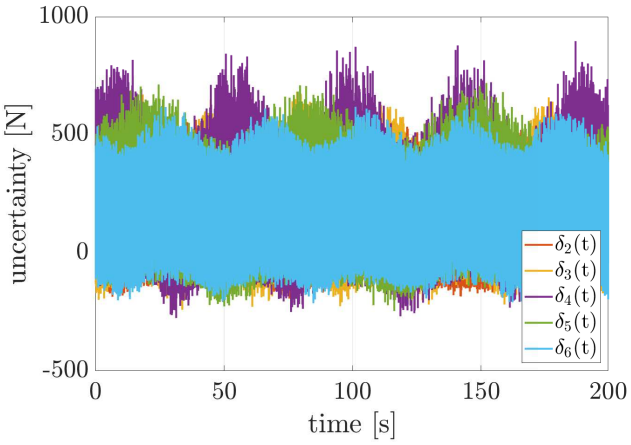

Figure 3.4: Example of the uncertainty used in simulation.

at random initial positions, with random initial velocities. Throughout the simulation, it is evidenced that the vehicles are able to merge into a platoon (see Figures 3.5 and 3.6). In the former phase, the shape of velocity of the followers is evidently smoother than that of the leader, and so is the acceleration. Thus, an overall decrease in the energy waste can reasonably be inferred as the consequence of the underlying behavior of the DMPC controllers.

Notice how, for the sake of the simulation, the leader follows a velocity profile that for some time becomes negative[12] (see Figure 8). While this does not represent a likely scenario, such behavior is enforced to highlight the effectiveness of the proposed strategy even in more extreme conditions. Despite that, it can be evidenced how the positive velocity constraint is kept effectively by all of the followers.

During the second phase, in which the platoon instead cruises, coherence is enforced by the introduction of the ISM correction term, as it is evidenced in Figure 3.7. The distances between vehicles are almost identical in both cases when the robust controller (compare Figures 3.5(b) and 3.6(b)) is employed, highlighting the insensitivity of the proposed scheme to uncertainty in spite of the fact that the MPC sampling time is as high as $T_s = 2s$ and could be in principle increased even more.

[12]This is not in contrast with Assumptions 9 and 8, since the leader is not controlled in this case.

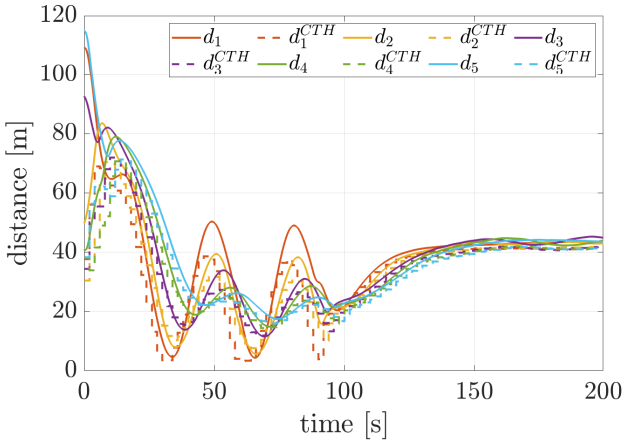

(a) Optimal control only.

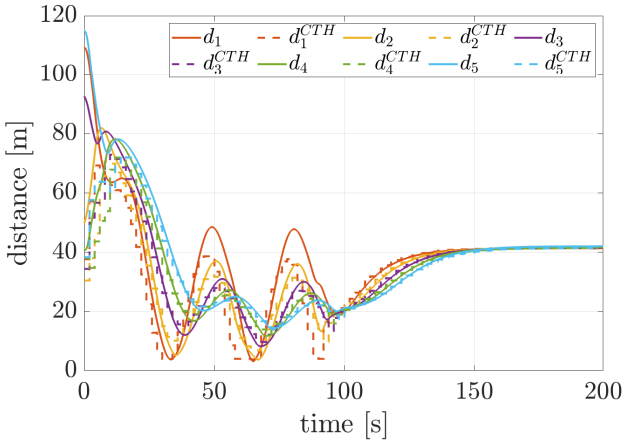

(b) ISM-robustified optimal control.

Figure 3.5: *Case 1:* Distances between the vehicles. Solid lines refer to actual distances, dashed ones are the respective CTH references.

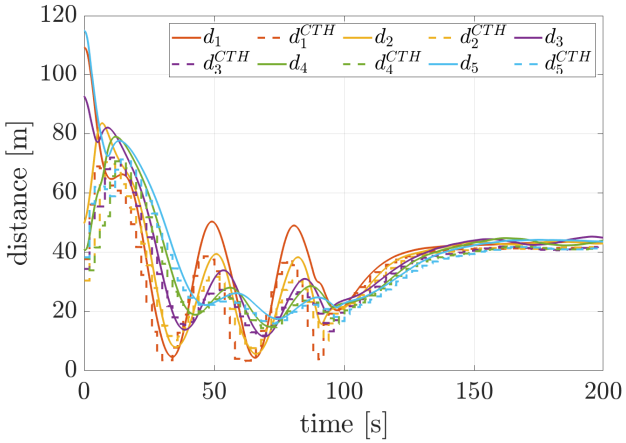

(a) Optimal control only.

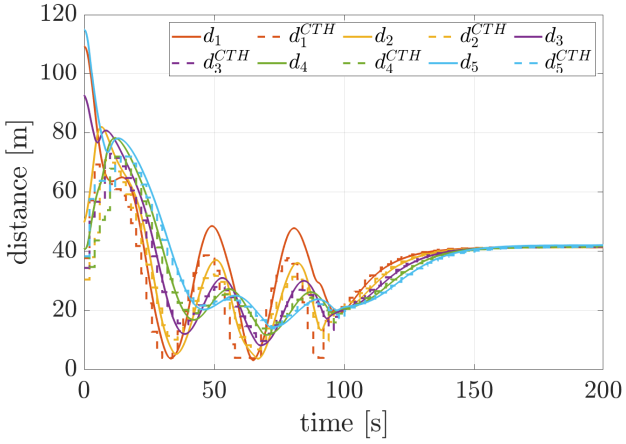

(b) ISM-robustified optimal control.

Figure 3.6: *Case 2:* Distances between the vehicles. Solid lines refer to actual distances, dashed ones are the respective CTH references.

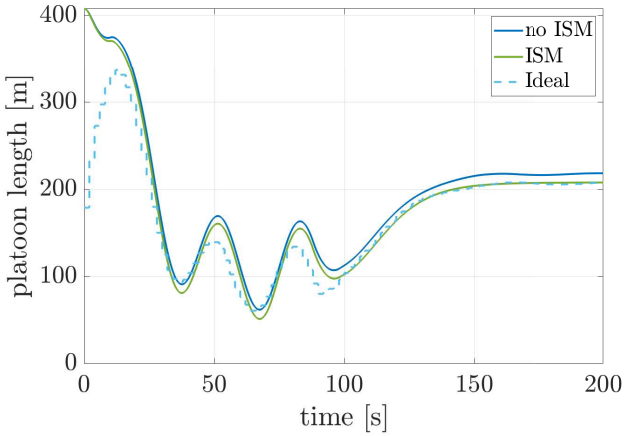

(a) *Case 1.*

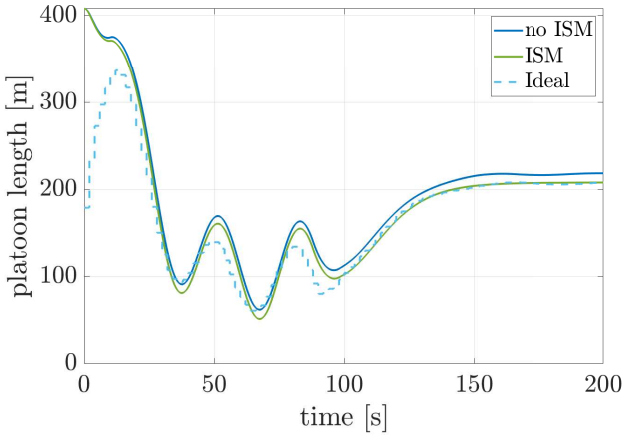

(b) *Case 2.*

Figure 3.7: Total platoon length. The oscillations which appear in the second half of the maneuver, which are more and more present as the number of vehicles increase and represent lack of coherence, are canceled by the ISM.

3.4 Second-Order Sliding Modes Generation for Robust Disturbance String Stable Platoon Control

As a second possible solution to the problem of robust platoon control, in the following discussion original results are reported evidencing how the generation of second-order sliding modes, locally in the vehicles composing the platoon, can lead to robust control in terms of both local and string stability. In particular, the results are shown to be rather general: on one hand, they hold for vehicles described by the model in (3.5), which encompasses almost all the longitudinal dynamics descriptions adopted in the literature and the possible uncertainties (both matched and unmatched). On the other hand, as it will be made evident in the remainder of this section, it is proved that the adoption of a special formulation for the (local) sliding variables guarantees a very general form of string stability. This latter considers both non-null initial perturbations and time-varying uncertainty affecting the dynamics of the vehicles. Specifically, it is shown that the resulting platoon is Disturbance String Stable, as per the Definition 2 reported below.

A novel spacing policy is adopted, based on the idea that in some cases the tracking of a desired velocity prescribed in space would be more suited for the particular application. Especially in the presence of heavy-duty vehicles, in fact, there may be for instance situations in which high road slopes can lead to input power saturation. This, in turn, implies perturbations in the velocity (and, as a consequence, in the position) of the vehicles. This leads to the undesirable possibility of having a too high required velocity in a portion of the road where it cannot be physically reached, thus disrupting the overall performance.

To overcome this issue, the adoption of a policy able to pursue at the same time a predefined inter-vehicle distance while tracking a reference velocity in space is proposed. Namely, the considered objective is that of establishing

$$d_i^*(t) = d_s \tag{3.44}$$

$$v_i(t) \to v_{ref}(s_i(t)) \tag{3.45}$$

with $v_{ref}(s(t))$ a space-dependent reference velocity common to all the ve-

hicles. The following assumption on such velocity reference is made:

Assumption 10. *The designed velocity $v_{ref}(s)$ must be twicely differentiable in time, with*

$$|\dot{v}_{ref}(s)| \leq V_1, \quad |\ddot{v}_{ref}(s)| \leq V_2 \tag{3.46}$$

for some known positive constants V_1 and V_2.

Remark 9. *The policy in Equations* (3.44) *and* (3.45) *is based on considerations made in [30], where the authors propose a Delay-Based strategy which reads as*

$$s_i^*(t) = s_{i-1}(t - \Delta t) \tag{3.47}$$

with $s_i^*(t)$ as the reference position for vehicle i and $\Delta t > 0$ the chosen time delay. In the mentioned work, it is shown that the proposed control strategy (which is designed in the spatial domain) is able to enforce both (3.47) *and* (3.45) *at the same time. As a consequence, the inter-vehicle distance varies when the velocity $v_{ref}(s(t))$ changes. With the choices suggested in this Dissertation, instead, a prescribed distance is pursued as the main control objective and, thus, is the consequent time delay which is possibly subject to changes.*

The task of robustly achieving (3.44) while tracking (3.45) in spite of the disturbances (as modelled in (3.5)) is the main aim of the work developed in the remaining of this discussion. In addition, the novel notion of Disturbance String Stability (DSS, introduced in [30]) is employed to study the string stability of the resulting platoon, which allows one to consider non-zero initial conditions as well as the effects of exogenous disturbances acting on a cascade of interconnected systems. Thus, it provides a great tool for the assessment of platoon control systems performance, with particular reference to string stability. To formally introduce the notion of DSS for cascades of $N + 1$ interconnected systems (platoons, in this case), systems in the form

$$\begin{cases} \dot{x}_0(t) = f(x_0(t), 0, w_0(t)) \\ \dot{x}_i(t) = f(x_i(t), x_{i-1}(t), w_i(t)) \end{cases} \tag{3.48}$$

are considered for $i = 0, \cdots, N$. In Equation (3.48), $x_i(t) \in \mathbb{R}^n$, and $w(t) =$

$[w_i(t) \cdots w_N(i)]^T$ represents a generic disturbance vector.

The following definition, rephrased here for the sake of the reader's convenience, introduces formally the concept of Disturbance String Stability (DSS) [30, Def. 3]

Definition 2. *System* (3.48) *is said to be disturbance string stable (DSS) if there exist functions* $\bar{\beta}$ *and* $\bar{\sigma}$ *of class* $\mathcal{KL}$ *and* $\mathcal{K}$ *respectively, and constants* $\bar{c} > 0$, $\bar{c}_w > 0$ *such that, for any initial condition* $x_i(t_0)$ *and disturbance* $w_i(t)$ *such that*

$$X = \sup_i |x_i(t_0)| < \bar{c}, \quad W = \sup_i ||w_i(t)||_\infty^{[t_0,t]} < \bar{c}_w \tag{3.49}$$

hold, the solution $x_i(t)$ *exists for all* $t \geq t_0$ *and is such that*

$$\sup_i |x_i(t)| \leq \bar{\beta}\left(X, t - t_0\right) + \bar{\sigma}\left(W\right) \tag{3.50}$$

for $i = 0, \cdots, N$, *where* $N \in \mathbb{N}$. *If, moreover,* $\bar{c}$ *and* $\bar{c}_w$ *can be taken as* $\bar{c} = \bar{c}_w = \infty$, *then the platoon is said to be globally disturbance string stable (GDDS).*

Remark 10. *The Definition 2 allows to consider both the effects of initial state perturbations and external disturbances at the same time, and can be seen as a sort of input-to-state stability for the entire platoon system. In particular, one can see that in absence of disturbances (i.e. for* $w_j = 0,\ j = 0, \cdots, N$*), the definition coincides with that of the classical asymptotic string stability formerly introduced in [196].*

The next theorem [30, Th. 2], reported here in a simplified form sufficient for the particular considered case, can be used to prove DSS on the basis of local properties. It will be useful in the remaining of the discussion.

Theorem 3. *Consider system* (3.48) *and let each vehicle* i *be input-to-state stable with respect to the same inputs* $x_{i-1}(t)$ *and* $w_i(t)$, *i.e. there exist a function* β_x *of class* $\mathcal{KL}$, *and functions* γ_x *and* σ_x *of class* $\mathcal{K}_\infty$ *such that, for some constants* $c > 0$ *and* $c_w > 0$ *such that*

$$|x_i(t_0)| < c, \quad ||x_{i-1}(t)||_\infty < c, \quad ||w_i(t)||_\infty < c_w \tag{3.51}$$

hold, the relationship

$$\begin{aligned} |x_i(t)| \leq \beta_x(|x_i(t_0)|, t - t_0) + \gamma_x(||x_{i-1}(t)||_\infty^{[t_0,t]}) \\ + \sigma_x(||w_i(t)||_\infty^{[t_0,t]}), \quad \forall t \geq 0 \end{aligned} \tag{3.52}$$

holds too. Then, considering $\sigma_x = 0$, if the function γ_x satisfies

$$\gamma_x(r) \leq \bar{\gamma} r, \quad \forall r \geq 0, \quad \bar{\gamma} < 1 \tag{3.53}$$

the platoon in (3.48) *is DSS. If, in addition, c and c_w can be chosen such that $c = \infty$ and $c_w = \infty$, then the platoon is Globally Disturbance String Stable (GDSS).*

3.4.1 The Proposed Strategy

With the aim of designing a distributed controller achieving conditions (3.44) and (3.45), one may define first the following quantities

$$\Delta_i(t) = s_i(t) - s_{i-1}(t) + d_s \tag{3.54}$$

$$\Delta_i^0(t) = s_i(t) - s_0(t) + id_s \tag{3.55}$$

$$e_i(t) = v_i(t) - v_{ref}(s_i(t)) \tag{3.56}$$

Notice that Equation (3.54) refers to the inter-vehicle spacing error between vehicle i and its predecessor, $i-1$, with respect to the desired distance d_s. Instead, the quantity in (3.55) refers to the distance error between i and the leader, while Equation (3.56) refers to the velocity tracking error.

The leader is considered as controlled, but for it a different choice of the quantities in (3.54), (3.55) and (3.56) must be made due to the fact that its preceding vehicle does not exist. Therefore, relationships

$$\Delta_0(t) = s_0(t) - s_0(t_0) - \int_{t_0}^{t} v_{ref}(s_0(\sigma))\, d\sigma \tag{3.57}$$

$$\Delta_0^0(t) = \Delta_0(t), \quad e_0(t) = v_0(t) - v_{ref}(s_0(t)) \tag{3.58}$$

are introduced and considered.

Proceeding with the design of the local sliding mode controllers, the

proposed sliding variable for the i-th vehicle is to be defined as

$$\zeta_{1,i}(t) = (1-\kappa_0)\Delta_i(t) + \kappa_0\Delta_i^0(t) + \kappa e_i(t) \tag{3.59}$$

with $\kappa > 0$ and $0 \leq \kappa_0 < 1$.

Remark 11. *Note that, for $\kappa_0 > 0$, the information on the leader position is required for every follower. This feature, in view of the discussions proposed in the introductory part of this dissertation, can be enabled through suitable V2V or V2I architectures.*

The pair $\{\zeta_{1,i}(t), u_i(t)\}$ exhibits relative degree $r = 2$ considering relationship (3.5) (see, for instance, [99]) and so it induces a diffeomorphism Ω[13] transforming (3.5) into its normal form ([91]). The choice of considering the spacing error (3.54) is made here for the internal dynamics of the transformed system, so that

$$\Omega\left(\begin{bmatrix} s_i(t) \\ v_i(t) \\ a_i(t) \end{bmatrix}\right) = \begin{bmatrix} \Delta_i(t) \\ \zeta_{1,i}(t) \\ \zeta_{2,i}(t) \end{bmatrix} \tag{3.60}$$

is taken, with

$$\begin{aligned} \zeta_{2,i}(t) &= \dot{\zeta}_{1,i}(t) \\ &= v_i(t) - (1-\kappa_0)v_{i-1}(t) - \kappa_0 v_0(t) \\ &+ \kappa(a_i(t) + \phi_i(t) - \dot{v}_{ref}(s_i(t))) \end{aligned} \tag{3.61}$$

The resulting dynamics, thus, read as

$$\begin{cases} \dot{\Delta}_i(t) & = \frac{1}{\kappa}\left(\zeta_{1,i}(t) - \Delta_i(t) - \Delta_{i-1}^0\right) - e_{i-1}(t) \\ \dot{\zeta}_{1,i}(t) & = \zeta_{2,i}(t) \\ \dot{\zeta}_{2,i}(t) & = a_i(t) + \phi_i(t) - (1-\kappa_0)(a_{i-1}(t) + \phi_{i-1}(t)) \\ & - \kappa_0(a_0(t) + \phi_0(t)) + \kappa(-a_i(t) + \gamma_i(t) \\ & + \dot{\phi}_i(t) - \ddot{v}_{ref}(t)) + \kappa u_i(t) \\ & = h(x_i(t), t) + g u_i(t) \end{cases} \tag{3.62}$$

[13] Ω is guaranteed to exist, at least locally. However, one can see that (3.60) holds also globally in $\mathbb{R}^3 \times \mathbb{R}$ (see [91, Chapter 13] for reference)

which can be used to prove local finite-time convergence to the sliding set $(\zeta_{1,i}(t), \zeta_{2,i}(t)) = 0$ and the subsequent GDDS of the platoon.

Remark 12. *Notice that the dynamics of* $\zeta_{2,i}(t)$ *in* (3.62) *has been kept expressed in the original coordinates, to make the following discussion more intuitive. Anyway, if necessary, an expression in the new coordinate system can be computed straightforwardly by means of the defined diffeomorphism* $\Omega(\cdot)$.

3.4.2 Local Stability

The choice of the particular SOSM control algorithm does not influence the resulting features of the platoon (under the respect of Assumptions 9 and 8) once the motion is established. Similar considerations with respect to these made in the following can be easily carried out to assess the local convergence of different controllers as described in Section 2.1.2. However, for the sake of completeness, the Sub-Optimal strategy (see Section 2.1.2) is proposed and analysed here. Thus, in this case, the next proposition follows:

Proposition 3. *For systems* (3.5) *under Assumptions 7 and 8 and the choice of the sliding variable* (3.59)*, the design of a local controller in the form*[14]

$$u_i(t) = -K sign\left(\zeta_{1,i}(t) - \frac{\zeta^*_{1,i}}{2}\right) \tag{3.63}$$

where $\zeta^*_{1,i}$ *is the last value in time of* $\zeta_{1,i}(t)$ *for which* $\zeta_{2,i}(t) = 0$ *held, with*

$$K > \frac{4(A+\Phi)}{\kappa} + 2\left(A + \Gamma + \hat{\Phi} + V_2\right) \tag{3.64}$$

guarantees the finite-time convergence of $\zeta_{1,i}(t)$ *and* $\zeta_{2,i}(t)$ *to the origin.*

Proof. It is sufficient to evidence that in (3.62), due to the assumptions made, for the dynamics of $\zeta_{2,i}(t)$ conditions

$$\Phi = 2(A+\Phi) + \kappa(A + \Gamma + \hat{\Phi} + V_2) \tag{3.65}$$

$$P_1 = P_2 = \kappa \tag{3.66}$$

[14] See the Sub-Optimal formulation in Section 2.1.2 or [20].

hold. Then, with the choice (3.64), the proof for the establishment of a SOSM follows straightforwardly from the results presented in [20] (considered, in the referred paper, $\alpha^* = 1$). □

Remark 13. *The requirement that $\kappa > 0$ is of primary importance. In fact, $\kappa = 0$ would lead to an increase in the relative degree exhibited by the pair $\{\zeta_{1,i}(t), u_i(t)\}$, while for $\kappa < 0$ an inversion in the sign of the input control action would be produced, leading to instability.*

3.4.3 String Stability

In order to prove (Global) Disturbance String Stability, the zero dynamics obtained for (3.62) during the sliding motion must be considered, leading consequently to

$$\begin{cases} \kappa\dot{\Delta}_0(t) = -\Delta_0(t) \\ \kappa\dot{\Delta}_i(t) = -\Delta_i(t) + (1-\kappa_0)\Delta_{i-1}(t) \end{cases} \tag{3.67}$$

where the condition $\zeta_{1,i}(t) = 0$ is introduced, holding during sliding, together with the relationship

$$\Delta_i^0(t) = \Delta_i(t) + \Delta_{i-1}^0(t) \tag{3.68}$$

which is easily verifiable by substitution.

Notice that the velocity tracking error can be expressed as a function of $\Delta_i(t)$, as a consequence of the dynamic order reduction (see Section 2.1). Namely,

$$e_i(t) = -\frac{1}{\kappa}\left(\Delta_i(t) - \kappa_0\Delta_{i-1}^0(t)\right) \tag{3.69}$$

holds as an algebraic constraint.

The following theorem summarizes the results obtained so far:

Theorem 4 ([224])**.** *Consider a platoon of vehicles described by the (perturbed) dynamics in* (3.5) *under Assumptions 7 and 8, controlled by a properly designed SOSM law. Then, the choice of the sliding manifold* (3.59)*, with $\kappa > 0$ and $0 \leq \kappa_0 < 1$, guarantees the establishment of a Globally Disturbance String Stable platoon with respect to the objectives specified in* (3.44) *and* (3.45)*.*

Proof. From system (3.5), by means of the diffeomorphism (3.60), (3.62) can be obtained. The design of a proper SOSM control law, which always can be found due to the assumptions made (an example is given by Proposition 3) guarantees that the sliding variable and its first time derivative vanish in a finite time. Then, the dynamics of the system can be completely characterized by the reduced order dynamics in (3.67) and the algebraic constraints obtained from $\zeta_{1,i} = 0$ and $\zeta_{2,i} = 0$. In particular, expression (3.69) holds for the velocity tracking error. Solving (3.67) in time (here only the followers will be considered, since for the leader an obviously exponentially stable dynamics is in place), one obtains

$$|\Delta_i(t)| \leq |e^{-\frac{t-t_0}{\kappa}}||\Delta_i(t_0)| + (1-\kappa_0)\|\Delta_{i-1}(t)\|_\infty^{[t_0,t]} \tag{3.70}$$

Therefore, one can easily derive that the conditions required by Theorem 3 hold with

$$\beta_x = |e^{-\frac{t-t_0}{\kappa}}||\Delta_i(t_0)|, \quad \gamma_x = \bar{\gamma}\|\Delta_{i-1}(t)\|_\infty^{[t_0,t]} \tag{3.71}$$

Since $\bar{\gamma} = (1-\kappa_0) < 1$, Disturbance String Stability follows. Moreover, the constant c can be chosen as $c = \infty$, and thus platoon (3.5) is Globally Disturbance String Stable. The velocity tracking error $e_i(t)$ depends algebraically from $\Delta_i(t)$ and $\Delta_{i-1}^0(t)$, and therefore it is sufficient to see that it is bounded and decreasing for bounded and decreasing $\Delta_i(t)$ and $\Delta_{i-1}^0(t)$. □

Remark 14. *Theorem 4 established the possibility of obtaining a GDSS platoon by means of any SOSM Control algorithm, independently of the actually adopted strategy. Proposition 3 gives sufficient conditions for the employment of the Sub-Optimal law.*

Remark 15. *The uncertainty considered in* (3.5)*, which comprises both matched and unmatched components, is entirely compensated by the adopted control strategy. In fact, to counter the term $\gamma_i(t)$ (matched uncertainty), a proper choice of the gain as in* (3.64) *is sufficient. The $\phi_i(t)$ term (unmatched) is instead compensated through a dynamic adjustment of the acceleration, and therefore it does not appear anymore in the dynamics of the velocity. In particular, one has that*

$$a_i(t) = -\frac{1}{\kappa}\left(e_i(t) - (1-\kappa_0)e_{i-1}(t) - \dot{v}_{ref}(t)\right) + \phi(t) \tag{3.72}$$

which remains bounded for bounded velocity errors. Additionally, it is worth noticing how higher values of κ result in lower values of the acceleration, which can be controlled also acting on the first time derivative of the prescribed velocity $\dot{v}_{ref}(t)$ so as to take into account the saturations naturally present in the vehicles actuators.

3.4.4 Simulation Results

In the following, simulation results obtained applying the control system previously described to a platoon of 6 vehicles (a leader and 5 followers) are reported. The initial velocities and displacements are randomly generated with the aim of presenting a meaningful scenario. The parameters for the (sinusoidal) injected uncertainties are sampled from uniform random distributions (their plots are reported in Figures 3.8 and 3.9). The goal inter-vehicle distance is chosen as $d_s = 10\,m$, and the reference velocity $v_{ref}(s(t))$ is generated in the space domain according to the function depicted in Figure 3.10[15]. The values $\kappa = 1$ and $\kappa_0 = 0.5$ are selected for the parameters of the distributed controllers. As visible in Figure 3.11, the local controllers are able to produce local convergence to the selected sliding manifolds in a finite time, thus effectively enforcing the sliding modes.

The consequent evolution of the quantities $\Delta_i(t)$ and $v_i(s)$ is reported in Figures 3.12 and 3.13 (where also the reference velocities are plotted, in the time domain) for all the considered vehicles. The validity of the present proposal in robustly attaining the desired platoon features is made evident: in particular, besides the asymptotic convergence to zero of the spacing errors, it is possible to notice how they do not amplify in the upstream direction, making the GDSS of the proposed strategy evident.

[15]Notice how the transition between the different constant reference velocities is smooth, so that Assumption 8 is well respected.

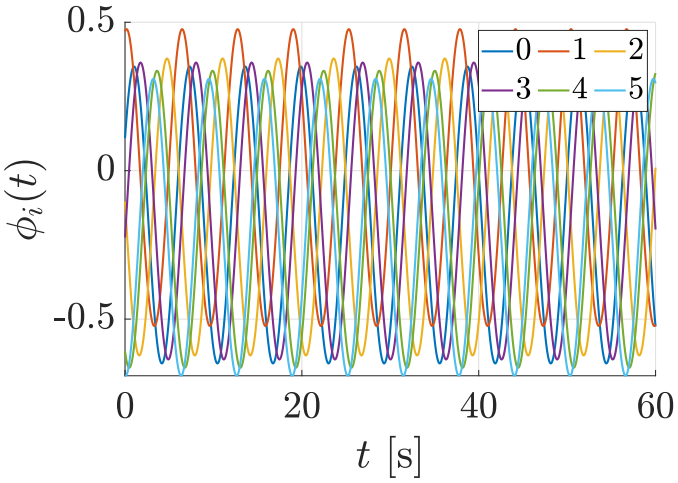

Figure 3.8: Disturbances $\phi_i(t)$. *From [224].*

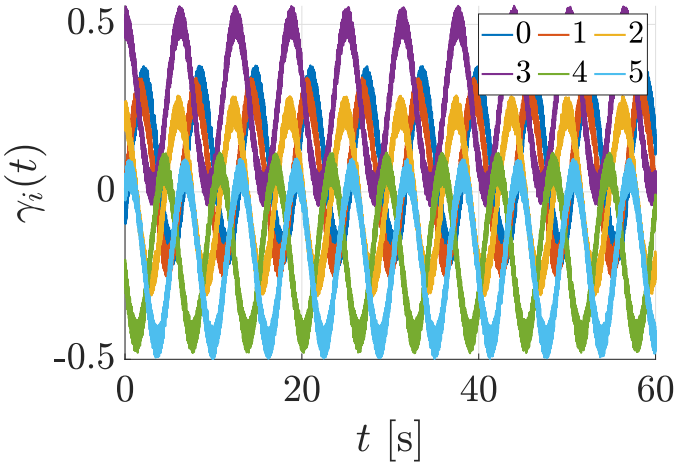

Figure 3.9: Disturbances $\gamma_i(t)$. *From [224].*

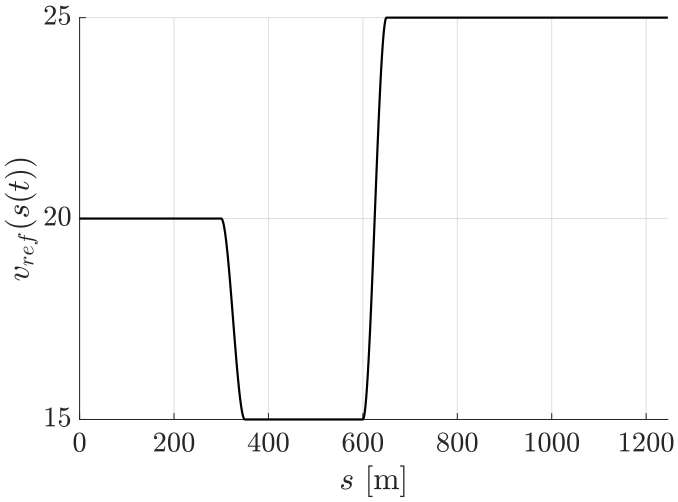

Figure 3.10: Reference speed in the space domain. *From [224].*

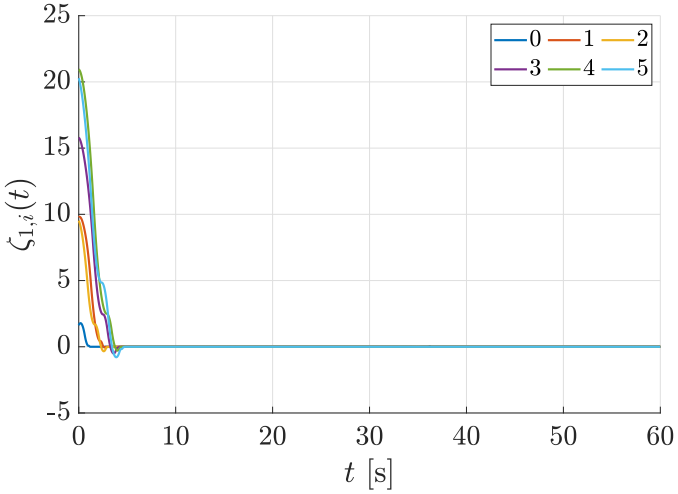

Figure 3.11: Local sliding variables. *From [224].*

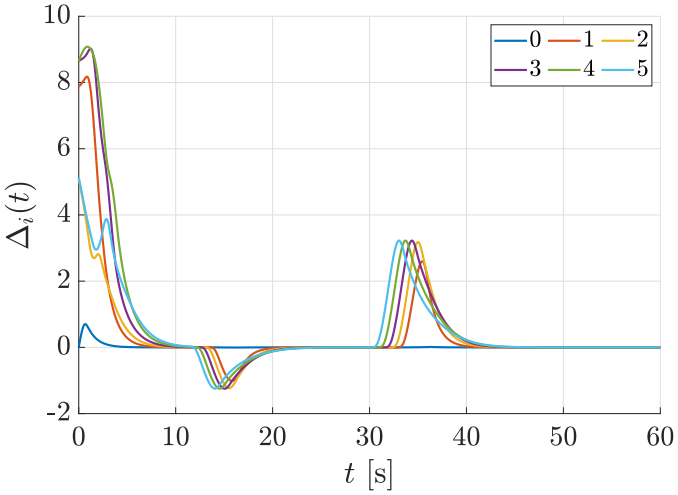

Figure 3.12: Spacing errors. *From [224].*

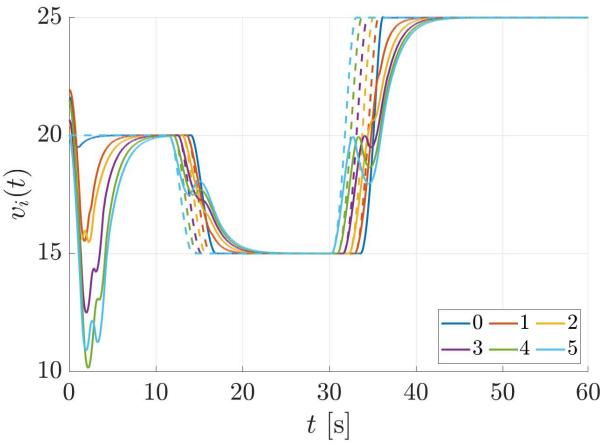

Figure 3.13: Vehicles velocities. *From [224].*

Chapter 4

Formation Control on Highways

This Chapter presents a novel algorithm for the on-line creation and dynamic reshaping of heterogeneous formations of automated ground vehicles in highways scenarios, which relies upon a two-step iterative procedure. The controlled vehicles are required to be CAVs, or semi-automated vehicles able to exhibit CAV capabilities on demand. A global coordinator must exist, that is able to communicate with every involved vehicle and perform basic coordination operations. This latter can easily be integrated in a multi-level traffic control architecture which computes on-line the required formation size, shape, position and velocity. A preliminary implementation of the algorithm is published in [221], where its validity has been assessed experimentally on small-scale trucks (as reported in Section 4.3), while a more extensive proposal is developed in [227].

Before proceeding with the description of the adopted strategy, in Section 4.1 the so-called *single-track model* is presented[1], which is a commonly adopted model for the vehicles longitudinal and lateral dynamics. Then, in Section 4.2, the original approach described above is presented and discussed, providing experimental results in a preliminary case and simulation results in more advanced scenarios.

[1] A dynamic model for the vehicles dynamics is here employed due to the fact that high-speed lateral maneuvers excite complex behaviors which need to be considered. On the other hand, the single-track model is simple enough to be usually suitable for on-line prediction in the MPC controllers.

4.1 Vehicles Dynamics Modelling

The Single-Track model [95, 76, 162] (often informally referred to also as "bicycle model") is a commonly adopted simplified 3-states model for both the longitudinal and lateral dynamics of non-holonomic ground vehicles. It is derived assuming that no moment is generated by differences among the forces applied on the two wheels of the same axle, and that the steering angles are equal for the two front wheels. As a direct consequence, the vehicles can be considered as formally having a unique wheel for each axle (from which the name follows). The resulting dynamic equations, which describe the longitudinal and lateral velocities $v_x(t)$ and $v_y(t)$, respectively, and the yaw angle velocity $r(t)$ (the *yaw rate*) in the vehicle reference frame are then

$$\begin{cases} \dot{v}_x(t) = v_y(t)r(t) + \frac{1}{m}\left(F_x(t) - F_{loss}(t)\right) \\ \dot{v}_y(t) = -v_x(t)r(t) + \frac{1}{m}\left(F_{y,f}(t) + F_{y,r}(t)\right) \\ \dot{r}(t) = \frac{1}{J_z}\left(l_f F_{y,f}(t) - l_r F_{y,r}(t)\right) \end{cases} \tag{4.1}$$

where m and J_z are, respectively, the mass and the moment of inertia of the vehicle. The inputs are the total longitudinal forces $F_{l,f}(t)$ and $F_{l,r}(t)$ exerted, respectively, by the front and rear wheels and the steering angle $\delta(t)$. The total longitudinal force $F_x(t) = F_{x,f}(t) + F_{x,r}(t)$ is then obtained projecting the input forces exerted by the wheels with respect to the vehicle reference frame, induced by the steering angle $\delta(t)$, i.e.

$$F_{x,f}(t) = F_{l,f}(t)\cos(\delta(t)) + F_{c,f}(t)\sin(\delta(t)) \tag{4.2}$$

$$F_{x,r}(t) = F_{l,r}(t) \tag{4.3}$$

Similarly to (4.2), the lateral forces $F_{y,f}(t)$ and $F_{y,r}(t)$ are obtained projecting the cornering forces $F_{c,f}(t)$ and $F_{c,r}(t)$ in the vehicle reference frame. These are obtained resorting to a linear description of the tire-road interaction forces [76] in terms of the wheels sideslip angles $\alpha_f(t)$ and $\alpha_r(t)$, i.e.

$$F_{c,f}(t) = -\alpha_f(t)C_f, \quad F_{c,r}(t) = -\alpha_r(t)C_r \tag{4.4}$$

where

$$\alpha_f(t) = \beta(t) + l_f \frac{r(t)}{v(t)} - \delta(t) \tag{4.5}$$

$$\alpha_r(t) = \beta(t) - l_r \frac{r(t)}{v(t)} \tag{4.6}$$

with

$$v(t) = \sqrt{v_x^2(t) + v_y^2(t)}, \quad \beta(t) = \arctan\left(\frac{v_y(t)}{v_x(t)}\right) \tag{4.7}$$

and C_f, C_r are the cornering stiffness coefficients for the front and rear wheels. The $F_{loss}(t)$ term in Equation (4.1) accounts for the aerodynamic and rolling resistance losses as in Equation (**??**), while l_f and l_r are, respectively, the distances between the front and rear axle and the vehicle center of mass.

Remark 16. *In the following of the discussion, the assumption that the input forces $F_{l,f}(t)$ and $F_{l,r}(t)$ are actually exerted on the corresponding axles will be made. In this respect, it is worth noticing that, in practice, the actually controllable inputs are torques, which interact with the ground and generate forces according to the tire-road interaction characteristic and the wheels dynamics. Thus, the reasonable assumption that fast-enough low-level slip controllers are available is usually made (see, e.g. [4]) so that the input (reference) forces can safely be confused with these actually exerted. Regarding the cornering forces, in standard conditions ($\beta \simeq 0$) the linearity assumption is well respected. Nevertheless, low-level stability control systems can be included to ensure that the cornering tire-road characteristic curve remains in the linear region during all the maneuvers.*

Since equations (4.1) describe quantities in the vehicle reference frame, in order to obtain the positions in the global reference frame the following

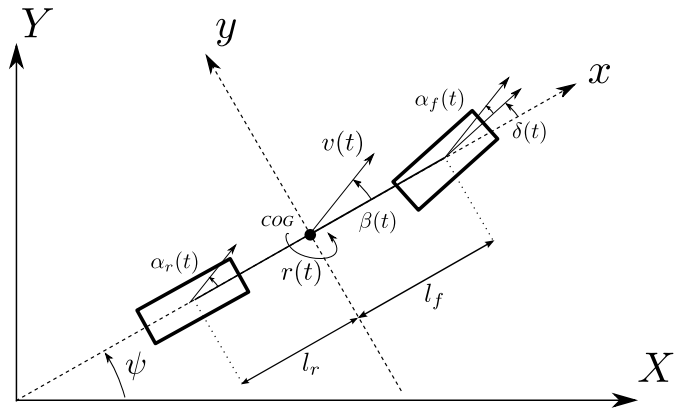

Figure 4.1: Schematic representation of the single track model. In this depiction, the reference frame XY is intended as being the global (world) reference frame, while the reference xy is attached to the vehicle. Additionally, COG denotes the center of gravity of the vehicle, assumed at the center of the vehicle with respect to the y axis.

kinematic model is considered[2]:

$$\begin{cases} \dot{p}_x(t) = v_x(t)\cos(\psi(t)) - v_y(t)\sin(\psi(t)) \\ \dot{p}_y(t) = v_y(t)\cos(\psi(t)) + v_x(t)\sin(\psi(t)) \\ \dot{\psi}(t) = r(t) \end{cases} \tag{4.8}$$

Please refer to figure 4.1 for a comprehensive schematic representation of the adopted model.

[2]The assumption $\beta \simeq 0$ is here made, since it is the standard condition in absence of sharp maneuvers intended to generate a drifting behavior of the vehicle. Additionally, low-level stability controllers can ensure the condition is kept (see Remark 16)

4.2 Two-Step Event-Triggered Iterative Algorithm for Formation Control in Highway Scenarios

The core idea of the present formation control strategy resides in the construction of a virtual reference frame attached to a virtual leader, which enables the construction of a (virtual) grid covering the involved portion of the highway and allowing for the subsequent two-step iterative procedure. The two stages involve a discretized and a continuous space framework which allow to flexibly address different problems. Specifically:

1. During the first stage, a discrete subdivision of the considered portion of the highway is performed and exploited to find the best path each vehicle would be required to follows in order to reach and join the formation through Dynamic Programming (DP). At this level, cost functions can be specifically designed at runtime to pursue particular requirements or encourage/discourage certain behaviors, for the sake of performance, safety or contingent external factors (for instance, one may want to discourage lane changes to reduce lateral maneuvers, or encourage joins of vehicles from lanes which may become unavailable in the near future). Additionally, an arbitrary number of pseudo-parallel DPs can be specified in order to improve the formation creation performance in terms of duration, without affecting any other aspect of the strategy.

2. The subsequent stage involves the creation of a smooth local trajectory able to move the vehicle along the previously computed (optimal) path, which is then followed making use of Model Predictive Control (MPC) and a single-track vehicle model. At this level safety and comfort can be considered, while taking into account physical constraints specific to the single vehicles.

Among the benefits of such approach, the main ones can be identified in the fact that

- The most critical operations (in terms of duration magnitude and variability) are carried out in a safe environment where only a small subset of controlled vehicles has non-zero relative velocity with respect to the rest of the formation;

- The presented framework possesses a great structural flexibility given by both the iterative and mixed discrete-continuous nature, which make it straightforward to include more advanced features and expand the already present ones or tailor them to specific needs;

- The inclusion of a mechanism to arbitrarily reshape the formation allows one to consider many practical cases (for instance, the restriction of the available road due to e.g. working sites or the dynamic join/leave of particular vehicles), while the adoption of an MPC formulation enables stable high-speed maneuvers.

Notice that, as already discussed in Section 1.1.3, the on-line creation (and reshape) of formations can be seen as a way of introducing moving bottlenecks in highways with aim of regulating the traffic flow. Although this is not the only possible way of exploiting formations of CAVs, in this work the situation in which an high-level traffic controller exists and dictates the characteristics of the formation(s) to be created is made.

In the remainder of the chapter, the problem addressed by the proposed algorithm is first formalized (in 4.2.1). Then, the strategy is introduced and thoroughly described in 4.2.2, relying on the model introduced in Section 4.1. At the end, examples of application are provided to highlight the validity of the presented control framework. In particular, in 4.3 an experimental validation carried out on small-scale trucks is presented for a preliminary formulation of the problem, which does not cover the most advanced features. These latter, in fact, have been developed later and validated in simulation during complex high-speed maneuvers, as reported in 4.4.

4.2.1 Problem Statement

In order to formalize the formation control problem under consideration, one may define a highway $H = \{1, 2, \cdots, N_l\}$ as a set of N_l lanes of uniform and constant width w_l, indexed in ascending order by starting from the rightmost lane. A number N of CAVs, which are required to implement autonomous driving features involving both longitudinal and lateral dynamics at high speed, is considered in the set of indices $\mathcal{V} = \{1, 2, \cdots, N\}$. Such vehicles start initially uncontrolled and proceed, scattered on the highway according to usual traffic patterns, with velocities $v_i(t) > 0, i \in \mathcal{V}$.

Due to the need for communication between the vehicles, a reliable information exchange mechanism must be in place through either V2V or V2I architectures, or a mixture of the two. A sufficiently accurate position measurement system (relying for instance on GPS) is also required, while the vehicles need local sensors (or observation systems) to close the MPC feedback loop.

Assumption 11. *The quantities necessary to close the local MPC control loops are readily and precisely available. Similarly, an effective communication is put in place between every vehicle and the formation coordinator*[3]*.*

Remark 17. *In practice, sensors and observers are employed to guarantee the access to such measurements, as these proposed in e.g. [177, 34, 17, 200, 161]. The adoption of such strategies is anyway out of the scope of the present work.*

For the sake of the discussion, a generic framework is adopted where at some point in time t_1 a signal generated by a high-level controller triggers the creation of a formation in a designed area of the highway. The formation is required to cover a certain area, with a specific shape, and proceed at a predefined speed $\bar{v} > 0$ (that is supposed to be constant in the initial phase).

The shape of the formation can be arbitrarily defined, provided that a grid-like underlying pattern is respected. This means that the required formation must be representable by a matrix $G = \{g_{hj}\}$ of dimension $N_l \times L_v$ (with g_{hj} being the element in the h-th row and j-th column), where L_v is the number of subdivisions of the considered space for every lane. It must be greater or equal than the longitudinal extension of the formation itself, and such that an area is covered large enough to comprise all the vehicles in $\mathcal{V}$. Such matrix can then be defined by using zero entries except in positions where a vehicle must be placed to construct the formation. For instance

$$G_1 = \begin{bmatrix} 0 & 0 & 0 \\ 1 & 1 & 0 \\ 1 & 1 & 0 \end{bmatrix}, \; G_2 = \begin{bmatrix} 0 & 1 & 0 & 1 \\ 1 & 0 & 1 & 0 \\ 0 & 1 & 0 & 1 \end{bmatrix} \tag{4.9}$$

[3] As will be evident from the development of the algorithm, it is not necessary that the coordinator is one of the vehicles. In fact, it may also be the infrastructure itself, with the only constraint that a sufficient computational and communication capability is available.

represent a square 2×2 (G_1) and a lattice formation on a highway with 3 lanes (G_2), respectively.

The matrix G can change arbitrarily over time, to dynamically address different objectives. In spite of the generality of such mechanism, practical considerations lead to consider simple shapes, often composed of lines of vehicles of arbitrary length covering the various lanes. The specific case in which the formation covers an arbitrary subset of lanes $\bar{H} \in H$ with lengths specified in number of vehicles is addressed specifically in [225].

In order to translate the matrix representation of the formation in a spatial description, the width of the lanes is naturally exploited in determining the cells width. For the length, an additional parameter $d > 0$ specifying the inter-vehicle distance is considered (see Figure 4.2 for a schematic representation of the concept, where the red dots correspond to the elements of the considered matrix). This latter is crucial in defining the overall length of the formation, and plays an important role in safety: in fact, longer distances lead to an improved safety at the expense of a coarser formation description.

Assumption 12. *The length dL_v of the portion of highway covered by the adopted discretization includes all of the vehicles to consider for control.*

Assumption 13. *All of the vehicles present in the considered region must actually be under control, with the ability of performing the required communication and control tasks.*

Remark 18. *Assumption 13 allows one to effectively implement the strategy presented in this article, but nevertheless in practice it can sometimes be slightly relaxed. For instance, the considered highway H may include only a contiguous subset of physical lanes, so that the ones not considered can be populated and traversed by uncontrolled vehicles. Notice additionally that the vehicles are required to implement a normal operating mode, since emergency situations will not be considered in the present work. Nevertheless, strategies to deal with such extraordinary contingencies are required in practice to be considered and included separately.*

Flexibility and scalability are two crucial characteristics for multi-agent control systems, and therefore are here addressed as specific requirements. The former relates, on one hand, to the possibility for the algorithm to be effective in a broad range of scenarios and, on the other hand, to the

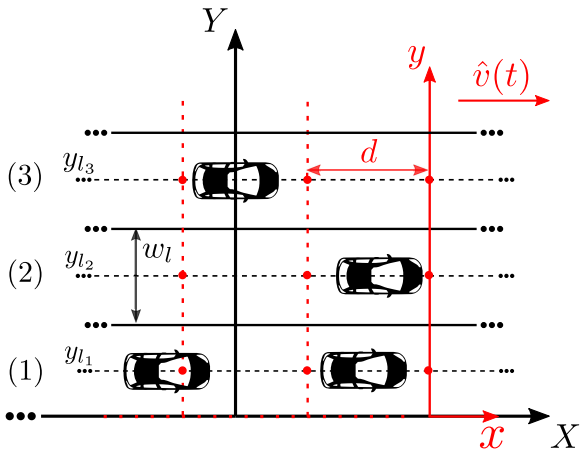

Figure 4.2: A generic three-lanes highway, i.e. $H = \{1, 2, 3\}$.

possibility of implement changes in parts of the algorithm without affecting the others. Scalability is, instead, related to the guarantee of an effective and efficient process in the presence of an arbitrarily high number N of considered vehicles, which should not require major changes in the control architecture both from an algorithmic and an infrastructural point of view.

To formally state the problem, a global reference frame XY is introduced for the highway such that the lanes are parallel to the X axis and the edge of lane 1 coincides with $Y = 0$ (see Figure 4.2). Additionally, a reference frame xy is considered with the same orientation as XY but moving in the positive X direction with velocity $\hat{v}(t) > 0$. In both the frames, the y-position of the center of the j-th lane is

$$Y_{l_h} = y_{l_h} = \frac{w_l}{2} + (h-1)w_l, \ h \in H \tag{4.10}$$

as evident from Figure 4.2. Given all the considerations made in this section, the problem can be summarized as follows:

Problem 3. *Find a scalable (for $N \to \infty$) and flexible control strategy for the set of vehicles $\mathcal{V}$ with positions $p_i(t) = [p_{x,i}(t) \quad p_{y,i}(t)]^T$ with respect to the frame xy such that they converge to a rigid position-based formation specified, for any time instant, by the reference formation matrix $G(t)$. Specifically, after having defined the desired formation in space as the set*

$$\mathcal{F}(G, d) = \left\{\bar{p}_{h,j} = [-(j-1)d \quad y_{l_h}]^T \, \forall (h, j) : g_{hj} = 1\right\} \tag{4.11}$$

with $\sum_{h,j} g_{hj}(t) \leq N$, $\forall t$, *a strategy must be found such that*

$$\forall \bar{p}_{h,j} \in \mathcal{F} \quad \exists! \quad i \in \mathcal{V} \ : \ p_i(t) \to \bar{p}_{h,j} \tag{4.12}$$

and, at the same time,

$$v_i(t) \to \bar{v}(t) > 0, \quad \forall i \in \mathcal{V} \tag{4.13}$$

with $\bar{v}(t)$ *the required speed for the formation, under the constraints*

$$0 < y_i(t) < N_l w_l, \quad \forall i \in \mathcal{V} \tag{4.14}$$

and without collisions between vehicles, independently of their geometrical and dynamical characteristics (heterogeneous formations).

4.2.2 The Proposed Strategy

In this section, the proposed formation control strategy is presented, starting from the generic situation in which, at time t_1, a higher-level control layer selects the parameters G, d, and $\bar{v}$ in order to pursue a particular objective on a specified section of the highway. The whole procedure is composed of two sequential, independent phases: an initialization phase (described in 4.2.3), to be performed once for a set of controlled vehicles, and an iterative phase composed of two successive steps (presented in 4.2.4) which starts after the initialization and remains active throughout the whole control time to provide reshaping capabilities.

An event-triggered approach is adopted to provide an asynchronous activation of the different steps (see Figure 4.3), while a sharp separation is put in place between global procedures (cheaper, carried out by the coordinator) and the local ones (more expensive, implemented in a distributed way at the vehicles level). Specifically, the general strategy is designed such that vehicles receive position references from the coordinator, and trigger it back when specific events occur. An high-level schematic representation of the proposed procedure is presented in Figure 4.4.

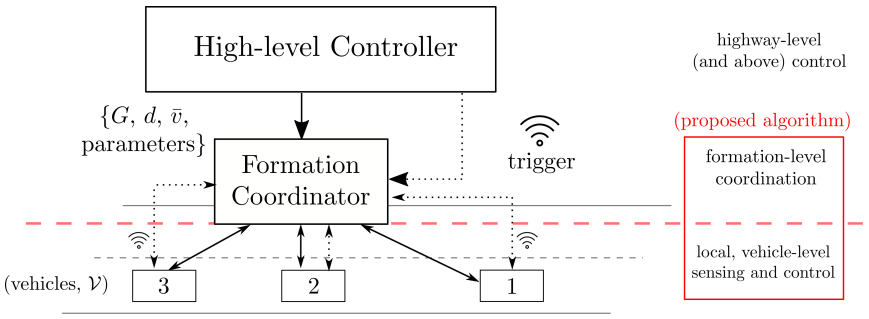

Figure 4.3: Schematic representation of the formation control architecture.

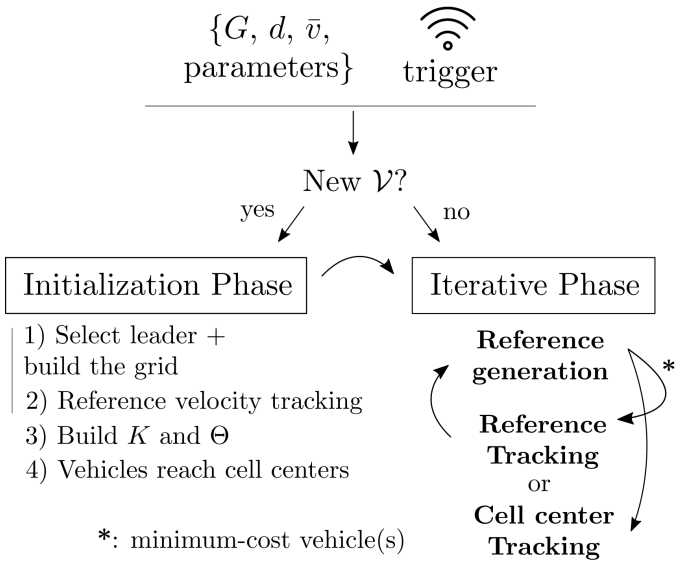

Figure 4.4: Schematic representation of the proposed algorithm, where the specific functioning modes and the information exchange paths are omitted for the sake of clarity.

4.2.3 Initialization Phase

The initialization phase is started as soon as the coordinator receives an update signal from the high-level controller, which also provides the formation parameters. Such phase is crucial in enabling the subsequent iterative phase, and thus it must be performed once for every different selection, i.e. every considered set $\mathcal{V}$, of vehicles. Among them, the vehicle with highest (global) X coordinate is designated as the virtual leader and referred to as vehicle 1 without loss of generality. Then, a virtual grid, which constitutes one of the key concepts of the proposed strategy, is built in the moving reference

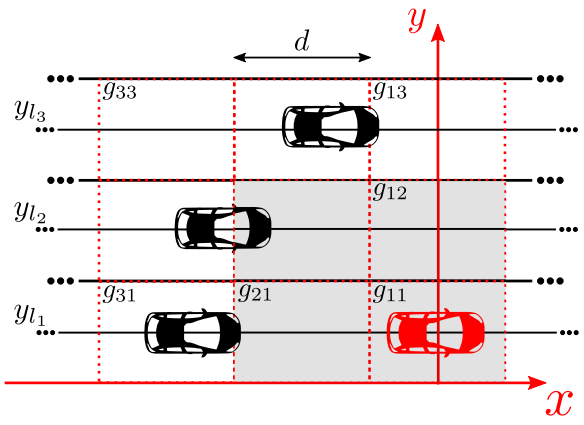

Figure 4.5: Grid designed with $G = G_1$ as in Equation (4.9). The grey cells must be "covered" to obtain the desired formation.

frame xy of the formation (see Section 4.2.1 for its definition). The grid is attached to it in such a way that the x position of the leader $p_{x,1}$ coincides with the center of the cells corresponding to the first row of the matrix G (see g_{11}, g_{12} and g_{13} in Figure 4.5), while the first lane of the highway is occupied by the cells corresponding to the first column of G (see Figure 4.5). This, in turn, means that the grid moves instantaneously with the velocity of the leader, i.e. $\hat{v}(t) = v_1(t)$.

The grid is formally defined in terms of its cells, that are indexed in the space $S = \{1, 2, \cdots, N_l\} \times \{1, 2, \cdots, L_v\}$. A map K is defined, which assigns to every cell the spatial coordinates of its center in the frame xy, i.e.

$$K(h, j) = \begin{bmatrix} -(j-1)d & y_{l_h} \end{bmatrix}^T, \quad (h, j) \in S \tag{4.15}$$

All the vehicles are subsequently required to attain and keep the reference velocity $\bar{v}$, which is constant in this phase and communicating to the coordinator when the objective is attained by means of a trigger signal. This is performed passing to the vehicles successive position references to track, with the x coordinate obtained integrating discretely the required velocity $\bar{v}$ in time. Once a trigger is received from all of the vehicles (meaning that they exhibit no relative velocity with respect to the virtual grid), a static association map $\Theta : S \mapsto \mathcal{V}$ is defined basing on the relationship in (4.15),

such that

$$\Theta(h,j) = i, \quad (h,j) \in S,\ i \in \mathcal{V} \tag{4.16}$$

if vehicle i is the nearest to $K(h,j)$ along the x axis at the time instant in which the evaluation is performed. Subsequently, an occupation map $\Omega : S \mapsto \{0,1\}$ is also introduced, where

$$\Omega(h,j) = \begin{cases} 1 & \text{if } (h,j) \text{ is occupied} \\ 0 & \text{otherwise} \end{cases} \tag{4.17}$$

Notice that the vehicles communicate to the coordinator their position, and this latter performs internally the construction of suitable maps Θ and Ω. All the process occurs at constant velocity $\bar{v}$, so that vehicles maintain the communicated position throughout all of it independently of the time taken to perform computations and communication.

Remark 19. *In practice, possible cases in which overlapping associations could occur must be addressed properly. For instance, if two vehicles concur for cell (h,j), the preceding of the two shall be assigned the preceding cell $(h,j-1)$ if this is available.*

At this point the coordinator starts to send to the involved vehicles (except the leader, thus belonging to the set $\bar{\mathcal{V}} = \mathcal{V} \backslash \{1\}$) a reference position to track, which corresponds to the center of the assigned cell. Again, when convergence to a neighborhood of the (moving) reference position is attained, the coordinator is notified by the vehicles. At the end of the initialization phase, every controlled vehicle is placed, within a designed tolerance, at the center of a moving cell, and no relative speed is present between the vehicles. In such conditions, at time $t_2 > t_1$, the core procedure of the proposed algorithm, i.e. the iterative phase, is started.

4.2.4 Iterative Phase

Each iteration in the iterative phase is composed of two distinct steps, namely the generation of reference positions for the vehicles to compose and keep the formation (computed by the coordinator and described in 4.2.4) and a reference tracking procedure (reported in 4.2.4), carried out by the

Table 4.1: Main Algorithm Parameters

Parameter	Values	Meaning
`vehicles_approach`	$\in \{0, 1\}$	Whether vehicles not performing trajectory tracking can move towards the formation
`free_cells_ahead`	$\in \mathbb{N}^+$	Specifies `vehicles_approach`, see 4.2.4
`outer_lanes_go_backwards`	$\in H$	Lanes to be considered as "out" of the formation, and thus to be freed
`outer_lanes_discount`	$\in \mathbb{R}^+$	Negative bias in the cost of actions for vehicles in outer lanes
`free_cells_behind`	$\in \mathbb{N}^+$	Specifies `lanes_go_backwards`, see 4.2.4
`max_cells_dist_behind`	$\in \mathbb{N}^+$	Specifies `lanes_go_backwards`, see 4.2.4
`init_distance_threshold`	$\in \mathbb{R}^+$	Radius of the neighborhood of the cells centers to be considered as reached in 4.2.3
`goal_distance_threshold`	$\in \mathbb{R}^+$	Radius of the neighborhood of the cells centers to be considered as reached in 4.2.4
`new_dp_after_completion`	$\in \{0, 1\}$	Replanning flag: new iteration after a single vehicle finished trajectory tracking
`max_parallel_dps`	$\in \mathbb{N}^+$	Maximum number of pseudo-parallel DPs to be performed in one iteration

vehicles independently. Specific features of the proposed approach can be controlled by means of the parameters reported in Table 4.1, which will be better described in the subsequent discussion.

First Step - Reference Generation

As a first step, the generation of optimal paths through the grid cells is performed for all the involved vehicles, if at least one candidate goal cell is available, through Dynamic Programming [29]. In particular, the goal cells are chosen among the currently non-occupied cells which are marked as to be covered to build the formation according to a selection policy. In this work, it considers cells with successive rows (first) and columns (then) indices, but it can be substituted by any other algorithm. If no cells are available at the current iteration, a flag is activated indicating that no further DP steps may be carried out until a new reference formation is provided. Otherwise, a prediction horizon $P_{DP} \in \mathbb{N}$ is selected depending on L_v so that a feasible path is always possible to obtain, if existent, towards any goal cell. This can be formalized using an increasing integer subscript $p \in \mathbb{N}^+$ associated to every subsequent considered DP problem. Additionally, every cell in the grid $c \in S$ is considered as a discrete state $g_p(q) \in S$ visited at step q during task p, with $q = 1, 2, \cdots, P_{DP}$ and $g_p(q)$ a map associating, for every problem p, a cell to the time step q. A set of state-dependent feasible actions $\bar{\mathcal{A}}(g_p(q)) \subseteq \mathcal{A}$ is then defined, with

$$\mathcal{A} = \{F, B, R, L, S\} \tag{4.18}$$

corresponding to *forward*, *backward*, *right*, *left* and *still*, respectively. The direction is referred to the relative frame, i.e. a *still* action still requires

that the vehicle keeps the velocity of the reference frame, and the left and right actions entail also a shift forward of one cell to better account for the non-holonomicity of the vehicles while encouraging motion towards the formation.

A cost function $c(u(q))$ is specified by the high-level controller (and/or the coordinator itself) at any iteration for every feasible action $u(q) \in \bar{\mathcal{A}}(g_p(q))$. Notice that this way of defining the states and costs leads to the fact that space constraints (the vehicles must not go past the width of the highway) are automatically considered.

Based on the occupation map Ω_p considered during the p-th DP task in the current iteration), a goal cell g_p^* is chosen. The problem can then be formally stated as that of finding an optimal actions sequence $u_{i,p}^* = \left(u_{i,p}^*(0), u_{i,p}^*(1), \cdots, u_{i,p}^*(P_{DP}-1)\right)$ leading from the location $g_{p,i}(0)$ to the goal state g_p^*, for every vehicle $i \in \bar{\mathcal{V}}$. Based on the Bellman's optimality principle, this translates in solving iteratively the optimization problems

$$\begin{aligned} J_i(q) = \min_{u_i(q) \in \bar{U}(g_i(q))} & c(u_i(q)) + J_i(q+1), \\ & q = P_{DP}-1, P_{DP}-2 \cdots, 0 \end{aligned} \tag{4.19}$$

where the cost function $J_i(q)$ is defined so that

$$g_{p,i}(P_{DP}) = g_p^* \quad \text{with} \quad J_i(P_{DP}) = 0, \quad \forall i \in \mathcal{V} \tag{4.20}$$

As a consequence of relationships (4.19) and (4.20), one has that $J_i(0)$ is the total optimal cost for vehicle i. A minimum-cost vehicle i^* can then be found as that associated with the lowest cost. An optimal states (cells) sequence $G_p^{i^*} = (g_{i^*}^*(0), \cdots, g_{i^*}^*(P_{dp}-1))$ is then considered as that induced by the optimal action sequence $u_{i^*,p}^*$.

The occupation map is then updated marking all of the cells in $G_p^{i_p^*}$ as occupied, adding also the cell adjacent to all the couples of cells associated to lane changes, in order to mathematically avoid the possibility of trajectory crossings (refer to Figure 4.6 for a clarification). The procedure is then repeated, for a number of times less or equal than that specified in `max_parallel_dps`, considering the new occupation map Ω_{p+1}. Specifically, the step is stopped if either the threshold `max_parallel_dps` is hit or none of the currently available vehicles can find an optimal path to the goal,

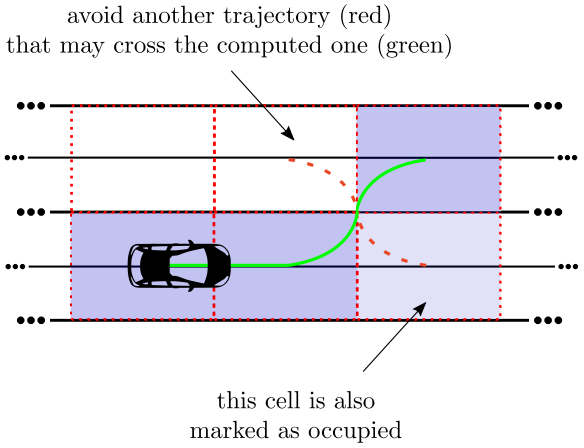

Figure 4.6: The light purple cell is marked as occupied even though it does not belong to the cells composing the optimal path (darker shaded), in order to avoid the possibility of generating another path (corresponding to the dashed red trajectory) that would cross the already composed path (solid green).
meaning that a feasible path is not physically available.

The reference generation is then performed as a subsequent task, which periodically updates position references $\bar{p}_i,\ i \in \bar{\mathcal{V}}$ (they may be in the global or local reference frames) based on the task to be performed by every vehicle[4]. In particular, the vehicles which are marked as minimum-cost in the DP (and thus, have a minimum-cost path $G_p^{i_p^*}$ for some p in the current iteration) are assigned references taken by a smooth trajectory generated using the centers of the cells in $G_p^{i_p^*}$. A third-order curve is adopted here to generate position and yaw references in time and space domain, but any trajectory generation procedure providing sufficiently smooth paths can be effectively adopted.

For all of the other vehicles, which are not associated with a minimum-cost path, the references generation mechanism comprises the possibility of adopting different strategies depending of the particular situation and the algorithm settings. The default reference is the center of the cell currently associated to the considered vehicle, but two different flags can be employed to modify the behavior of the vehicles not performing trajectory tracking.

[4]Although in the present proposal the trajectory planning is entirely carried out in the coordinator, in principle local, distributed strategies can be adopted so that each vehicle constructs its own trajectory given the control points (i.e. the centers of the respective cells). This, on one hand, would increase complexity. On the other hand, though, it would allow for instance to generate trajectories dependent on the specific model of the vehicle.

The `vehicles_approach` flag enables the possibility for the vehicles to approach the formation, being associated sequentially to free cells (if existent) ahead of the currently occupied one. In doing so, a minimum number of cells `free_cells_ahead` is to be kept free between the final position of the considered vehicle and the "last" (with highest h-index in the G matrix) cell composing the formation or the next cell occupied by a vehicle. The main advantage of such an approach is that the vehicles safely traverse in parallel and independently cells that otherwise would require the subsequent trajectories to be longer, thus leading to appreciable increases in the formation creation speed.

As an additional mechanism, a subset of lanes `outer_lanes_go_backwards` $\subset H$ can be defined such that the vehicles assigned to cells belonging to these lanes are successively assigned as reference the center of cells at the back of the currently occupied one. The variable `free_cells_behind` can be set so that, in assigning new cells to the considered vehicles, a number of cells is kept free with respect to the closest vehicle in the same lane. A maximum distance, in terms of cells, between the farthest cell that can be assigned with respect to the formation and the formation itself can be specified in the flag `max_cells_dist_behind`. This particular feature is included so that peculiar situations can be considered where vehicles are required to join the formation from specific lanes (for instance in case the presence of construction sites ahead requires them to be freed). To this end, a discount factor (`outer_lanes_discount`) is also included so that lane changes performed from the lanes specified in `outer_lanes_go_backwards` are discounted, thus encouraging inclusion of the vehicles in the formation.

Notice that in order to implement the local MPC control loops, a sequence of P successive references, computed considering a sampling time T_s which must match in the coordinator and the single vehicles, is actually transmitted to the vehicles to consider the whole prediction horizon. Additionally, a reference yaw angle $\bar{\psi}_i$ is included, so that at each sampling time a reference sequence

$$\bar{r}_k^{(i)} = \left(r_{k+1}^{(i)}, r_{k+2}^{(i)}, \cdots, r_{k+P}^{(i)} \right) \tag{4.21}$$

where

$$r_k^{(i)} = \begin{bmatrix} \bar{p}_{x,i}(kT_s) & \bar{p}_{y,i}(kT_s) & \bar{\psi}_i(kT_s) \end{bmatrix}^T \tag{4.22}$$

is a generic reference vector for the vehicle i.

The references generation is entirely carried out inside of the coordinator, which provides the reference positions to the respective vehicles. Given that the formation moves uniformly at the reference speed $\bar{v}$, an easy interpolation mechanism can be included to improve robustness with respect to possible delays and packet losses.

At this point the reference tracking step (described in 4.2.4) is performed by the subset of vehicles obtaining a minimum-cost path in the DP step. While all of them need to trigger the coordinator once they reach the last cell in the associated sequence, the information about the subset of vehicles in charge of performing trajectory tracking is particularly important. In fact, if the flag `new_dp_after_completion` is set, the iteration finishes as soon as one vehicle finished trajectory tracking, while if it is not the coordinator waits for all of the minimum-cost vehicles to carry out their associated task before starting the successive iteration.

Second Step - Reference Tracking

For each of the vehicles required to implement local control loops, a reference sequence (4.21) is received from the coordinator for the 2D position and the yaw angle. On the basis of this information, an MPC reference tracking problem is formulated as a quadratic program. In order to do so, the single-track dynamic model is adopted foe every vehicle, as described in Section 4.1.

In order to implement the local position-tracking feature at vehicles level, Model Predictive Control (MPC) is exploited, see e.g. [118]. To describe the particular adopted strategy, a sampling time T_s is introduced along with a prediction horizon $P \in \mathbb{N}$ (based on which the references in (4.21) are generated), which induces a sequence of inputs

$$\bar{u}_k = (u_k, u_{k+1}, \cdots, u_{k+P-1}) \tag{4.23}$$

for every sampling step k (corresponding to the sampling instant kT_s).

Please note that the formulation adopted in this work relies on a continuous time framework, so that the input signal is to be considered as a piece-wise constant function, namely

$$u(t) = u_k, \quad kT_s \leq t < (k+1)T_s \tag{4.24}$$

With respect to the problem under consideration, the vehicle inputs are taken as $u(t) = [F_{l,f}(t)\ F_{l,r}(t)\ \delta(t)]^T$ (see in particular Equations (4.1) and Remark 16).

Then, since a model of the vehicles dynamics is required to implement the MPC strategy, a successively linearized version of the model in (4.1) and (4.8) is computed on the basis of the initial vehicle state for each step k, so that a system in the form

$$\Delta\dot{x}_k(t) = f(x(kT_s)) + A_k\Delta x_k(t) + B_k\Delta u_k(t) \tag{4.25}$$

is obtained, where $f(\cdot)$ is the vector function obtained stacking the right-hand sides of (4.1) and (4.8) (thus representing the derivative of the complete vehicle model), while $A_k \in \mathbb{R}^{6\times6}$ and $B_k \in \mathbb{R}^{6\times3}$ are obtained through a standard linearization procedure around the reference state x_k and the reference input $u_k = [0, 0, 0]^T$. These latter are therefore the jacobians of $f(\cdot)$ with respect of $x(t)$ and $u(t)$, respectively. As a consequence, $\Delta x_k(t) = x(t) - x_k$, while $\delta u_k(t) = u(t)$.

The MPC cost function is then defined to reflect the control objectives on the prediction horizon, namely the tracking of the references (4.21), by means of the diagonal matrix $Q \succeq 0$. The diagonal matrix $R \succ 0$ is also employed to consider the cost associated with the magnitude of the inputs, so that the final expression is

$$J(x(kT_s), \bar{u}_k) = \sum_{l=k}^{k+P-1} \left(\hat{r}_{l+1}^T Q \hat{r}_{l+1} + u_l^T R u_l\right) \tag{4.26}$$

where $\hat{r}_l = \hat{x}_l - r_l$, with r_l as defined in Equation (4.22), and $\hat{x}_l$ is the vector of predicted states at step l according to model (4.8) starting from $x(kT_s)$ and sampled over the considered prediction horizon, i.e. at time instants $(k+1)T_s, \cdots, (k+P)T_s$. Thus, $\hat{r}_l$ represents the predicted tracking error at the time step l, obtained sampling the trajectories computed inside the

MPC procedure, dependent on the input sequence $\bar{u}_k$.

Apart from the linear dynamics constraints given by (4.25), a set of convex constraints is introduced for the states and inputs. In particular, the relationships

$$F_f^- \leq u_1(t) \leq F_f^+,\ F_r^- \leq u_2(t) \leq F_r^+,\ \Delta^- \leq u_3(t) \leq \Delta^+ \tag{4.27}$$

are enforced for the inputs, while

$$V^- \leq v_x(t) \leq V^+ \tag{4.28a}$$

$$A^- \leq \frac{v(t) - v(t_-)}{T_s} \leq A^+ \tag{4.28b}$$

$$J^- \leq \frac{v(t) - 2v(t_-) + v(t_{--})}{T_s^2} \leq J^+ \tag{4.28c}$$

where (4.28b) and (4.28c) allow to consider, respectively, the acceleration and jerk in terms of the velocity by means of the backward finite-difference method. Specifically, in (4.28) the term $v(t_-)$ and $v(t_{--})$ are the velocities sampled one and two previous sampling instants, respectively. Notice that this formulation, as well as the adoption of the relationships (4.25), (4.26), (4.27) and (4.28), allows to cast the MPC optimization problem into the form of a quadratic program. Once obtained the optimal sequence, according to the receding horizon approach, only the first input vector, u_k^*, is actually applied for $t \in [kT_s, (k+1)T_s)$.

The coordinator is periodically updated by the vehicles as soon as they enter a neighborhood of one cell (control point) of predefined radius, so that the considered cell is assigned to it in the map Θ and all of the cells behind it, previously occupied, are freed in Ω. This is crucial, especially if `new_dp_after_completion` is set, in maintaining a coherent description of the cells status. In any case, the vehicles trigger the coordinator as soon as they enter a neighborhood of the center of the last cell in the sequence.

Remark 20. *The linear MPC formulation adopted here focuses on the adoption of a QP formulation to keep complexity low, thus constituting a rather basic but performing solution which can be further extended. For instance, in order to introduce robustness, one could resort to the introduction of integral sliding modes (ISM). With this respect, works as [170, 165] propose a multi-rate architecture in which a fast ISM correction term is aimed at rejecting*

the matched disturbances with negligible increase in complexity. Additionally, the linearization strategy proposed in [151] can be straightforwardly adopted with possible improvements in prediction accuracy. While the mentioned strategies preserve the QP nature of the optimization problem, the introduction of nonlinear constraints and cost functions can be exploited to consider, e.g., explicit safety constraints or efficiency-related metrics. The adoption of such modifications and the assessment of the trade-off between the increase in computational complexity with respect to the practical improvement is currently under investigation, and thus not addressed in the current work.

(a) (b)

Figure 4.7: Small-scale automated trucks employed in the experimental tests. *From [221].*

4.3 Experimental Results

In this section experimental results carried out on a simplified version of the strategy described above are reported, to testify the effectiveness of the proposal in real-life conditions. In particular, the experiments have been conducted on three small-scale vehicles at the *Institute of Automation and Control* of the *Graz University of Technology* employing the testbed describe thoroughly in [174, 173]. The coordinator, in particular, is embedded into an external computation unit (simulating, thus, a V2I approach), which communicated with the vehicles through a UDP connection. A sampling time of $0.01s$ is considered, for control and information retrieval. In particular, the position and orientation measurements are given by cameras mounted on the ceiling, which emulate a GPS tracking system.

Notice that the algorithm employed is the one described in [221], which presents these main simplifications with respect to the more extended approach described in this Chapter:

- Only the creation of formations is allowed, and no on-line reshape. In particular, the formations must be described via the composition of arbitrary-length strings of vehicles occupying each available lane;
- Only one DP is allowed per iteration;
- The trajectory following task is carried out with model-free local Stanley controllers [203] for the steering angle and a simple PI controller for velocity tracking[5].

[5]The choice of using such algorithms instead of MPC for trajectory tracking follows

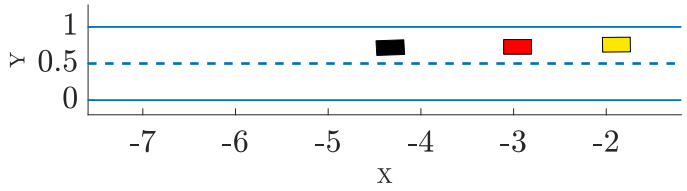

(a) Until $t = t_1$, the vehicles proceed on the highway.

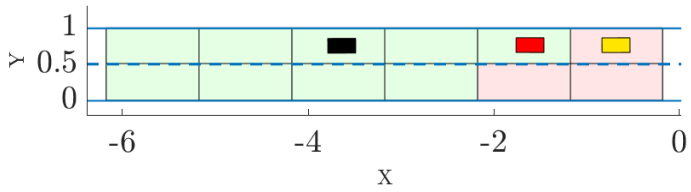

(b) The grid is created and the vehicles are required to reach and keep the center of the nearest cell. The first DP is performed by the black and the red trucks.

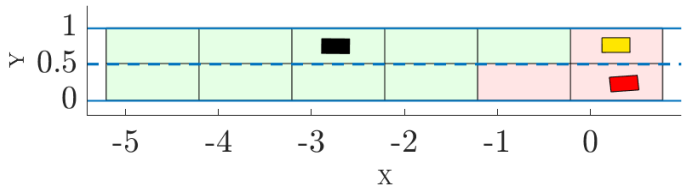

(c) Once the red truck reached the goal cell, another DP is performed (only by the black truck).

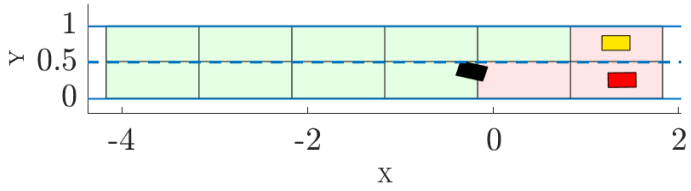

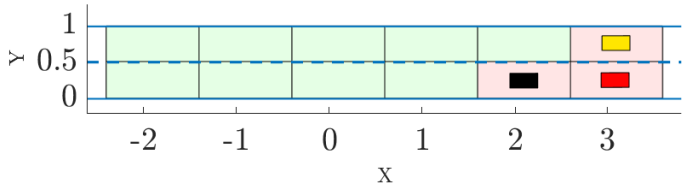

(e) The formation is finally created and maintained.

Figure 4.8: Frames of the first formation creation experiment. *From [221].*

from the fact that the small-scale trucks possess very low velocities. Dynamic models cannot represent low-speed situations (see, for instance, how Equations (4.5) and (4.7)

Two experiments are reported here: in the first one, three trucks should achieve a triangular formation proceeding at a velocity of $0.1m/s$ on both lanes of a two-lane road. At the beginning of the experiment the vehicles $A = \{1, 2, 3\}$ (respectively, the yellow, red and black truck) proceed uncontrolled on the left lane, as depicted in Figure 4.8, where frames of the experiment over time are reported. At time $t = t_1 = 3s$, the trigger signal is received and the virtual grid is created with respect to the yellow truck as explained in Section 4.2.3. Then, basing on the position of the followers, the nearest cell is assigned to each of them. In particular, the map Θ defined in (4.16) is such that $\Theta(1) = (1, 2)$, $\Theta(2) = (1, 1)$ and $\Theta(3) = (2, 1)$. The vehicles are controlled to reach and keep the center of the corresponding cells, as depicted in Figure 4.8(b). From Figure 4.8 it is evident that in the considered case $L_v = 6$ has been chosen, while the portion of the road to be covered by the formation based on the requirements (in the leaders reference frame) is constituted by the three red cells.

Once the distance between the center of all the assigned cells and the respective vehicles becomes lower than a predefined threshold of $5cm$, the second phase is started and the first of the stages described in Section 4.2.4 is carried out by vehicles 2 and 3 at time $t = 13.72s$, with the considered goal cell being $(1, 1)$. The cost for going forward has been set to 1, to go left and right 5, to go backwards 2 and to stay still 0. Consequently, the vehicle with minimum cost is the red one ($J_2^* = 5$), which then reaches the goal cell as reported in Figure 4.8(c) with $\alpha = 1.15$ chosen as a fixed design parameter. Finally, the last iteration is performed by vehicle 3 only at time $t = 21.38s$, which then reaches its position in the grid with cost $J_3^* = 7$. Notice that, in this case, it is obviously not necessary since vehicle 3 is the only one left. As represented in Figure 4.8(d), at $t = 50s$ the formation is created as required and kept throughout all the subsequent time. The evolution of the X and Y coordinates over time of the involved vehicles are reported in Figure 4.9 to show the working principles of the employed algorithm. In particular, it is worth noticing how the reference $\bar{Y}_i$ changes as soon as the corresponding vehicle i is selected as that in charge of reaching the goal. At the same time, the velocity (slope of the reference $\bar{X}_i$ curve) increases accordingly. The

degenerate for $v(t) \to 0$), and simple proportional-integral controllers are simple to implement but yet very effective. Other strategies, anyway, could have been resorted to (see, e.g. [139])

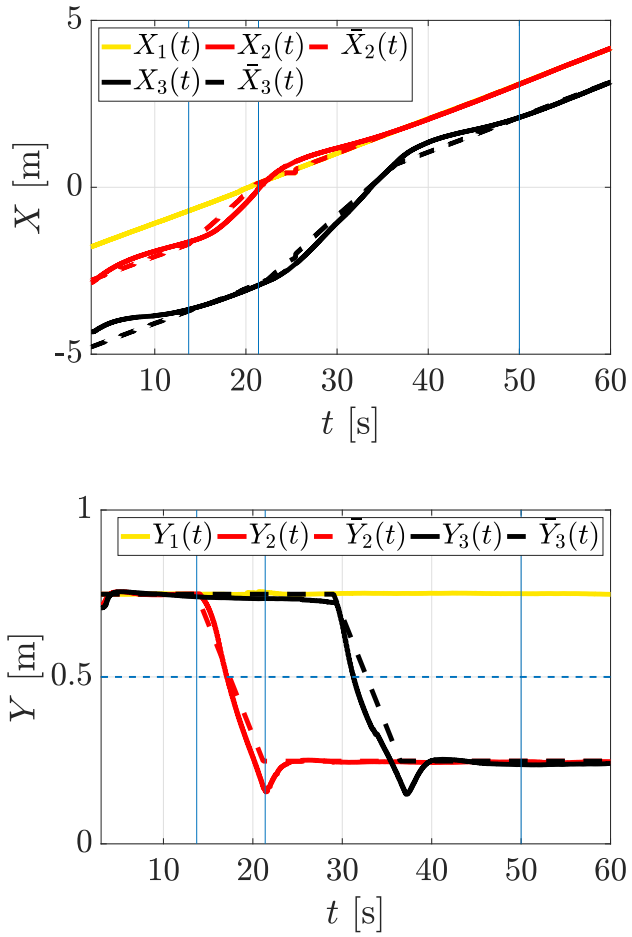

Figure 4.9: X_i and Y_i coordinates of the trucks $i = \{1, 2, 3\}$ during the first experiment. The vertical lines correspond to the time instants reported in the results discussion and the frames reported in Figure 4.8. *From [221].*

maneuvers are safe and no collisions occur during the experiment, since d is chosen sufficiently high.

A second experiment, on a three-lanes road, has been performed and reported in Figures 4.10 and 4.11. All the design choices have been kept equal to those of the first experiment, but with different initial conditions. Also in this case the algorithm proves to be effective and no collisions occur, reinforcing the soundness of the presented approach in a realistic scenario where not considered delays and other nonidealities are present.

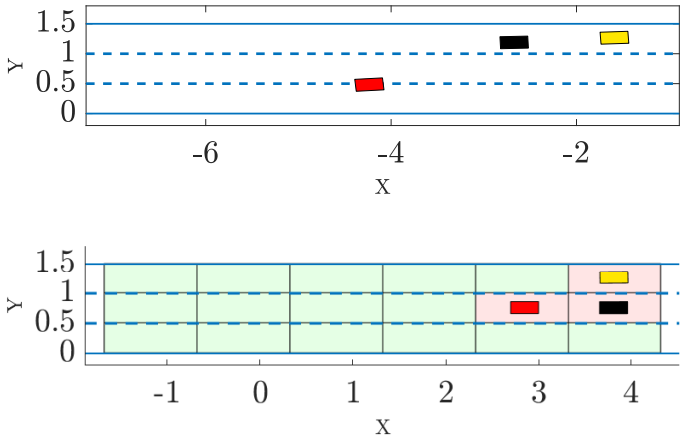

Figure 4.10: Initial (upper plot) and final (lower plot) frame of the second experiment. *From [221].*

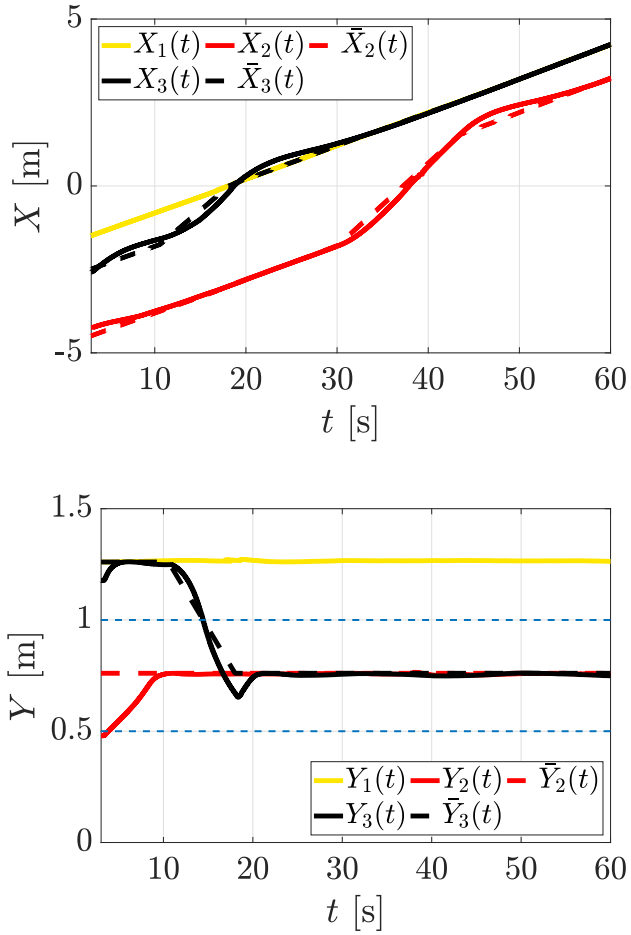

Figure 4.11: X_i and Y_i coordinates of the trucks $i = \{1, 2, 3\}$ during the second experiment. *From [221].*

4.4 Simulation Results

Two different simulation scenarios are here considered in order to exemplify the proposed (extended) approach and show the flexibility of the adopted strategy. In the first simulation (described in 4.4), a rectangular formation is created and then reshaped in order to allow vehicles to leave a lane (the first) free. This maneuver highlights the capability of the algorithm to effectively create the formation from the initial traffic flow and to straightforwardly adopt reconfiguration mechanisms when required, just acting on the external signals coming from the high-level controller and the algorithm parameters in Table 4.1. The second simulation, discussed in 4.4, is proposed in order to evidence the ability of creating and reshaping formations with arbitrary disposition of vehicles. In particular, the possibility of dynamically reconfigure the formation to allow a vehicle to exit the highway is shown.

Formation Creation

A 2×4 rectangular formation is created in the first two lanes as the first task addressed in this scenario, starting from $N = 8$ vehicles randomly placed on the highway. Although similar to the maneuvers proposed in [221], here a higher number of vehicles is considered and proceed at high speed ($\bar{v} = 30m/s$). Additionally, vehicles are equipped with local MPC controllers and a maximum of 3 pseudo-parallel iterations is considered (`max_parallel_dps`$= 3$). The approach mechanism is exploited for vehicles not performing trajectory tracking, with `free_cells_ahead`$= 1$. The considered highway comprises 3 lanes (i.e. $H = \{1, 2, 3\}$) of width $w_l = 4m$, and the dynamics of the vehicles follow the description in (4.1) and (4.8).

The local MPC loops consider a prediction horizon $P = 8$ with sampling time $T_s = 0.3s$. For all of the vehicles, considered as having random mass ($m \in [800, 1400]kg$) and moment of inertia ($J_z \in [900, 1300]kgm^2$), the same input constraints are considered. Specifically, the total input force is such that $F^- = F^+ = 3000N$ while the steering angle is constrained to be such that $\delta(t) \in [-0.2, 0.2]$ during trajectory tracking and $\delta(t) \in [-0.025, 0.025]$ during the tracking of the cells centers. The (longitudinal) velocity of the vehicles is imposed to be such that $0.8\hat{v} \leq v_x(t) \leq 1.2\hat{v}$, while horizontal and lateral accelerations as well as the respective jerks are

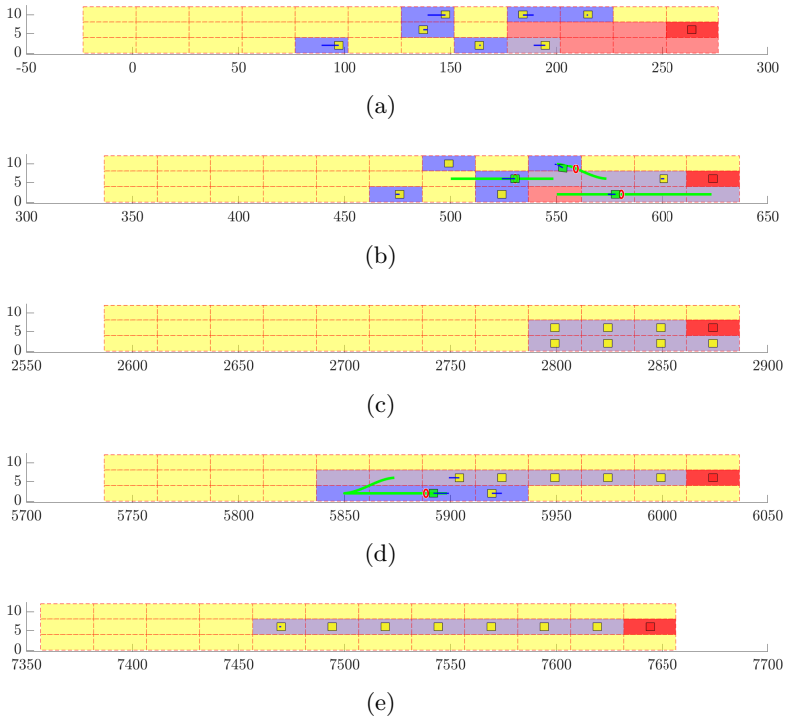

Figure 4.12: Frames of the first simulation.

all constrained in the range $[-1.5, 1.5]$ (see equations (4.27) and (4.28)). Notice that the latter constraints are softened in the final formulation to improve the feasibility of the optimization task. The utilized weights are such that $Q = diag\,([0\ 0\ 0\ 1\ 1\ 100])$ and $R = diag\,([0.8\ 0.8\ 1])$.

Both the continuous-time dynamics simulations and the MPC optimizations are carried out, for the two considered simulation scenarios, in Matlab using the CasADi framework [7].

In Figure 4.12, some key frames of the simulation are reported. The vehicles start in random positions on the lanes of the highway. Frame 4.12(a) depicts a situation in which the initialization phase is in progress, with the grid already been constructed (with the cells $d = 25m$ in length) and attached to the leader (colored in red). The cells to be occupied by the formation are highlighted in red, while the blue segments link the vehicles with the respective associated cell centers. In frame 4.12(b), taken during the iterative phase, it can be highlighted how three different trajectories have been generated (green curves) with respect to three different goal cells in the formation (`max_parallel_dps`= 3). No replanning is considered for

this particular situation (`new_dp_after_completion`= 0), and therefore all of the parallel DPs are carried out for every iteration. In frame (4.12(c)) it is possible to evidence how the formation is effectively created (just after about 200 seconds). The reshaping occurs from 450 seconds on, and entails moving all of the vehicles to the second lane, to free the first one. To do so, it is only required that the high-level controller passes to the coordinator the new reference disposition and triggers is for an update. The iterative phase is then carried out as usual, only considering the new reference cells as successive goals. In this particular case one can see how the vehicles move backwards to achieve the new shape (frame 4.12(d)) due to the fact that, additionally with respect to the results from the DP stages (in this case, `max_parallel_dps` is lowered to 1), a mechanism for which in the first lane the vehicles are encouraged to decelerate is employed (i.e. `outer_lanes_go_backward`= {1}), with `free_cells_behind`= 0. In Frame 4.12(e) the new disposition is finally attained.

Formation Reshape

In the second maneuver, formation creation is followed by a situation in which a vehicle not occupying the rightmost lane needs to exit the highway, and therefore has to leave the formation. To do so, an online reconfiguration maneuver is required to be performed so that space is left for the considered vehicle to safely reach the rightmost lane and, consequently, be able to leave the highway. For the sake of simplicity, the same parameters employed for the previous simulation are kept, so that the only difference lies in the number of vehicles ($N = 9$ in this case), the initial positions and velocities, and the reference shape of the formation, which covers all the 3 lanes of the highway and is 3 cells long.

In the first simulation frame 4.13(a) the initial vehicles disposition is depicted, together with the cells to be occupied in order to cover the reference formation shape. Frame 4.13(b) represents a situation in which, during the iterative phase, the vehicles move towards goal cells, independently and in parallel. The final disposition of the vehicles is reported in frame 4.13(c). Then, the vehicle which needs to leave the highway triggers a leave request to the coordinator, and this latter reshapes the formation as little as possible to allow the vehicle reaching the rightmost lane through free cells (see the new reference cells in Frame 4.13(d)). Frame 4.13(e) reports the backup

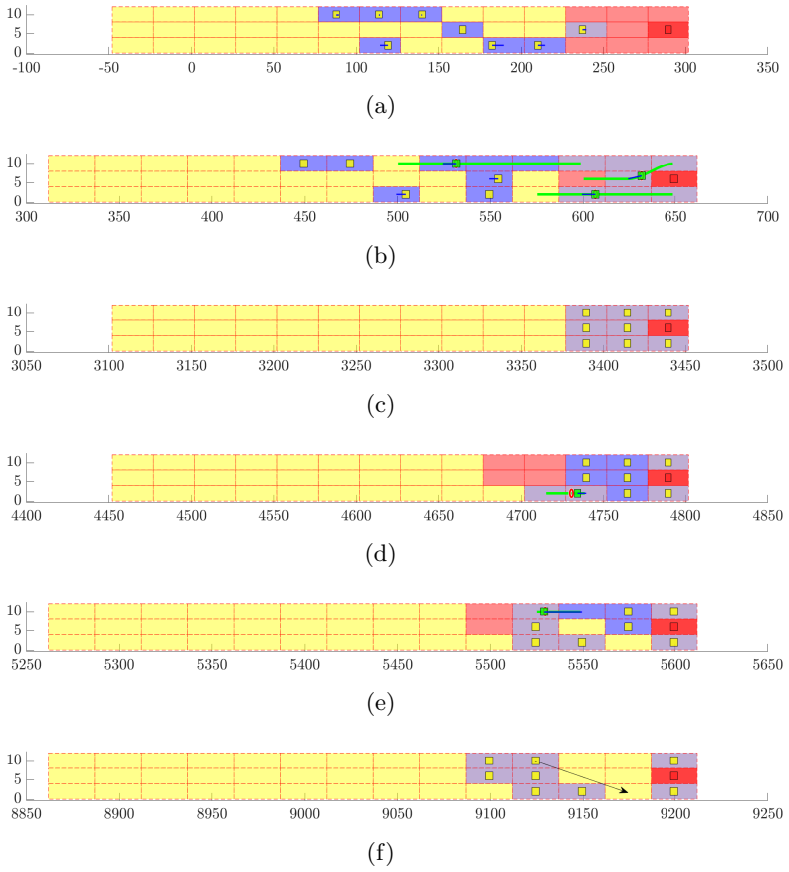

Figure 4.13: Frames of the second simulation.

movements of nearby vehicles to achieve such disposition, while the final shape is achieved in Frame 4.13(f). This highlights the fact that arbitrary dispositions can be imposed as reference online, and the algorithms underlying structure takes care of moving the vehicles appropriately and in a completely automatic way. Following the marked arrow, then, the interested vehicle can safely move to the first lane and then exit, implementing the same trajectory generation and following technique proposed here or any other control strategy guaranteeing collision avoidance in the traversing of the cells.

Chapter 5

Conclusions

The present Dissertation introduces original advanced techniques for the control of automotive systems, based mainly on MPC and SMC. Different aspects of the automotive control are presented, starting from the control of single vehicles and extending the considered systems to unidimensional and bidimensional formations.

Novel results concerning the robust yaw-rate control of EVs are briefly introduced, along with an original observation system for the online reconstruction of the tire-road interaction forces, though not exhaustively presented. Instead, the main focus in the discussion of this Thesis is devoted to the multi-agent case, which covers both (robust) platoon control and formation control (this latter, in the specific case of highway scenarios).

Specifically, the solutions to the former problem aim mainly at providing robust schemes, which rely on the introduction of a multi-rate ISM correction loop in non-cooperative distributed MPC schemes and an SMC-based distributed control architecture, respectively. Besides providing increases in safety, efficiency, and road infrastructure exploitation, it is made evident in the literature how platoons can be exploited as dynamic actuators for traffic control. Therefore, improvements in this direction could be made by developing integrated solutions comprising high-level traffic controllers and lower-level platoon control algorithms. Many possible scenarios could be envisaged considering this topic, dependent on the adopted infrastructure, architecture, and communication system.

Additionally, an effort could be made in the direction of effectively address the problem of energy efficiency, which nowadays is of paramount

importance. Again, considering explicitly this issue in the design of the control architecture could open a wide range of possibilities worth investigating especially in view of the possibilities offered by EVs/HEVs.

The proposed novel formation control algorithm possesses peculiar features, broadly discussed in the related Chapter, which make it particularly interesting. Among many others, the possibility of greatly extending it opens to many improvement directions. In particular, the inclusion of more advanced techniques such as, for instance, machine learning to account for a broader range of situations (e.g. the presence of uncontrolled vehicles in the considered area of the highway) may lead to the direction of state-of-the-art results enabling a completely new paradigm in the control of formations of commercial (unmanned) vehicles. At the same time, also in this case the development of integrated solutions encompassing high-level traffic controllers, road infrastructure design, and communication systems development could profoundly change the nature of highway travels, improving the safety and comfort of the passengers.

As side results, developed together with the presented works, some further original pieces of literature are reported. In particular, while introducing the basics of Sliding Mode Control a general overview of the employment of SMC in Consensus control is given, providing also a novel algorithm for the robust finite-time leader-follower consensus reaching of MAS. Though not directly employed in the proposed developments, the possibility of adopting consensus-based solutions is broadly investigated in research and could constitute a promising direction in the improvement of already existing or newly designed control systems in the automotive field. Similarly, a brief digression is provided on robust consensus control, which again is not directly employed in the proposed works but could be investigated as a straightforward way of considering constraints in real-life implementations of the proposed strategies.

Appendix A

Peer-Reviewed Scientific Publications

Journals:

- M. Zambelli, M. Steinberger, M. Horn, and A. Ferrara. Two-step event-triggered iterative formation control for heterogeneous vehicles in highwayscenarios. In *(Submitted to) IEEE Transactions on Intelligent Vehicles*, 2020
- A. Pozzi, M. Zambelli, A. Ferrara, and D. M. Raimondo. Balancing-aware charging strategy for series-connected lithium-ion cells: A nonlinear model predictive control approach. *IEEE Transactions on Control Systems Technology*, pages 1–16, 2020
- E. Regolin, A. Alatorre, M. Zambelli, A. Victorino, A. Charara, and A. Ferrara. A sliding-mode virtual sensor for wheel forces estimation with accuracy enhancement via ekf. *IEEE Transactions on Vehicular Technology*, 68(4):3457–3471, 2019

Book Chapters:

- M. Zambelli and A. Ferrara. *Emerging Trends in Sliding Mode Control – Theory and Application*, chapter Sliding Modes in Consensus Control. Springer, 2021
- M. Zambelli and A. Ferrara. *Variable-Structure Systems and Sliding-Mode Control: From Theory to Practice*, chapter Constrained Sliding-

Mode Control: A Survey, pages 149–175. Springer International Publishing, Cham, 2020

Conference Proceedings:

- M. Zambelli and A. Ferrara. Second-order sliding modes generation for robust disturbance string stable platoon control. In *2020 European Control Conference (ECC)*, pages 1879–1884. IEEE, 2020[1]
- M. Zambelli, P. Carulli, M. Steinberger, M. Horn, and A. Ferrara. A novel formation creation algorithm for heterogeneous vehicles in highway scenarios: Assessment and experimental validation. In *IFAC-PapersOnLine: Proceedings of the 21st IFAC World Congress*, 2020
- M. Zambelli and A. Ferrara. Robustified distributed model predictive control for coherence and energy efficiency-aware platooning. In *2019 American Control Conference (ACC)*, pages 527–532, July 2019
- A. Ferrara and M. Zambelli. Integral second-order sliding modes for robust prescribed-time leader-follower consensus control with partial information. In *Proceedings of the 58th Conference on Decision and Control*, 2019
- E. Regolin, M. Zambelli, M. Vanzulli, and A. Ferrara. A path tracking approach for autonomous driving on slippery surfaces. In *2019 IEEE International Conference on Connected Vehicles and Expo (ICCVE)*, pages 1–6, 2019
- M. Zambelli and A. Ferrara. Linearization-based integral sliding mode control for a class of constrained nonlinear systems. In *2018 15th International Workshop on Variable Structure Systems (VSS)*, pages 402–407, 2018
- E. Regolin, M. Zambelli, and A. Ferrara. A multi-rate ism approach for robust vehicle stability control during cornering. *IFAC-PapersOnLine*, 51:249–254, 2018
- E. Regolin, M. Zambelli, and A. Ferrara. Wheel forces estimation via adaptive sub-optimal second order sliding mode observers. *Proceedings*

[1] 2020 European Control Conference Best Student Paper Award finalist

of the 2017 XXVI International Conference on Information, Communication and Automation Technologies (ICAT 2017), Oct. 2017

Bibliography

[1] S. Al-Sultan, M. M. Al-Doori, A. H. Al-Bayatti, and H. Zedan. A comprehensive survey on vehicular ad hoc network. *Journal of network and computer applications*, 37:380–392, 2014.

[2] A. A. Alam, A. Gattami, and K. H. Johansson. An experimental study on the fuel reduction potential of heavy duty vehicle platooning. In *13th International IEEE Conference on Intelligent Transportation Systems*, pages 306–311, Sep. 2010.

[3] M. Amodeo, A. Ferrara, R. Terzaghi, and C. Vecchio. Slip control for vehicles platooning via second order sliding modes. In *2007 IEEE Intelligent Vehicles Symposium*, pages 761–766, June 2007.

[4] M. Amodeo, A. Ferrara, R. Terzaghi, and C. Vecchio. Wheel slip control via second-order sliding-mode generation. *IEEE Transactions on Intelligent Transportation Systems*, 11(1):122–131, 2009.

[5] M. Amoozadeh, H. Deng, C.-N. Chuah, H. M. Zhang, and D. Ghosal. Platoon management with cooperative adaptive cruise control enabled by vanet. *Vehicular communications*, 2(2):110–123, 2015.

[6] B. D. Anderson, B. Fidan, C. Yu, and D. Walle. Uav formation control: Theory and application. In *Recent advances in learning and control*, pages 15–33. Springer, 2008.

[7] J. A. Andersson, J. Gillis, G. Horn, J. B. Rawlings, and M. Diehl. Casadi: a software framework for nonlinear optimization and optimal control. *Mathematical Programming Computation*, 11(1):1–36, 2019.

[8] N. Ando and H. Fujimoto. Yaw-rate control for electric vehicle with active front/rear steering and driving/braking force distribution of rear

wheels. In *2010 11th IEEE International Workshop on Advanced Motion Control (AMC)*, pages 726–731. IEEE, 2010.

[9] D. Angeli, R. Amrit, and J. B. Rawlings. On average performance and stability of economic model predictive control. *IEEE transactions on automatic control*, 57(7):1615–1626, 2011.

[10] A. Askari, M. Mortazavi, and H. Talebi. Uav formation control via the virtual structure approach. *Journal of Aerospace Engineering*, 28(1):04014047, 2015.

[11] G. Baffet, A. Charara, and G. Dherbomez. An observer of tire–road forces and friction for active security vehicle systems. *IEEE/ASME TRANSACTIONS ON MECHATRONICS*, 12(6):651–661, 12 2007.

[12] G. Baffet, A. Charara, and D. Lechner. Estimation of vehicle sideslip, tire force and wheel cornering stiffness. *Control Engineering Practice*, 17(11):1255–1264, 2009.

[13] G. Baffet, A. Charara, D. Lechner, and D. Thomas. Experimental evaluation of observers for tire–road forces, sideslip angle and wheel cornering stiffness. *Vehicle System Dynamics*, 46(6):501–520, 2008.

[14] T. Balch and R. C. Arkin. Behavior-based formation control for multirobot teams. *IEEE Transactions on Robotics and Automation*, 14(6):926–939, 1998.

[15] B. Bamieh, M. R. Jovanovic, P. Mitra, and S. Patterson. Coherence in large-scale networks: Dimension-dependent limitations of local feedback. *IEEE Transactions on Automatic Control*, 57(9):2235–2249, Sept 2012.

[16] L. Barnes, M. Fields, and K. Valavanis. Unmanned ground vehicle swarm formation control using potential fields. In *2007 Mediterranean Conference on Control & Automation*, pages 1–8. IEEE, 2007.

[17] C. Barrios and Y. Motai. Improving estimation of vehicle's trajectory using the latest global positioning system with kalman filtering. *IEEE Transactions on Instrumentation and Measurement*, 60(12):3747–3755, 2011.

[18] G. Bartolini, A. Ferrara, A. Levant, and E. Usai. On second order sliding mode controllers. In *Variable structure systems, sliding mode and nonlinear control*, pages 329–350. Springer, 1999.

[19] G. Bartolini, A. Ferrara, and E. Usai. Output tracking control of uncertain nonlinear second-order systems. *Automatica*, 33(12):2203 – 2212, 1997.

[20] G. Bartolini, A. Ferrara, and E. Usai. Chattering avoidance by second-order sliding mode control. *IEEE Transactions on Automatic Control*, 43(2), 02 1998.

[21] G. Bartolini, A. Pisano, E. Punta, and E. Usai. A survey of applications of second-order sliding mode control to mechanical systems. *International Journal of control*, 76(9-10):875–892, 2003.

[22] L. D. Baskar, B. De Schutter, J. Hellendoorn, and Z. Papp. Traffic control and intelligent vehicle highway systems: a survey. *IET Intelligent Transport Systems*, 5(1):38–52, 2011.

[23] M. Batty, K. W. Axhausen, F. Giannotti, A. Pozdnoukhov, A. Bazzani, M. Wachowicz, G. Ouzounis, and Y. Portugali. Smart cities of the future. *The European Physical Journal Special Topics*, 214(1):481–518, 2012.

[24] C. E. Beal and J. C. Gerdes. Model predictive control for vehicle stabilization at the limits of handling. *IEEE Transactions on Control Systems Technology*, 21(4):1258–1269, 2012.

[25] R. W. Beard, J. Lawton, and F. Y. Hadaegh. A coordination architecture for spacecraft formation control. *IEEE Transactions on control systems technology*, 9(6):777–790, 2001.

[26] R. W. Beard, T. W. McLain, D. B. Nelson, D. Kingston, and D. Johanson. Decentralized cooperative aerial surveillance using fixed-wing miniature uavs. *Proceedings of the IEEE*, 94(7):1306–1324, 2006.

[27] A. Bemporad and M. Morari. Robust model predictive control: A survey. In *Robustness in identification and control*, pages 207–226. Springer, 1999.

[28] L. Bertoni, J. Guanetti, M. Basso, M. Masoero, S. Cetinkunt, and F. Borrelli. An adaptive cruise control for connected energy-saving electric vehicles. *IFAC-PapersOnLine*, 50(1):2359 – 2364, 2017.

[29] D. P. Bertsekas, D. P. Bertsekas, D. P. Bertsekas, and D. P. Bertsekas. *Dynamic programming and optimal control*, volume 1. Athena scientific Belmont, MA, 1995.

[30] B. Besselink and K. H. Johansson. String stability and a delay-based spacing policy for vehicle platoons subject to disturbances. *IEEE Transactions on Automatic Control*, 62(9):4376–4391, Sep. 2017.

[31] B. Burmeister, A. Haddadi, and G. Matylis. Application of multi-agent systems in traffic and transportation. *IEE Proceedings-Software*, 144(1):51–60, 1997.

[32] E. F. Camacho and C. B. Alba. *Model predictive control*. Springer Science & Business Media, 2013.

[33] E. Camponogara, D. Jia, B. H. Krogh, and S. Talukdar. Distributed model predictive control. *IEEE control systems magazine*, 22(1):44–52, 2002.

[34] F. Caron, M. Davy, E. Duflos, and P. Vanheeghe. Particle filtering for multisensor data fusion with switching observation models: Application to land vehicle positioning. *IEEE transactions on Signal Processing*, 55(6):2703–2719, 2007.

[35] A. Carvalho, Y. Gao, A. Gray, H. E. Tseng, and F. Borrelli. Predictive control of an autonomous ground vehicle using an iterative linearization approach. In *16th International IEEE Conference on Intelligent Transportation Systems (ITSC 2013)*, pages 2335–2340. IEEE, 2013.

[36] Z. Chao, S.-L. Zhou, L. Ming, and W.-G. Zhang. Uav formation flight based on nonlinear model predictive control. *Mathematical Problems in Engineering*, 2012, 2012.

[37] L. Chen and C. Englund. Cooperative intersection management: A survey. *IEEE Transactions on Intelligent Transportation Systems*, 17(2):570–586, 2015.

[38] Y. Q. Chen and Z. Wang. Formation control: a review and a new consideration. In *2005 IEEE/RSJ International conference on intelligent robots and systems*, pages 3181–3186. IEEE, 2005.

[39] H. Cherouat and S. Diop. An observer and an integrated braking/traction and steering control for a cornering vehicle. In *Proceedings of the 2005, American Control Conference, 2005.*, pages 2212–2217. IEEE, 2005.

[40] W. Cho, J. Yoon, J. Kim, J. Hur, and K. Yi. An investigation into unified chassis control scheme for optimised vehicle stability and manoeuvrability. *Vehicle System Dynamics*, 46(S1):87–105, 2008.

[41] L. Consolini, F. Morbidi, D. Prattichizzo, and M. Tosques. Leader–follower formation control of nonholonomic mobile robots with input constraints. *Automatica*, 44(5):1343–1349, 2008.

[42] C. Cooper, D. Franklin, M. Ros, F. Safaei, and M. Abolhasan. A comparative survey of vanet clustering techniques. *IEEE Communications Surveys Tutorials*, 19(1):657–681, 2017.

[43] E. Cruz-Zavala, J. A. Moreno, and L. M. Fridman. Uniform robust exact differentiator. *IEEE Transactions on Automatic Control*, 56(11):2727–2733, 2011.

[44] R. Cui, S. S. Ge, B. V. E. How, and Y. S. Choo. Leader–follower formation control of underactuated autonomous underwater vehicles. *Ocean Engineering*, 37(17-18):1491–1502, 2010.

[45] B. Das, B. Subudhi, and B. B. Pati. Cooperative formation control of autonomous underwater vehicles: An overview. *International Journal of Automation and computing*, 13(3):199–225, 2016.

[46] R. De Castro, R. E. Araújo, and D. Freitas. Wheel slip control of evs based on sliding mode technique with conditional integrators. *IEEE Transactions on Industrial Electronics*, 60(8):3256–3271, 2012.

[47] L. De Novellis, A. Sorniotti, and P. Gruber. Wheel torque distribution criteria for electric vehicles with torque-vectoring differentials. *IEEE Transactions on Vehicular Technology*, 63(4):1593–1602, 2013.

[48] L. De Novellis, A. Sorniotti, P. Gruber, and A. Pennycott. Comparison of feedback control techniques for torque-vectoring control of fully electric vehicles. *IEEE Transactions on Vehicular Technology*, 63(8):3612–3623, 2014.

[49] R. A. DeCarlo, S. H. Zak, and G. P. Matthews. Variable structure control of nonlinear multivariable systems: a tutorial. *Proceedings of the IEEE*, 76(3):212–232, Mar 1988.

[50] M. Defoort, T. Floquet, A. Kokosy, and W. Perruquetti. Sliding-mode formation control for cooperative autonomous mobile robots. *IEEE Transactions on Industrial Electronics*, 55(11):3944–3953, 2008.

[51] M. Defoort, A. Polyakov, G. Demesure, M. Djemai, and K. Veluvolu. Leader-follower fixed-time consensus for multi-agent systems with unknown non-linear inherent dynamics. *IET Control Theory Applications*, 9(14):2165–2170, 2015.

[52] K. C. Dey, L. Yan, X. Wang, Y. Wang, H. Shen, M. Chowdhury, L. Yu, C. Qiu, and V. Soundararaj. A review of communication, driver characteristics, and controls aspects of cooperative adaptive cruise control (cacc). *IEEE Transactions on Intelligent Transportation Systems*, 17(2):491–509, 2015.

[53] M. Di Bernardo, A. Salvi, and S. Santini. Distributed consensus strategy for platooning of vehicles in the presence of time-varying heterogeneous communication delays. *IEEE Transactions on Intelligent Transportation Systems*, 16(1):102–112, 2014.

[54] F. Dinuzzo and A. Ferrara. Higher order sliding mode controllers with optimal reaching. *IEEE Transactions on Automatic Control*, 54(9):2126–2136, 2009.

[55] K. D. Do and J. Pan. Nonlinear formation control of unicycle-type mobile robots. *Robotics and Autonomous Systems*, 55(3):191–204, 2007.

[56] X. Dong, B. Yu, Z. Shi, and Y. Zhong. Time-varying formation control for unmanned aerial vehicles: Theories and applications. *IEEE Transactions on Control Systems Technology*, 23(1):340–348, 2014.

[57] M. Doumiati, A. Charara, A. Victorino, and D. Lechner. *Vehicle dynamics estimation using Kalman filtering: experimental validation.* John Wiley & Sons, 2012.

[58] M. Doumiati, A. Victorino, A. Charara, and D. Lechner. A method to estimate the lateral tire force and the sideslip angle of a vehicle: Experimental validation. In *Proceedings of the 2010 American Control Conference*, pages 6936–6942, June 2010.

[59] M. Doumiati, A. Victorino, D. Lechner, G. Baffet, and A. Charara. Observers for vehicle tyre/road forces estimation: experimental validation. *Vehicle System Dynamics*, 48(11):1345–1378, 2010.

[60] M. Doumiati, A. C. Victorino, A. Charara, and D. Lechner. Onboard real-time estimation of vehicle lateral tire–road forces and sideslip angle. *IEEE/ASME Transactions on Mechatronics*, 16(4):601–614, 2010.

[61] W. Dunbar and D. S. Caveney. Distributed receding horizon control of vehicle platoons: Stability and string stability. *IEEE Transactions on Automatic Control*, 57:620–633, 03 2012.

[62] W. B. Dunbar and R. M. Murray. Distributed receding horizon control for multi-vehicle formation stabilization. *Automatica*, 42(4):549 – 558, 2006.

[63] C. Edwards and S. Spurgeon. *Sliding mode control: theory and applications.* Crc Press, 1998.

[64] M. Ehsani, Y. Gao, and J. M. Miller. Hybrid electric vehicles: Architecture and motor drives. *Proceedings of the IEEE*, 95(4):719–728, 2007.

[65] A. Emadi, Y. J. Lee, and K. Rajashekara. Power electronics and motor drives in electric, hybrid electric, and plug-in hybrid electric vehicles. *IEEE Transactions on industrial electronics*, 55(6):2237–2245, 2008.

[66] J. Eyre, D. Yanakiev, and I. Kanellakopoulos. A simplified framework for string stability analysis of automated vehicles. *Vehicle System Dynamics*, 30(5):375–405, 1998.

[67] A. Ferrara and G. P. Incremona. Design of an integral suboptimal second-order sliding mode controller for the robust motion control of robot manipulators. *IEEE Transactions on Control Systems Technology*, 23(6):2316–2325, 2015.

[68] A. Ferrara and M. Rubagotti. A sub-optimal second order sliding mode controller for systems with saturating actuators. *IEEE Transactions on Automatic Control*, 54(5):1082–1087, May 2009.

[69] A. Ferrara, S. Sacone, and S. Siri. *Freeway Traffic Modelling and Control*. Springer International Publishing, 2018.

[70] A. Ferrara and C. Vecchio. Controlling a platoon of vehicles via a second order sliding mode approach. *IFAC Proceedings Volumes*, 39(12):439 – 444, 2006.

[71] A. Ferrara and M. Zambelli. Integral second-order sliding modes for robust prescribed-time leader-follower consensus control with partial information. In *Proceedings of the 58th Conference on Decision and Control*, 2019.

[72] A. Filippov. *Differential Equations with Discontinuous Righthand Sides*. Springer Netherlands, 1988.

[73] T. Floquet, C. Edwards, and S. K. Spurgeon. On sliding mode observers for systems with unknown inputs. *International Journal of Adaptive Control and Signal Processing*, 21(8-9):638–656, 2007.

[74] Y. Furukawa and M. Abe. Advanced chassis control systems for vehicle handling and active safety. *Vehicle System Dynamics*, 28(2-3):59–86, 1997.

[75] C. E. Garcia, D. M. Prett, and M. Morari. Model predictive control: theory and practice—a survey. *Automatica*, 25(3):335–348, 1989.

[76] G. Genta. *Motor vehicle dynamics: modeling and simulation*, volume 43. World Scientific, 1997.

[77] Y. A. Ghoneim, W. C. Lin, D. M. Sidlosky, H. H. Chen, and Y.-K. Chin. Integrated chassis control system to enhance vehicle stability. *International Journal of Vehicle Design*, 23(1-2):124–144, 2000.

[78] T. Goggia, A. Sorniotti, L. De Novellis, A. Ferrara, P. Gruber, J. Theunissen, D. Steenbeke, B. Knauder, and J. Zehetner. Integral sliding mode for the torque-vectoring control of fully electric vehicles: Theoretical design and experimental assessment. *IEEE Transactions on Vehicular Technology*, 64(5):1701–1715, 2014.

[79] G. Guo and W. Yue. Autonomous platoon control allowing range-limited sensors. *IEEE Transactions on vehicular technology*, 61(7):2901–2912, 2012.

[80] A. Harifi, A. Aghagolzadeh, G. Alizadeh, and M. Sadeghi. Designing a sliding mode controller for slip control of antilock brake systems. *Transportation research part C: emerging technologies*, 16(6):731–741, 2008.

[81] H. Her, Y. Koh, E. Joa, K. Yi, and K. Kim. An integrated control of differential braking, front/rear traction, and active roll moment for limit handling performance. *IEEE Transactions on Vehicular Technology*, 65(6):4288–4300, 2015.

[82] Y. Hong, J. Hu, and L. Gao. Tracking control for multi-agent consensus with an active leader and variable topology. *Automatica*, 42(7):1177–1182, 2006.

[83] L. Imsland, T. A. Johansen, T. I. Fossen, H. F. Grip, J. C. Kalkkuhl, and A. Suissa. Vehicle velocity estimation using nonlinear observers. *Automatica*, 42(12):2091–2103, 2006.

[84] G. P. Incremona, A. Ferrara, and L. Magni. Hierarchical model predictive/sliding mode control of nonlinear constrained uncertain systems. *IFAC-PapersOnLine*, 48(23):102 – 109, 2015. 5th IFAC Conference on Nonlinear Model Predictive Control NMPC 2015.

[85] G. P. Incremona, A. Ferrara, and L. Magni. Asynchronous networked mpc with ism for uncertain nonlinear systems. *IEEE Transactions on Automatic Control*, 62(9):4305–4317, Sept 2017.

[86] G. P. Incremona, S. C. Strada, M. Tanelli, and A. Ferrara. Switched integral suboptimal second-order sliding mode control. In *2017 American Control Conference (ACC)*, pages 5842–5847, 2017.

[87] D. Jia, K. Lu, J. Wang, X. Zhang, and X. Shen. A survey on platoon-based vehicular cyber-physical systems. *IEEE Communications Surveys Tutorials*, 18(1):263–284, Firstquarter 2016.

[88] T. A. Johansen, I. Petersen, J. Kalkkuhl, and J. Ludemann. Gain-scheduled wheel slip control in automotive brake systems. *IEEE Transactions on Control Systems Technology*, 11(6):799–811, 2003.

[89] S. Kato, S. Tsugawa, K. Tokuda, T. Matsui, and H. Fujii. Vehicle control algorithms for cooperative driving with automated vehicles and intervehicle communications. *IEEE Transactions on intelligent transportation systems*, 3(3):155–161, 2002.

[90] T. Keviczky, F. Borrelli, K. Fregene, D. Godbole, and G. J. Balas. Decentralized receding horizon control and coordination of autonomous vehicle formations. *IEEE Transactions on Control Systems Technology*, 16(1):19–33, 2007.

[91] H. K. Khalil. *Nonlinear systems*. Pearson, 2002.

[92] S. Khoo, L. Xie, and Z. Man. Integral terminal sliding mode cooperative control of multi-robot networks. In *2009 IEEE/ASME International Conference on Advanced Intelligent Mechatronics*, pages 969–973, July 2009.

[93] S. Khoo, L. Xie, and Z. Man. Robust finite-time consensus tracking algorithm for multirobot systems. *IEEE/ASME Transactions on Mechatronics*, 14(2):219–228, April 2009.

[94] U. Kiencke and A. Daiß. Observation of lateral vehicle dynamics. *Control Engineering Practice*, 5(8):1145–1150, 1997.

[95] U. Kiencke and L. Nielsen. *Automotive Control Systems - For Engine, Driveline, and Vehicle*. Springer-Verlag Berlin Heidelberg, 2005.

[96] J. Kim and H. Kim. Electric vehicle yaw rate control using independent in-wheel motor. In *2007 Power Conversion Conference-Nagoya*, pages 705–710. IEEE, 2007.

[97] J. Larminie and J. Lowry. *Electric vehicle technology explained*. John Wiley & Sons, 2012.

[98] J. Larson, K.-Y. Liang, and K. H. Johansson. A distributed framework for coordinated heavy-duty vehicle platooning. *IEEE Trans. Intelligent Transportation Systems*, 16(1):419–429, 2015.

[99] A. Levant. Sliding order and sliding accuracy in sliding mode control. *International Journal of Control*, 58(6):1247–1263, 1993.

[100] A. Levant. Robust exact differentiation via sliding mode technique. *Automatica*, 34(3):379 – 384, 1998.

[101] A. Levant. Higher-order sliding modes, differentiation and output-feedback control. *International journal of Control*, 76(9-10):924–941, 2003.

[102] A. Levant. Quasi-continuous high-order sliding-mode controllers. In *42nd IEEE International Conference on Decision and Control (IEEE Cat. No. 03CH37475)*, volume 5, pages 4605–4610. IEEE, 2003.

[103] A. Levant. Homogeneity approach to high-order sliding mode design. *Automatica*, 41(5):823–830, 2005.

[104] A. Levant. Non-homogeneous finite-time-convergent differentiator. In *Proceedings of the 48h IEEE Conference on Decision and Control (CDC) held jointly with 2009 28th Chinese Control Conference*, pages 8399–8404. IEEE, 2009.

[105] A. Levant. Chattering analysis. *IEEE transactions on automatic control*, 55(6):1380–1389, 2010.

[106] A. Levant and L. Alelishvili. Integral high-order sliding modes. *IEEE Transactions on Automatic Control*, 52(7):1278–1282, 2007.

[107] H. Li, P. Xie, and W. Yan. Receding horizon formation tracking control of constrained underactuated autonomous underwater vehicles. *IEEE Transactions on Industrial Electronics*, 64(6):5004–5013, 2016.

[108] L. Li, Y. Lu, R. Wang, and J. Chen. A three-dimensional dynamics control framework of vehicle lateral stability and rollover prevention via active braking with mpc. *IEEE Transactions on Industrial Electronics*, 64(4):3389–3401, 2016.

[109] L. Li, D. Wen, and D. Yao. A survey of traffic control with vehicular communications. *IEEE Transactions on Intelligent Transportation Systems*, 15(1):425–432, 2013.

[110] P. Y. Li and A. Shrivastava. Traffic flow stability induced by constant time headway policy for adaptive cruise control vehicles. *Transportation Research Part C: Emerging Technologies*, 10(4):275–301, 2002.

[111] S. Li, H. Du, and X. Lin. Finite-time consensus algorithm for multi-agent systems with double-integrator dynamics. *Automatica*, 47(8):1706–1712, 2011.

[112] S. E. Li, Y. Zheng, K. Li, and J. Wang. An overview of vehicular platoon control under the four-component framework. In *2015 IEEE Intelligent Vehicles Symposium (IV)*, pages 286–291, June 2015.

[113] Y. Li, C. Tang, K. Li, X. He, S. Peeta, and Y. Wang. Consensus-based cooperative control for multi-platoon under the connected vehicles environment. *IEEE Transactions on Intelligent Transportation Systems*, 20(6):2220–2229, 2018.

[114] F. Lin, M. Fardad, and M. R. Jovanović. Optimal control of vehicular formations with nearest neighbor interactions. *IEEE Transactions on Automatic Control*, 57:2203–2218, 2012.

[115] J. A. P. Lopes, F. J. Soares, and P. M. R. Almeida. Integration of electric vehicles in the electric power system. *Proceedings of the IEEE*, 99(1):168–183, 2010.

[116] M. Lu, K. Wevers, and R. V. D. Heijden. Technical feasibility of advanced driver assistance systems (adas) for road traffic safety. *Transportation Planning and Technology*, 28(3):167–187, 2005.

[117] Q. Lu, P. Gentile, A. Tota, A. Sorniotti, P. Gruber, F. Costamagna, and J. De Smet. Enhancing vehicle cornering limit through sideslip and yaw rate control. *Mechanical Systems and Signal Processing*, 75:455–472, 2016.

[118] J. M. Maciejowski. *Predictive Control with Constraints*. Pearson Education, 2002.

[119] L. Magni, G. De Nicolao, R. Scattolini, and F. Allgöwer. Robust model predictive control for nonlinear discrete-time systems. *International Journal of Robust and Nonlinear Control: IFAC-Affiliated Journal*, 13(3-4):229–246, 2003.

[120] S. Mammar, S. Glaser, and M. Netto. Vehicle lateral dynamics estimation using unknown input proportional-integral observers. In *2006 American control conference*, pages 6–pp. IEEE, 2006.

[121] D. Q. Mayne, J. B. Rawlings, C. V. Rao, and P. O. Scokaert. Constrained model predictive control: Stability and optimality. *Automatica*, 36(6):789–814, 2000.

[122] D. Q. Mayne, M. M. Seron, and S. Raković. Robust model predictive control of constrained linear systems with bounded disturbances. *Automatica*, 41(2):219–224, 2005.

[123] A. Mesbah. Stochastic model predictive control: An overview and perspectives for future research. *IEEE Control Systems Magazine*, 36(6):30–44, 2016.

[124] M. Mesbahi and M. Egerstedt. *Graph theoretic methods in multiagent networks*, volume 33. Princeton University Press, 2010.

[125] N. Michael, J. Fink, and V. Kumar. Cooperative manipulation and transportation with aerial robots. *Autonomous Robots*, 30(1):73–86, 2011.

[126] V. Milanés, S. E. Shladover, J. Spring, C. Nowakowski, H. Kawazoe, and M. Nakamura. Cooperative adaptive cruise control in real traffic situations. *IEEE Transactions on intelligent transportation systems*, 15(1):296–305, 2013.

[127] S. Mondal, J. Ghommam, and M. Saad. Homogeneous finite-time consensus control for higher-order multi-agent systems by full order sliding mode. *Journal of Systems Science and Complexity*, 31(5):1186–1205, Oct 2018.

[128] S. Monteiro and E. Bicho. A dynamical systems approach to behavior-based formation control. In *Proceedings 2002 IEEE International Con-*

ference on Robotics and Automation (Cat. No. 02CH37292), volume 3, pages 2606–2611. IEEE, 2002.

[129] R. M. Murray. Recent Research in Cooperative Control of Multivehicle Systems. *Journal of Dynamic Systems, Measurement, and Control*, 129(5):571–583, 05 2007.

[130] W. Ni and D. Cheng. Leader-following consensus of multi-agent systems under fixed and switching topologies. *Systems & Control Letters*, 59(3-4):209–217, 2010.

[131] J. J. Oh and S. B. Choi. Vehicle velocity observer design using 6-d imu and multiple-observer approach. *IEEE Transactions on Intelligent Transportation Systems*, 13(4):1865–1879, 2012.

[132] R. Okuda, Y. Kajiwara, and K. Terashima. A survey of technical trend of adas and autonomous driving. In *Technical Papers of 2014 International Symposium on VLSI Design, Automation and Test*, pages 1–4, 2014.

[133] R. Olfati-Saber. Flocking for multi-agent dynamic systems: Algorithms and theory. *IEEE Transactions on automatic control*, 51(3):401–420, 2006.

[134] R. Olfati-Saber, J. A. Fax, and R. M. Murray. Consensus and cooperation in networked multi-agent systems. *Proceedings of the IEEE*, 95(1):215–233, 2007.

[135] R. Olfati-Saber and R. M. Murray. Consensus problems in networks of agents with switching topology and time-delays. *IEEE Transactions on Automatic Control*, 49(9):1520–1533, Sep. 2004.

[136] E. Ono, Y. Hattori, Y. Muragishi, and K. Koibuchi. Vehicle dynamics integrated control for four-wheel-distributed steering and four-wheel-distributed traction/braking systems. *vehicle system dynamics*, 44(2):139–151, 2006.

[137] J. Orwell, S. Massey, P. Remagnino, D. Greenhill, and G. A. Jones. A multi-agent framework for visual surveillance. In *Proceedings 10th International Conference on Image Analysis and Processing*, pages 1104–1107. IEEE, 1999.

[138] M. Oudghiri, M. Chadli, and A. El Hajjaji. Robust observer-based fault-tolerant control for vehicle lateral dynamics. *International Journal of vehicle design*, 48(3-4):173–189, 2008.

[139] B. Paden, M. Čáp, S. Z. Yong, D. Yershov, and E. Frazzoli. A survey of motion planning and control techniques for self-driving urban vehicles. *IEEE Transactions on Intelligent Vehicles*, 1(1):33–55, 2016.

[140] J. H. Park and C. Y. Kim. Wheel slip control in traction control system for vehicle stability. *Vehicle system dynamics*, 31(4):263–278, 1999.

[141] K. Peng and Y. Yang. Leader-following consensus problem with a varying-velocity leader and time-varying delays. *Physica A: Statistical Mechanics and its Applications*, 388(2-3):193–208, 2009.

[142] G. Piacentini, P. Goatin, and A. Ferrara. Traffic control via moving bottleneck of coordinated vehicles. *IFAC-PapersOnLine*, 51(9):13 – 18, 2018.

[143] G. Piacentini, P. Goatin, and A. Ferrara. Traffic control via platoons of intelligent vehicles for saving fuel consumption in freeway systems. *IEEE Control Systems Letters*, 5(2):593–598, 2021.

[144] G. Piacentini, C. Pasquale, S. Sacone, S. Siri, and A. Ferrara. Multiple moving bottlenecks for traffic control in freeway systems. In *2019 18th European Control Conference (ECC)*, pages 3662–3667, June 2019.

[145] A. Pilloni, A. Pisano, M. Franceschelli, and E. Usai. Integral sliding modes for the robustification of consensus-based multi-agent based systems. In *2016 14th International Workshop on Variable Structure Systems (VSS)*, pages 222–227, June 2016.

[146] A. Pisano, M. Tanelli, and A. Ferrara. Combined switched/time-based adaptation in second order sliding mode control. *52nd IEEE Conference on Decision and Control*, 2013.

[147] J. Ploeg, B. T. Scheepers, E. Van Nunen, N. Van de Wouw, and H. Nijmeijer. Design and experimental evaluation of cooperative adaptive cruise control. In *2011 14th International IEEE Conference on Intelligent Transportation Systems (ITSC)*, pages 260–265. IEEE, 2011.

[148] J. Ploeg, D. P. Shukla, N. van de Wouw, and H. Nijmeijer. Controller synthesis for string stability of vehicle platoons. *IEEE Transactions on Intelligent Transportation Systems*, 15(2):854–865, 2014.

[149] J. Ploeg, N. van de Wouw, and H. Nijmeijer. Lp string stability of cascaded systems: Application to vehicle platooning. *IEEE Transactions on Control Systems Technology*, 22(2):786–793, 2014.

[150] M. Porfiri, D. G. Roberson, and D. J. Stilwell. Tracking and formation control of multiple autonomous agents: A two-level consensus approach. *Automatica*, 43(8):1318–1328, 2007.

[151] A. Pozzi, M. Torchio, R. D. Braatz, and D. M. Raimondo. Optimal charging of an electric vehicle battery pack: A real-time sensitivity-based mpc approach, 2019.

[152] A. Pozzi, M. Zambelli, A. Ferrara, and D. M. Raimondo. Balancing-aware charging strategy for series-connected lithium-ion cells: A nonlinear model predictive control approach. *IEEE Transactions on Control Systems Technology*, pages 1–16, 2020.

[153] R.-E. Precup, S. Preitl, M. Balas, and V. Balas. Fuzzy controllers for tire slip control in anti-lock braking systems. In *2004 IEEE International Conference on Fuzzy Systems (IEEE Cat. No. 04CH37542)*, volume 3, pages 1317–1322. IEEE, 2004.

[154] J. Qin, Q. Ma, Y. Shi, and L. Wang. Recent advances in consensus of multi-agent systems: A brief survey. *IEEE Transactions on Industrial Electronics*, 64(6):4972–4983, June 2017.

[155] J. Qin, G. Zhang, W. X. Zheng, and Y. Kang. Adaptive sliding mode consensus tracking for second-order nonlinear multiagent systems with actuator faults. *IEEE Transactions on Cybernetics*, pages 1–11, 2018.

[156] R. Rajamani, G. Phanomchoeng, D. Piyabongkarn, and J. Y. Lew. Algorithms for real-time estimation of individual wheel tire-road friction coefficients. *IEEE/ASME Transactions on Mechatronics*, 17(6):1183–1195, Dec 2012.

[157] R. Rajamani, D. Piyabongkarn, V. Tsourapas, and J. Y. Lew. Parameter and state estimation in vehicle roll dynamics. *IEEE Transactions on Intelligent Transportation Systems*, 12(4):1558–1567, 2011.

[158] Z. Ramezani, D. Gagliardi, and L. Del Re. A risk-constrained and energy efficient stochastic approach for autonomous overtaking. In *Proceedings of the 2018 European Control Conference*, 2018.

[159] S. Rao and D. Ghose. Sliding mode control-based autopilots for leaderless consensus of unmanned aerial vehicles. *IEEE Transactions on Control Systems Technology*, 22(5):1964–1972, Sep. 2014.

[160] J. J. Rath, K. C. Veluvolu, M. Defoort, and Y. C. Soh. Higher-order sliding mode observer for estimation of tyre friction in ground vehicles. *IET Control Theory & Applications*, 8(6):399–408, 2014.

[161] E. Regolin, A. Alatorre, M. Zambelli, A. Victorino, A. Charara, and A. Ferrara. A sliding-mode virtual sensor for wheel forces estimation with accuracy enhancement via ekf. *IEEE Transactions on Vehicular Technology*, 68(4):3457–3471, 2019.

[162] E. Regolin, G. P. Incremona, and A. Ferrara. *Sliding mode control of vehicle dynamics*, chapter Longitudinal Vehicle Dynamics Control via Sliding Modes Generation, pages 33–76. IET, London, 2017.

[163] E. Regolin, D. Savitski, V. Ivanov, K. Augsburg, and A. Ferrara, 2017.

[164] E. Regolin, M. Zambelli, and A. Ferrara. Wheel forces estimation via adaptive sub-optimal second order sliding mode observers. *Proceedings of the 2017 XXVI International Conference on Information, Communication and Automation Technologies (ICAT 2017)*, Oct. 2017.

[165] E. Regolin, M. Zambelli, and A. Ferrara. A multi-rate ism approach for robust vehicle stability control during cornering. *IFAC-PapersOnLine*, 51:249–254, 2018.

[166] E. Regolin, M. Zambelli, M. Vanzulli, and A. Ferrara. A path tracking approach for autonomous driving on slippery surfaces. In *2019 IEEE International Conference on Connected Vehicles and Expo (ICCVE)*, pages 1–6, 2019.

[167] B. Ren, H. Chen, H. Zhao, and L. Yuan. Mpc-based yaw stability control in in-wheel-motored ev via active front steering and motor torque distribution. *Mechatronics*, 38:103–114, 2016.

[168] W. Ren and R. W. Beard. *Distributed consensus in multi-vehicle cooperative control*. Springer, 2008.

[169] J. Rios-Torres and A. A. Malikopoulos. A survey on the coordination of connected and automated vehicles at intersections and merging at highway on-ramps. *IEEE Transactions on Intelligent Transportation Systems*, 18(5):1066–1077, 2016.

[170] M. Rubagotti, A. Estrada, F. Castanos, A. Ferrara, and L. Fridman. Integral sliding mode control for nonlinear systems with matched and unmatched perturbations. *IEEE Transactions on Automatic Control*, 56(11):2699–2704, Nov 2011.

[171] A. Rupp, M. Reichhartinger, and M. Horn. String stability analysis for sliding mode controllers in platoons with unmodeled actuator dynamics: A frequency domain approach. In *2019 18th European Control Conference (ECC)*, pages 4067–4072, 2019.

[172] A. Rupp, M. Steinberger, and M. Horn. Sliding mode based platooning with non-zero initial spacing errors. *IEEE Control Systems Letters*, 1(2):274–279, 2017.

[173] A. Rupp, M. Steinberger, and M. Horn. *Sliding-Mode-Based Platooning: Theory and Applications*, pages 393–431. Springer International Publishing, Cham, 2020.

[174] A. Rupp, M. Tranninger, J. Zubača, M. Steinberger, M. Horn, and R. Wallner. Fast and low-cost testing of advanced driver assistance systems using small-scale vehicles. In *9th IFAC International Symposium on Advances in Automotive Control*, volume 52 (5), pages 34–39, 9 2019.

[175] A. Rupp, R. Wallner, S. Koch, M. Reichhartinger, and M. Horn. Sliding mode based platooning with actuator dynamics. In *15th International Workshop on Variable Structure Systems*, 2018.

[176] J. Ryu and J. C. Gerdes. Estimation of vehicle roll and road bank angle. In *Proceedings of the 2004 American control conference*, volume 3, pages 2110–2115. IEEE, 2004.

[177] J. Ryu, E. J. Rossetter, and J. C. Gerdes. Vehicle sideslip and roll parameter estimation using gps. In *Proceedings of the AVEC International Symposium on Advanced Vehicle Control*, pages 373–380, 2002.

[178] F. R. Salmasi. Control strategies for hybrid electric vehicles: Evolution, classification, comparison, and future trends. *IEEE Transactions on vehicular technology*, 56(5):2393–2404, 2007.

[179] H. Santana, G. Ramalho, V. Corruble, and B. Ratitch. Multi-agent patrolling with reinforcement learning. In *Proceedings of the Third International Joint Conference on Autonomous Agents and Multiagent Systems-Volume 3*, pages 1122–1129, 2004.

[180] K. Santhanakrishnan and R. Rajamani. On spacing policies for highway vehicle automation. *IEEE Transactions on intelligent transportation systems*, 4(4):198–204, 2003.

[181] S. Santini, A. Salvi, A. S. Valente, A. Pescapè, M. Segata, and R. L. Cigno. A consensus-based approach for platooning with inter-vehicular communications. In *2015 IEEE Conference on Computer Communications (INFOCOM)*, pages 1158–1166, April 2015.

[182] A. Sciarretta, M. Back, and L. Guzzella. Optimal control of parallel hybrid electric vehicles. *IEEE Transactions on control systems technology*, 12(3):352–363, 2004.

[183] A. Sciarretta and L. Guzzella. Control of hybrid electric vehicles. *IEEE Control Systems Magazine*, 27(2):60–70, 2007.

[184] P. O. Scokaert, D. Q. Mayne, and J. B. Rawlings. Suboptimal model predictive control (feasibility implies stability). *IEEE Transactions on Automatic Control*, 44(3):648–654, 1999.

[185] E. Shaw and J. K. Hedrick. String stability analysis for heterogeneous vehicle strings. In *2007 American control conference*, pages 3118–3125. IEEE, 2007.

[186] Y. Shibahata. Progress and future direction of chassis control technology. *Annual Reviews in Control*, 29(1):151–158, 2005.

[187] S. E. Shladover, D. Su, and X.-Y. Lu. Impacts of cooperative adaptive cruise control on freeway traffic flow. *Transportation Research Record*, 2324(1):63–70, 2012.

[188] Y. Shoham and K. Leyton-Brown. *Multiagent systems: Algorithmic, game-theoretic, and logical foundations*. Cambridge University Press, 2008.

[189] Y. Shtessel, C. Edwards, L. Fridman, and A. Levant. *Sliding Mode Control and Observation*. Birkhäuser Basel, 2014.

[190] E. Siampis, M. Massaro, and E. Velenis. Electric rear axle torque vectoring for combined yaw stability and velocity control near the limit of handling. In *52nd IEEE conference on Decision and Control*, pages 1552–1557. IEEE, 2013.

[191] J. Stephant, A. Charara, and D. Meizel. Virtual sensor: Application to vehicle sideslip angle and transversal forces. *IEEE Transactions on industrial electronics*, 51(2):278–289, 2004.

[192] J. Stéphant, A. Charara, and D. Meizel. Evaluation of a sliding mode observer for vehicle sideslip angle. *Control Engineering Practice*, 15(7):803–812, 2007.

[193] A. Stotsky, C. C. Chien, and P. Ioannou. Robust platoon-stable controller design for autonomous intelligent vehicles. In *Proceedings of 1994 33rd IEEE Conference on Decision and Control*, volume 3, 1994.

[194] A. Stotsky and I. Kolmanovsky. Simple unknown input estimation techniques for automotive applications. In *Proceedings of the 2001 American Control Conference.(Cat. No. 01CH37148)*, volume 5, pages 3312–3317. IEEE, 2001.

[195] D. Swaroop. String stability of interconnected systems: An application to platooning in automated highway systems. 1997.

[196] D. Swaroop and J. K. Hedrick. String stability of interconnected systems. *IEEE Transactions on Automatic Control*, 41(3):349–357, 1996.

[197] D. Swaroop, J. K. Hedrick, and S. B. Choi. Direct adaptive longitudinal control of vehicle platoons. *IEEE transactions on vehicular technology*, 50(1):150–161, 2001.

[198] D. Swaroop and K. R. Rajagopal. A review of constant time headway policy for automatic vehicle following. In *ITSC 2001. 2001 IEEE Intelligent Transportation Systems. Proceedings (Cat. No.01TH8585)*, pages 65–69, Aug 2001.

[199] M. Tanelli and A. Ferrara. Switched second-order sliding mode control with partial information: Theory and application. *Asian Journal of Control*, 15(1):20–30, 2013.

[200] M. Tanelli, A. Ferrara, and P. Giani. Combined vehicle velocity and tire-road friction estimation via sliding mode observers. In *Proc. IEEE International Conference on Control Applications*, pages 130–135, Oct. 2012.

[201] H. G. Tanner, A. Jadbabaie, and G. J. Pappas. Flocking in fixed and switching networks. *IEEE Transactions on Automatic control*, 52(5):863–868, 2007.

[202] R. Tchamna and I. Youn. Yaw rate and side-slip control considering vehicle longitudinal dynamics. *International Journal of Automotive Technology*, 14(1):53–60, 2013.

[203] S. Thrun, M. Montemerlo, H. Dahlkamp, D. Stavens, A. Aron, J. Diebel, P. Fong, J. Gale, M. Halpenny, G. Hoffmann, K. Lau, C. Oakley, M. Palatucci, V. Pratt, P. Stang, S. Strohband, C. Dupont, L.-E. Jendrossek, C. Koelen, C. Markey, C. Rummel, J. van Niekerk, E. Jensen, P. Alessandrini, G. Bradski, B. Davies, S. Ettinger, A. Kaehler, A. Nefian, and P. Mahoney. *Stanley: The Robot That Won the DARPA Grand Challenge*, pages 1–43. Springer Berlin Heidelberg, Berlin, Heidelberg, 2007.

[204] L. Tolbert, F. Z. Peng, T. Cunnyngham, and J. N. Chiasson. Charge balance control schemes for cascade multilevel converter in hybrid electric vehicles. *IEEE transactions on industrial electronics*, 49(5):1058–1064, 2002.

[205] A. Trachtler. Integrated vehicle dynamics control using active brake, steering and suspension systems. *International Journal of Vehicle Design*, 36(1):1–12, 2004.

[206] V. Utkin and J. Shi. Integral sliding mode in systems operating under uncertainty conditions. In *Proceedings of 35th IEEE Conference on Decision and Control*, volume 4, pages 4591–4596 vol.4, Dec 1996.

[207] V. I. Utkin. *Sliding Modes in Control and Optimization*. Springer-Verlag, 1992.

[208] B. van Arem, C. J. G. van Driel, and R. Visser. The impact of cooperative adaptive cruise control on traffic-flow characteristics. *IEEE Transactions on Intelligent Transportation Systems*, 7(4):429–436, Dec 2006.

[209] D. Van der Walle, B. Fidan, A. Sutton, C. Yu, and B. D. Anderson. Non-hierarchical uav formation control for surveillance tasks. In *2008 American Control Conference*, pages 777–782. IEEE, 2008.

[210] P. Varaiya. Smart cars on smart roads: problems of control. *IEEE Transactions on automatic control*, 38(2):195–207, 1993.

[211] A. von Vietinghoff, M. Hiemer, and U. Kiencke. Nonlinear observer design for lateral vehicle dynamics. *IFAC Proceedings Volumes*, 38(1):988–993, 2005.

[212] J. Wang and M. Xin. Integrated optimal formation control of multiple unmanned aerial vehicles. *IEEE Transactions on Control Systems Technology*, 21(5):1731–1744, 2012.

[213] L. Wang and F. Xiao. Finite-time consensus problems for networks of dynamic agents. *IEEE Transactions on Automatic Control*, 55(4):950–955, April 2010.

[214] T. L. Willke, P. Tientrakool, and N. F. Maxemchuk. A survey of inter-vehicle communication protocols and their applications. *IEEE Communications Surveys & Tutorials*, 11(2):3–20, 2009.

[215] L. Xiao and F. Gao. Practical string stability of platoon of adaptive cruise control vehicles. *IEEE Transactions on Intelligent Transportation Systems*, 12(4):1184–1194, 2011.

[216] Z. Xiong, H. Sheng, W. Rong, and D. E. Cooper. Intelligent transportation systems for smart cities: a progress review. *Science China Information Sciences*, 55(12):2908–2914, 2012.

[217] D. Yanakiev and I. Kanellakopoulos. Nonlinear spacing policies for automated heavy-duty vehicles. *IEEE Transactions on Vehicular Technology*, 47(4):1365–1377, 1998.

[218] K. Yi, K. Hedrick, and S.-C. Lee. Estimation of tire-road friction using observer based identifiers. *Vehicle System Dynamics*, 31(4):233–261, 1999.

[219] J. Yoon, W. Cho, B. Koo, and K. Yi. Unified chassis control for rollover prevention and lateral stability. *IEEE Transactions on Vehicular Technology*, 58(2):596–609, 2008.

[220] F. Yu, D.-F. Li, and D. Crolla. Integrated vehicle dynamics control—state-of-the art review. In *2008 IEEE vehicle power and propulsion conference*, pages 1–6. IEEE, 2008.

[221] M. Zambelli, P. Carulli, M. Steinberger, M. Horn, and A. Ferrara. A novel formation creation algorithm for heterogeneous vehicles in highway scenarios: Assessment and experimental validation. In *IFAC-PapersOnLine: Proceedings of the 21st IFAC World Congress*, 2020.

[222] M. Zambelli and A. Ferrara. Linearization-based integral sliding mode control for a class of constrained nonlinear systems. In *2018 15th International Workshop on Variable Structure Systems (VSS)*, pages 402–407, 2018.

[223] M. Zambelli and A. Ferrara. Robustified distributed model predictive control for coherence and energy efficiency-aware platooning. In *2019 American Control Conference (ACC)*, pages 527–532, July 2019.

[224] M. Zambelli and A. Ferrara. Second-order sliding modes generation for robust disturbance string stable platoon control. In *2020 European Control Conference (ECC)*, pages 1879–1884. IEEE, 2020.

[225] M. Zambelli and A. Ferrara. *Variable-Structure Systems and Sliding-Mode Control: From Theory to Practice*, chapter Constrained Sliding-

Mode Control: A Survey, pages 149–175. Springer International Publishing, Cham, 2020.

[226] M. Zambelli and A. Ferrara. *Emerging Trends in Sliding Mode Control – Theory and Application*, chapter Sliding Modes in Consensus Control. Springer, 2021.

[227] M. Zambelli, M. Steinberger, M. Horn, and A. Ferrara. Two-step event-triggered iterative formation control for heterogeneous vehicles in highwayscenarios. In *(Submitted to) IEEE Transactions on Intelligent Vehicles*, 2020.

[228] A. Zanella, N. Bui, A. Castellani, L. Vangelista, and M. Zorzi. Internet of things for smart cities. *IEEE Internet of Things journal*, 1(1):22–32, 2014.

[229] J. Zhao, M. Oya, and A. El Kamel. A safety spacing policy and its impact on highway traffic flow. In *2009 IEEE Intelligent Vehicles Symposium*, pages 960–965. IEEE, 2009.

[230] L.-H. Zhao, Z.-Y. Liu, and H. Chen. Design of a nonlinear observer for vehicle velocity estimation and experiments. *IEEE Transactions on Control Systems Technology*, 19(3):664–672, 2010.

[231] W. Zhao, D. Ngoduy, S. Shepherd, R. Liu, and M. Papageorgiou. A platoon based cooperative eco-driving model for mixed automated and human-driven vehicles at a signalised intersection. *Transportation Research Part C: Emerging Technologies*, 95:802–821, 2018.

[232] Y. Zheng, S. E. Li, J. Wang, K. Li, et al. Influence of information flow topology on closed-loop stability of vehicle platoon with rigid formation. In *17th International IEEE Conference on Intelligent Transportation Systems (ITSC)*, pages 2094–2100. IEEE, 2014.

[233] H. Zhou and Z. Liu. Vehicle yaw stability-control system design based on sliding mode and backstepping control approach. *IEEE Transactions on Vehicular Technology*, 59(7):3674–3678, 2010.

[234] F. Zhu. State estimation and unknown input reconstruction via both reduced-order and high-order sliding mode observers. *Journal of Process Control*, 22(1):296–302, 2012.